TECHNISCHE UNIVERSITÄT WIEN

Diplomarbeit

Monitoring of *Corynebacterium glutamicum* cultivations by means of a genetically encoded fluorescence sensor

Ausgeführt am Institut für
Verfahrenstechnik,
Umwelttechnik und technische Biowissenschaften
der Technischen Universität Wien

Unter der Anleitung von
Univ. Prof. Dipl.–Ing. Dr. techn. Christoph Herwig
Peter Sinner, M.Sc.

durch

Lizaveta Sidarenka

01428448

Wien, 15.11.2019 _____

Die approbierte gedruckte Originalversion dieser Diplomarbeit ist an der TU Wien Bibliothek verfügbar.
The approved original version of this thesis is available in print at TU Wien Bibliothek.
TU Bibliothek Your knowledge hub WIEN

Table of contents

Acknowledgments 3

Abstract 4

Zusammenfassung 5

Abbreviations 6

1 Introduction 7

2 Aims of the Study 8

3 Theoretical background 9

3.1 *Corynebacterium glutamicum* 9

3.2 Intracellular pH and pH homeostasis 10

3.3 IPTG Induction of pHluorin fluorescence sensor protein 12

3.4 Genetically encoded pH-sensitive fluorescent sensors 14

3.5 Membrane stress inducers 15

3.6 Statistical methods for pHlourin calibration 16

4 Materials and Methods 20

4.1 Materials 20

4.1.1 Bacterial strain and plasmid 20

4.1.2 Chemicals 20

4.1.3 Equipment 23

4.2 Cultivation methods 23

4.2.1 Strain maintenance and pre-culture preparation 23

4.2.2 Microtiterplate cultivation 23

4.2.3 Shake flask cultivation 24

4.2.4 Cultivation in bioreactor 24

4.3 Analytical methods 26

4.3.1 Dry cell weight determination 26

4.3.2 Optical density measurement 26

4.3.3 Substrate and metabolite analytics 26

4.3.4 Fluorescence analysis of pHluorin 26

4.3.5 pHluorin sensor calibration 27

5 Results and Discussion 29

5.1 Fluorescence sensor calibration and validation 29

5.1.1 Calibration by means of CTAB 29

5.1.1.1 Polynomic function (CTAB) 29

5.1.1.2 Sigmoidal function (CTAB) 31

Die approbierte gedruckte Originalversion dieser Diplomarbeit ist an der TU Wien Bibliothek verfügbar.
The approved original version of this thesis is available in print at TU Wien Bibliothek.

TU Bibliothek Your knowledge hub WIEN

5.1.1.3 Linear function (CTAB) ... 32
5.1.2 Calibration by means of Nigericin ... 34
5.1.2.1 Polynomic function (Nigericin) ... 35
5.1.2.2 Sigmoidal function (Nigericin) ... 37
5.1.2.3 Linear function (Nigericin) ... 38
5.1.3 Sensor validation at different optical density levels ... 39
5.1.4 CTAB/Nigericin and pH range validation ... 42
5.2 Dynamics of intracellular pH and cell growth during batch cultivations in shake flasks ... 44
5.3 Tuning of sensor protein expression levels by high-throughput screening ... 46
5.4 Tuning of sensor protein expression levels in batch and fed-batch bioreactor cultivations 51
5.4.1 Intracellular sensor signal ... 51
5.4.2 Extracellular sensor signal ... 57
5.4.3 Relation of carbon dioxide evolution rate and pH gradient ... 59
5.4.4 Correlation of substrate uptake rate and pH gradient ... 61
5.5 Dynamics of pH_i during carbon starvation, external pH changes and Penicillin G addition .. 63
5.5.1 Batch & Fed-Batch cultivations ... 64
5.5.2 Batch cultivations ... 65
5.5.2.1 Intracellular sensor signal ... 67
5.5.2.2 Relation of carbon dioxide evolution rate and pH gradient ... 70
5.5.2.3 Correlation of substrate uptake rate/ respiration rates and pH gradient ... 71
6 Summary ... 73
7 Outlook ... 74
8 References ... 75
9 List of figures ... 82
10 List of tables ... 88
11 Attachments ... 89

Die approbierte gedruckte Originalversion dieser Diplomarbeit ist an der TU Wien Bibliothek verfügbar.
The approved original version of this thesis is available in print at TU Wien Bibliothek.

Acknowledgments

I would like to thank everyone who supported me during the course of my master thesis!

First of all, I would like to thank my supervisor Peter Sinner MSc for his continuous assistance over the course of my master thesis. In particular I am grateful for his encouragements, constant availability, insightful instruction and creative ideas. Especially for helping me develop what turned out to be an interesting and successful master thesis. I want to express my gratitude to Professor Christoph Herwig for offering me the opportunity to conduct my master thesis at his research group and for continuous contribution of potential paths along with constant supervision of my work. Furthermore, I would like to thank Dr. Julian Kager for openness and always wiliness to help, moreover, for the introduction to BPTT script that made the calculation of bioprocesses easier.

A special thanks to our master group for supporting each other, sharing scientific ideas and having lunch breaks together. Especially, I would like to thank Georg Scherfler for his consistently assistance with MATLAB and Marlene Stiegler for her cooperation during laboratory work.

On a more personal level I am thankful to my parents who make it possible for me to have an opportunity to study at Technical University of Vienna and to be able to live in such a beautiful city. I truly appreciate their continuous belief in me and for their support in up and downs in my life.

Furthermore, I want to express my gratefulness to the groups of Dr. Christian Riedel from University of Ulm and Associate Professor Dr. Gerd Seibold from Technical University of Denmark for providing us with the pHluorin expressing *C. glutamicum* strain they developed. Moreover, I want to appreciative acknowledge that this project has received funding from the Bio Based Industries Joint Undertaking under the European Union's Horizon 2020 research and innovation program under grant agreement N° 790507.

Die approbierte gedruckte Originalversion dieser Diplomarbeit ist an der TU Wien Bibliothek verfügbar.
The approved original version of this thesis is available in print at TU Wien Bibliothek.

Abstract

Intracellular pH (pH_i) measurement has gotten a strong interest in biotechnology and molecular biology over the last decades. Internal pH homeostasis is essential for all cellular functions and directly linked to membrane integrity and functionality of energy generation processes. Therefore, the internal pH in relation to the external pH is a valuable parameter to assess the physiological state and the viability of bacteria. In this work, *Corynebacterium glutamicum* was used with the plasmid containing genetically encoded pH-sensitive green fluorescent protein – pHluorin. The sensor expression is connected to an expression system that is induced under the addition of IPTG. This inducer activates the *tac*-promotor and allows conditional sensor production. The goals of the work were the following:

- To validate the production of the pHluorin protein and to check the sensor production dependency on biomass concentration
- To tune fluorescence sensor expression levels
- To investigate the influence of additional stress factors on the production of pHluorin sensor
- To monitor the protein production and to correlate the internal pH to process parameters and predict the performance of the process

The non-invasive sensor was calibrated by expressing it under IPTG induction at different extracellular pH values and adding membrane-disturbing chemicals (Nigericin and CTAB). The calibration allows the calculation of pH_i under experimental conditions. Also, the calibration showed no dependency on biomass concentration, meaning that no extra sample manipulations like dilution are necessary during bioreactor cultivation. As the next step, IPTG induction levels were tuned in order to find the appropriate inductor concentration, at which sensor production proved adequate to obtain a sufficiently strong fluorescent signal while minimizing the metabolic load on the strain, showing that low IPTG levels are already enough to observe an adequate signal.

Corynebacterium glutamicum is widely used in industry for its high glutamate production, which gives this bacteria industrial importance and plays a principal role in the progress of the amino acid fermentation. Glutamate is produced under the addition of membrane stress conditions. In this study, Tween 40 and Penicillin G were applied to investigate how the cells can handle additional stress conditions and how they influence the production of the pHluorin sensor.

The physiological response of the *C.glutamicum* cells under the production of the fluorescence pHluorin sensor was monitored. Internal pH homeostasis measurement showed the existence of a correlation of pH_i with other process variables, like the specific substrate uptake rate (q_s), respiration rates (q_{O2} and q_{CO2}) and its relation to the carbon dioxide evaluation rate (CER). This novelty shows that sensor production can be used to monitor process performance.

Die approbierte gedruckte Originalversion dieser Diplomarbeit ist an der TU Wien Bibliothek verfügbar.
The approved original version of this thesis is available in print at TU Wien Bibliothek.

Zusammenfassung

Intrazelluläre pH-Messung (pH_i) hat in den letzten Jahrzehnten eine steigende Bedeutung in Biotechnologie und Molekularbiologie erhalten. Die interne pH-Homöostase ist für alle zellulären Funktionen von wesentlicher Bedeutung und direkt mit der Membranintegrität und Funktionalität von Energieerzeugungsprozessen verbunden. Daher ist der interne pH-Wert im Verhältnis zum externen pH-Wert ein wichtiger Parameter zur Beurteilung des physiologischen Zustands von Bakterien. In dieser Masterarbeit wurde ein rekombinanter *Corynebacterium glutamicum* Stamm mit einem Plasmid kodierten pH-sensitiven grün fluoreszierende Protein pHluorin enthält, verwendet. Die Sensorexpression wurde durch Zugabe von IPTG induziert. Dieser Induktor aktiviert *tac*-promotor und ermöglicht die bedingte pHluorin Produktion. Die Ziele der Arbeit waren die folgende:

- Validierung der Produktion des pHluorin-Proteins und Überprüfung der Abhängigkeit der Sensorproduktion von der Biomassekonzentration
- Einstellung des Expressionsniveaus des Fluoreszenzsensors
- Untersuchung des Einflusses zusätzlicher Stressfaktoren auf die pHluorin Produktion
- Überwachung der Proteinproduktion und Korrelation des internen pH-Werts mit Prozessparametern und Vorhersage der Prozessleistung

Der nicht-invasive Sensor wurde kalibriert, indem er unter Zugabe membranstörender Chemikalien (Nigericin und CTAB) und mittels IPTG-Induktion bei verschiedenen extrazellulären pH-Werten exprimiert wurde. Die Kalibrierung erlaubt die Berechnung des intrazellulären pH-Wertes unter experimentellen Bedingungen. Durch die Kalibrationsversuche konnte gezeigt werden, dass der Sensor über einen weiten Konzentrationsbereich unabhängig von der Biomassekonzentration ist. Das bedeutet, dass während der Kultivierung des Bioreaktors keiner zusätzlichen Probenvorbereitung, wie Verdünnung, nötig ist. Als nächster Schritt wurden IPTG-Induktionsniveaus untersucht, um eine minimale Induktor Konzentration für ausreichende Sensorproduktion zu finden. Damit soll ein ausreichend starkes Fluoreszenzsignal und zudem eine minimierte metabolische Belastung des Stammes erzielt werden. Es wurde gezeigt, dass bereits niedrige IPTG-Konzentrationen genügen um ein adäquates Signal zu erhalten.

Corynebacterium glutamicum kann zur Produktion verschiedener Aminosäuren, etwa Glutamat und Lysin, verwendet werden, was diesem Bakterium industrielle Bedeutung verleiht. Glutamat wird unter Einwirkung äußerer Stressbedingungen hergestellt. In dieser Studie wurde mittels Tween 40 und Penicillin G untersucht, wie die Zellen auf induziertem Membranstress reagieren und wie sie die Produktion des pH-Fluorsensors beeinflussen.

Die physiologische Antwort der *C. glutamicum* Zellen während der Expression des fluoreszierenden pH Sensors wurde analysiert. Interne pH-Homöostase Messungen zeigten, dass eine Korrelation von pH_i mit anderen Prozessvariablen wie der spezifischen Substrataufnahmerate (q_s), Respirationsraten (q_{O2} und q_{CO2}) und ihre Beziehung zur Carbon Dioxide Evaluation Rate (CER) besteht. Auf Grundlage der Ergebnisse dieser Arbeit kann der genetisch kodierte Sensor nun zur Analyse und Überwachung unter Bioreaktorbedingungen verwendet werden.

Die approbierte gedruckte Originalversion dieser Diplomarbeit ist an der TU Wien Bibliothek verfügbar.
The approved original version of this thesis is available in print at TU Wien Bibliothek.

Abbreviations

ΔΨ – membrane potential
$\Delta\mu_{ion}$ – electrochemical potential
ΔpH – pH gradient
μ_{max} – maximum specific growth rate
P_i – inorganic phosphate
pH_i – intracellular pH
pCO2 – dissolved carbon dioxide concentration
pO2 – dissolved oxygen concentration
q_p – specific production rate
q_s – substrate uptake rate
q_{CO2} – specific carbon dioxide evolution rate
q_{O2} – specific oxygen uptake rate
ATP – adenosine triphosphate
ADP – adenosine diphosphate
CAC – citric acid cycle
CDW – cell dry weight
CER – carbon dioxide evolution rate
CTAB – cetyl trimethyl ammonium bromide
DO – dissolved oxygen
FCM – flow cytometry
FP – fluorescence protein
GFP – green fluorescent protein
IPTG – isopropyl β-D-1-thiogalactopyranoside
MLR – multiple linear regression
MOPS – 3-morpholino propane sulfonacid
NMR – nuclear magnetic resonance
OD – optical density
PBS – phosphate-buffered saline
PCA – principal component analysis
PenG – Penicillin G
PLS – partial least squares regression
PMF – proton motive force
RMSE – root mean squared error
TCA – tricarboxylic acid cycle
VIF – variance inflation factor

Die approbierte gedruckte Originalversion dieser Diplomarbeit ist an der TU Wien Bibliothek verfügbar.
The approved original version of this thesis is available in print at TU Wien Bibliothek.
TU Bibliothek Your knowledge hub WIEN

1 Introduction

Corynebacterium glutamicum is an aerobic, gram-positive bacterium that in order to survive has to manage with always changing environmental conditions (Follmann M, 2009). A crucial role in bacterial growth and survival plays the pH value, which is defined as the decimal logarithm of the reciprocal of the hydrogen ion activity, a_{H+}, in a solution. Even though bioreactor fermentation processes are generally carried out at a constant controlled pH of the culture media, internal pH can be expected to be widely different and variable during the fermentation process. The pH has a relevant impact on the solubility of nutrients and trace elements as well as on the whole cellular metabolism (Booth, 1985). The ability of an organism to maintain its internal pH (pH_i) at a constant level regardless of variations in external pH is termed pH homeostasis and is critical to the functionality and stability of the cellular enzymes. The internal pH of most bacteria is neutral to slightly alkaline (Booth, 1985). The range of pH-homeostasis of *C. glutamicum* of external pH is between 6 and 9, and the internal pH - 7 to 8.3 (Follmann M, 2009). This pH homeostasis is important for functionality of all cellular enzymes as well as their stability in all organisms (Orij R B. S., 2011). The pH gradient (ΔpH) determines the difference between extracellular pH and intracellular pH. The ΔpH across the membrane can be high at low pH values or can be reversed at high external pH values (Booth, 1985; Lund P, 2014). ΔpH represents the chemical constituent of the proton motive force (PMF) which is essential for generation of ATP by the F_1F_0-ATPase (Booth IR, 1983), thus pH homoeostasis is connected to the overall energetic status of the cell (Deamer DW, 1989). Effective pH-homeostasis was shown to be correlated with optimal growth of *C. glutamicum* (Follmann M, 2009) and substrate uptake rate, what was researched during this study.

In order to measure intracellular pH, several methods were established like measurement of in vivo 31P nuclear magnetic resonance (NMR) spectra (Gillies RJ, 1981), the fluorescence of specific chemical dyes (Chakraborty S, 2015), and analyses of the distribution of radioactively labelled weak organic acids (Kresnowati MTAP, 2007; Follmann M, 2009). The problem of these methods is that NMR and analyses of the distribution of organic acids are not easily accessible techniques and the fluorescence method is expensive, short-lived and requires a number of time-consuming manipulations (Chakraborty S, 2015). The alternative to these is the expression of the genes encoding fluorescent proteins such as the GFP-variant pHluorin (Miesenböck G, 1998; MJ, 2011; Shen Y, 2014; Arce-Rodríguez A, 2019) under the IPTG induction and the detection of the resulting fluorescence signals. It is an inexpensive and fast technique, enabling online measurements of pH_i in vivo in various microorganisms (Schuster, 2005; Orij R P. J., 2009; Morimoto Y V. C. Y.-S., 2010; Marešová, 2010; Valkonen M, 2013; Morimoto Y V. K.-i. N., 2016). The fast response of the non-invasive sensor to pH deviation (Martinez, 2012; Crauwels, 2018) enables fast detection of pH changes. The continuous expression of the protein allows for continuous analyses over long timescales. Therefore, adaptation of this method should be made to enable the usage of pHluorin fluorescence sensor as an at-line measurement parameter during bioreactor cultivation and to detect the correlation with other process variables.

Die approbierte gedruckte Originalversion dieser Diplomarbeit ist an der TU Wien Bibliothek verfügbar.
The approved original version of this thesis is available in print at TU Wien Bibliothek.
TU Bibliothek Your knowledge hub WIEN

2 Aims of the Study

The goal of this study was to calibrate the genetically encoded fluorescence sensor pHluorin in order to allow in situ monitoring of the intracellular pH and via the pH indirectly other critical process variables in a recombinant *Corynebacterium glutamicum* strain under bioreactor conditions.

First, the best calibration equation for intracellular pH evaluation needed to be determined. In order to obtain representative calibration equations, membrane disturbing chemical agents, which allow the proton concentration inside and outside the cell to equilibrate, like Nigericin and CTAB, were used and compared. Through statistical assessments the chemical which yields the more representative calibration equation was selected. The second task was to evaluate, which regression method/equation (linear, polynomial or Boltzmann sigmoidal curve) gives the best fit for the obtained dataset without overparameterizing. The third important question was to check if the fluorescence signal is dependent on the biomass concentration during cultivation process.

After successful identification of the most adequate calibration equation, the inducer (IPTG) concentration for the pHluorin fluorescence sensor needed to be tuned and optimized since the fluorescent signal strength needed to be sufficient while minimizing the metabolic load on the organism. Inducer tuning was initially tested in order to preselect an appropriate IPTG range using high-throughput screening methods in 96-well microplates with online optical density and fluorescence measurement. Once completed the selected concentrations were further analyzed in controlled bioreactor cultivations.

The second aspect of my goal was to investigate the response of the sensor to external stress conditions. This was simulated via the addition of chemicals like Tween 40 and Penicillin G, which are used for induction of glutamate production. For this investigation high-throughput screening in microtiter plates, shake flask cultivation, and bioreactor cultivations were conducted.

The final aspect of my master thesis was to determine if a correlation exists between pH gradient and process performance parameters, like substrate uptake rate (q_s), respiration rates (q_{o2} and q_{co2}) and the existence of an interrelationship with carbon dioxide evaluation rate (CER). These experiments were conducted in bioreactor cultivations during batch and fed-batch phases using substrate limitation, Penicillin G addition and pH shifts.

Die approbierte gedruckte Originalversion dieser Diplomarbeit ist an der TU Wien Bibliothek verfügbar.
The approved original version of this thesis is available in print at TU Wien Bibliothek.
TU Bibliothek Your knowledge hub WIEN

3 Theoretical background

3.1 *Corynebacterium glutamicum*

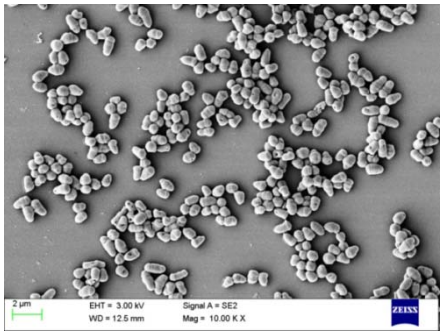

Figure 1: Scanning electron microscopy of *Corynebacteium glutamicum*. Scanning electron microscopy was performed in CeNSE, IISc, Bangalore. 2016-06-09. Author: Vader1941

Corynebacterium glutamicum is a non-pathogenic, aerobic, gram-positive bacterium (Figure 1) capable of growing on a variety of sugars or organic acids.

This strain represented the introduction of fermentation in the industrial production of L-amino acids, which was carried out by Kinoshita and colleagues of Kyowa Hakko (Tokyo, Japan) in 1957 (Kinoshita, 1957; Udaka, 1960). They reported a novel bacterium, *Corynebacterium glutamicum* (initially reported *as Micrococcus glutamicus*), with a unique ability to produce significant amounts of glutamate directly from cheap sugar and ammonia. Later advances in the amino acid industry are closely connected with the discovery of this microbe and subsequent development of production strains for various kinds of L-amino acids (Ikeda, 2003). In Figure 2 the history of fermentation of amino acids and strain development technology can be observed.

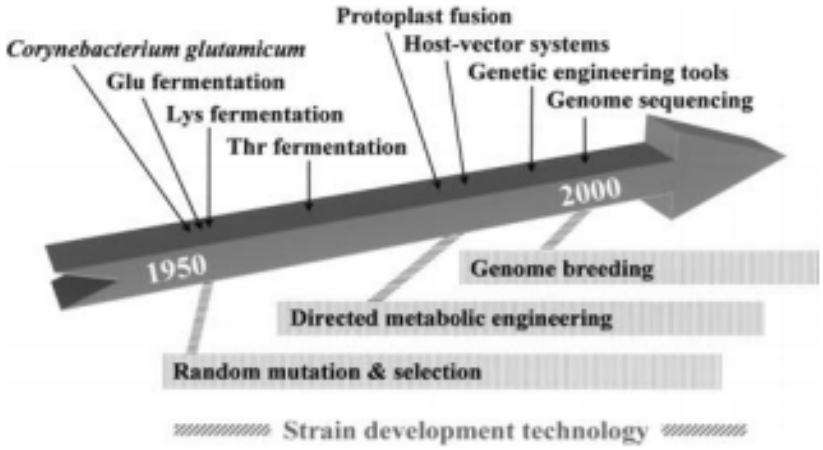

Figure 2: History of amino acid fermentation and strain development technology in *Corynebacterium glutamicum* (Ikeda, 2003).

Figure 2 shows the main topics of *Corynebacterium glutamicum* history and development. First development method was random mutation and selection, what generated a variety of mutants, such as auxotrophs, analog-resistant mutants, and transport mutants (Ikeda, 2003). These mutations allowed glutamate, lysine and threonine fermentations in industrial scale. In 1979, a procedure for protoplast fusion in this species was first reported by Kaneko and Sakaguchi (1979), which allowed genetic recombination in vivo (Karasawa M, 1986). Later, in the 1980s, host-vector system was developed (Katsumata R O. A., 1984). In the 1990s, directed metabolic engineering and genetic engineering tools of the bacteria were developed (Haynes JA, 1990; Schäfer A, 1990; Schwarzer A, 1991; Ikeda M, 1998; Rest ME van der, 1999) and are now being applied for enlargement of biosynthetic and transport capacity. At the same time with strain development, intensive biochemical and molecular analyses have advanced the knowledge of the molecular biology and physiology of *C.glutamicum* (Kinoshita S, 1978; Jetten MSM, 1995; Sekine H, 2001; Pfefferle W, 2003; Kimura, 2003). The fundamental information obtained has been the basis for further strain improvement.

Die approbierte gedruckte Originalversion dieser Diplomarbeit ist an der TU Wien Bibliothek verfügbar.
The approved original version of this thesis is available in print at TU Wien Bibliothek.

Corynebacterium glutamicum under optimal conditions is able to convert glucose into high yields of glutamic acid. Currently about 1×10^6 tons of glutamate are produced with this microorganism annually and used as a flavoring agent (Leuchtenberger, 1996). During the past 40 years, various mutants of *C. glutamicum* have been isolated with the capacity to produce significant amounts of different L-amino acids (Kalinowski, 2003). This strain is a potential platform organism for industrial biotechnology. *C. glutamicum* indicated the potential for anaerobic amino acid production by nitrate respiration (Takeno, 2007). The engineering *C. glutamicum* has ability for higher chain alcohol production like isobutanol and as byproducts 1-propanol, 2-methyl-1-butanol, 1-butanol, and 2-phenylethanol using the 2-keto acid pathways (Smith, 2010) as well as degradation and assimilation of aromatic compounds (Shen, 2012). It is concluded that *C. glutamicum* is a very useful model organism to disclose new knowledge of biochemistry, physiology, and genetics of the catabolism of aromatic compounds, and that the new physiological properties are potentially important for industrial applications of *C. glutamicum*.

3.2 Intracellular pH and pH homeostasis

The maintenance of internal pH in bacterial cells is challenged by natural stress conditions or in biotechnological production processes. Intracellular pH (pH_i) affects nearly all processes in a living cell. pHi directly influences the redox state of the cell by influencing the NAD^+/NADH equilibrium (Veine, 1998) and determines pH gradients necessary for transport over membranes (Goffeau, 1981; Wohlrab, 1982). Additionally, the effect of pH is very prominent in enzyme kinetics, as pH influences ionization states of acidic or basic amino acid side-chains and thereby influences the structure, solubility and activity of most enzymes (Orij R P. J., 2009).

Electron transport across the membrane requires multiple enzyme complexes embedded in the membrane (Figure 3). The two processes of membrane-bound electron transport and ATP synthesis are closely linked with each other. In general, neither of the two processes can take place without each other. In the full pathway, electrons are transferred from NADH via the electron transport chain to a terminal electron acceptor as which molecular oxygen (0_2) is served, which is later reduced to water. When electrons in the electron transport chain are transferred from one enzyme to the other, the energy or free enthalpy of the exergonic oxidation of NADH is gradually released by oxygen and used for the endergonic transfer of protons to a proton gradient from the cytoplasm into the membrane. This stores the released energy in a proton gradient over the membrane. The proton gradient drives the endergonic ATP synthesis catalyzed by ATP synthase, which eventually catalyzes the endergonic synthesis of ATP from ADP and P_i. This is driven by the proton gradient generated in the course of membrane-bound electron transport (H. Robert Horton, 2008). F_0F_1-ATPase/synthase catalyzes ATP synthesis/hydrolysis coupled with a transmembrane H^+ (proton)-translocation in bacteria (Boyer, 1997). The enzyme is composed of two portions (Figure 3), i.e. a water-soluble F_1, which has catalytic sites for ATP synthesis/hydrolysis, and a membrane-integrated F_0, which mediates proton translocation. The bacterial enzyme has the simplest subunit structure, $\alpha_3\beta_3\gamma_1\delta_1\varepsilon_1$ for F_1 and $a_1b_2c_{12}$ for F_0 (Suzuki, 2003). F_1 is reversibly detached from F_0 and is by itself a rotary motor driven by ATP hydrolysis (Berger, 1973) in which a central stalk made of γ and ε subunits rotates relative to the surrounding $\alpha_3\beta_3$ hexamer ring where hydrolysis occurs (Harold, 1969), (Evans, 1970). The remaining F_0 portion in the membrane acts as a proton channel that mediates passive proton translocation across the membrane (Klein, 1972).

Die approbierte gedruckte Originalversion dieser Diplomarbeit ist an der TU Wien Bibliothek verfügbar.
The approved original version of this thesis is available in print at TU Wien Bibliothek.

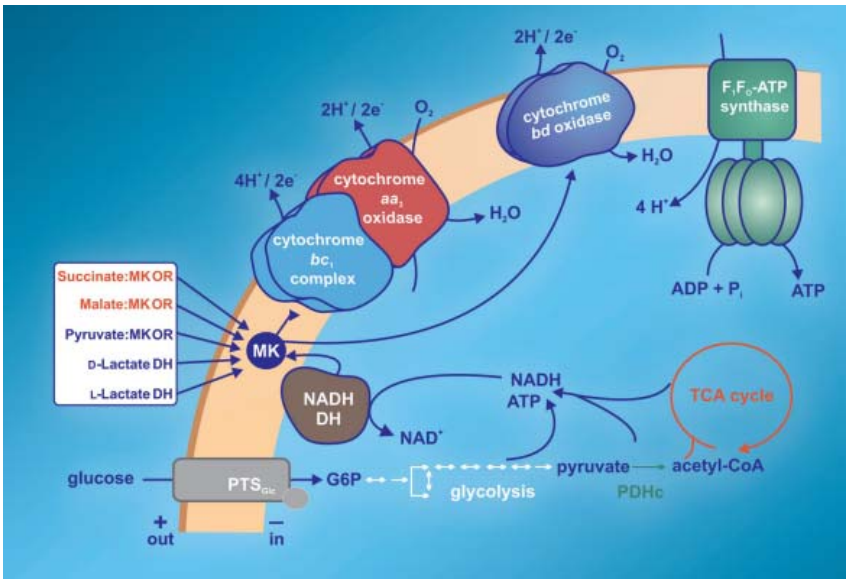

Figure 3: Overview of membrane-bound electron transport and ATP synthesis in *Corynebacterium glutamicum* (Koch-Koerfges, 2012). The energy released in the electron transport chain reactions is used to build up a proton concentration gradient across the membrane. For this purpose, protons are transported from the cytoplasm into the membrane, when electrons from reduced substrates flow through the complexes of the electron transport chain. At the time protons flow back into the cytoplasm through ATP synthase, the free enthalpy stored in the proton gradient is used for building ATP from ADP and P_i **(H. Robert Horton, 2008)**.

Studies on acidic pH response revealed the participation of multiple cellular processes in acclimatization of bacteria. Among them are the activation of the protein folding and stabilization machinery (Martin-Galiano AJ, 2005), the induction of iron uptake systems (Jakob K, 2007), or various metabolic adaptations (Roe AJ, 2002). Furthermore, observations were made indicating the occurrence of oxidative stress at low pH values (Fisher MA, 2002). A shift of the external pH seemed to act on various levels and affected a multiplicity of cellular processes finally limiting growth at non optimal pH conditions (Follmann, 2009).

At low external pH value the following adapting mechanisms are applied: the proton-impermeable cytoplasmic membrane and the buffering capacity of the cytoplasm (Booth, 1985). This buffer capacity is possible due to nucleic acids and the amino acid side chains of the proteins. Furthermore, in response to acid stress in bacterial cells, chaperone, DNA repair activity as well as proton export are increased in order to protect important cellular components (Cotter, 2003). At low external pH levels, potassium is essential for the growth of *C. glutamicum*, with the protein CglK being the main uptake system for potassium (Follmann M, 2009). The bacteria cannot maintain their internal pH at low external pH levels without potassium, but the exact mechanism of potassium-mediated acid tolerance is still unclear. Under neutral pH conditions, *C. glutamicum* has a low chemical proton gradient (ΔpH) across the membrane, which can be generated by proton motive force (PMF) (Ochrombel, 2011). By regulating the membrane potential (ΔΨ), *C. glutamicum* is able to produce the PMF that is essential for the generation of ATP via F_1F_0-ATPase (Boyer P. D., 1973).

pH homeostasis includes elevated levels of transporters and enzymes that promote proton capture and retention (e.g., the ATP synthase and monovalent cation/proton antiporters), metabolic changes that lead to increased acid production, and changes in the cell surface layers that contribute to cytoplasmic proton retention (Padan, 2005). The model of the pH homeostasis of *C. glutamicum* at low pH can be found in Figure 4.

Die approbierte gedruckte Originalversion dieser Diplomarbeit ist an der TU Wien Bibliothek verfügbar.
The approved original version of this thesis is available in print at TU Wien Bibliothek.

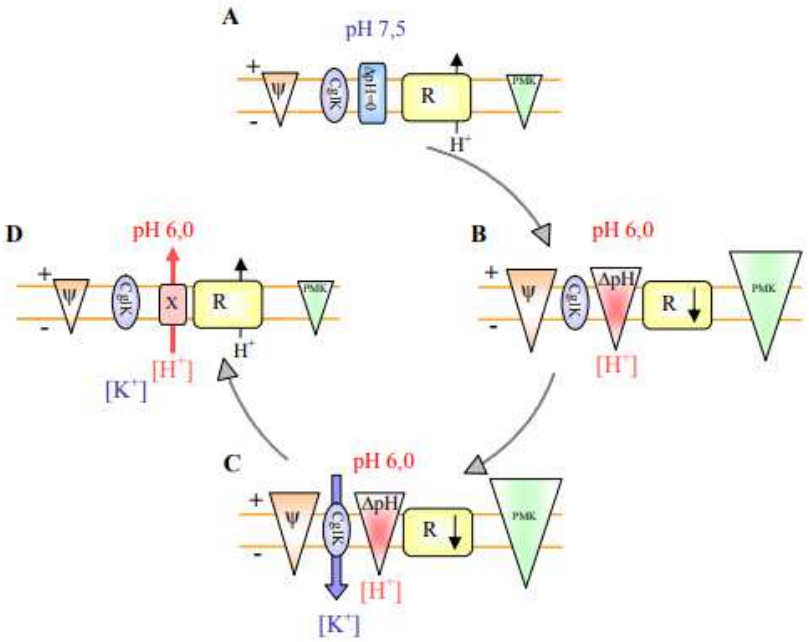

Figure 4: Model for the function of potassium in the pH homeostasis of *C.glutamicum.* Under neutral pH conditions at pH_{in} = pH_{ex} = 7.5, the proton motive force (PMK) is determined solely by the value of the membrane potential (Ψ), while the respiratory chain (R) is fully active ↑ **(A).** If the external pH drops to 6.0, a proton gradient (ΔpH) occurs across the membrane, which causes a higher PMK value. Due to the increased PMK, the respiratory chain (R) is only partially active ↓ and protons can enter the cell **(B)**. The influx of potassium ions by CglK into the cytoplasm leads to the lowering of membrane potential **(C)** due to the shift of positive charges. Thus, the PMK is also lowered, so that the respiratory chain is again fully active, and proton-exporting systems (X) can regulate the pH in the cell **(D) (Ochrombel, 2011)**.

From the Figure 4 can be seen that if the external pH decreases, the proton concentration in the medium increases, what results in development of the proton gradient across the membrane and therefore value of the PMF is being increased. This leads to a restriction of respiratory chain activity (Löffler G., 2007) (Figure 4, A-B). Increase of protons penetration through diffusion into the cytoplasm leads to the increase of the proton gradient, what influence further metabolic processes of the cell. When potassium ions flow into the cell through CglK protein, a shift in positive charges occurs, which is accompanied by a decrease in membrane potential and lowers the value of proton motive force (Figure 4, C). The restriction of respiratory chain activity is thus reversed, and it is again fully active. The increased proton-exporting system regulates the pH in the cytoplasm (Figure 4, D). The effect of potassium influx on respiratory chain activity under low pH conditions, and how potassium-mediated pH homeostasis works mechanistically, has not yet been clarified (Ochrombel, 2011).

3.3 IPTG Induction of pHluorin fluorescence sensor protein

Corynebacterium glutamicum carries pEKEx2_pHluorin plasmid, which holds *pHluorin* gene under control of *tac* promotor. This is a synthetically produced DNA promoter, produced from the combination of promoters from the *trp* and *lac* operons (De Boer, 1983). The *tac* promoter direct transcription approximately 10 times more efficiently than the derepressed parental *lac* promoter and approximately 3 times more efficiently than the *trp* promoter in the absence of the *trp* repressor (De Boer, 1983). The hybrid promoter can be repressed by the *lac* repressor and derepressed with isopropyl beta-D-thiogalactoside (IPTG) (De Boer, 1983). In contrast to the *trp* and the *lac* promoters, the *tac* promoter has not only a consensus -35 sequence but also a consensus Pribnow box sequence. This may explain the higher efficiency of this hybrid promoter with respect to either one of the parental promoters (De Boer, 1983). *Lac*-type promoter systems are the regulatory system from

Die approbierte gedruckte Originalversion dieser Diplomarbeit ist an der TU Wien Bibliothek verfügbar.
The approved original version of this thesis is available in print at TU Wien Bibliothek.
TU Bibliothek Your knowledge hub WIEN

the lac operon (Figure 5). This system contain the *lacI* gene, supplier of the *lac* repressor, which prevents transcription from the promoter itself by binding to the lac operator region situated next to the promoter. mRNA transcription starts when the repressor is removed from the operator by an inducer. The inducer used for induction of *tac* promoter system is IPTG. In opposition to lactose (also an inducer of these systems if altered by ß-galactosidase (Huber RE, 1976), what is not the case of *C.glutamicum*) IPTG is not a substrate for ß-galactosidase (the product of the *lacZ* gene) and is, therefore, not metabolized (Hansen, 1998). For efficient transcription from the promoter, the IPTG must enter the cells efficiently. This inducer is very expensive and may interfere with cell growth. Owing to the cost and possible toxic effect of IPTG, it would be advantageous to use less inducer to obtain the same level of transcription (Hansen, 1998). Therefore, during this study, different levels of IPTG induction were examined to find the lowest concentration, which need to be applied to receive sufficient protein production and therefore fluorescence signal intensity.

Table 1: Elements and their purpose in gene expression system under control of *lac* operon

Element	Purpose
lacI	Controls production of the repressor protein
Promoter	Binding site for RNA Polymerase
Operator	Binding site for repressor
Repressor	Gene encoding the lac repressor protein. Binds to DNA at the operator and blocks binding of RNA Polymerase at the promoter.

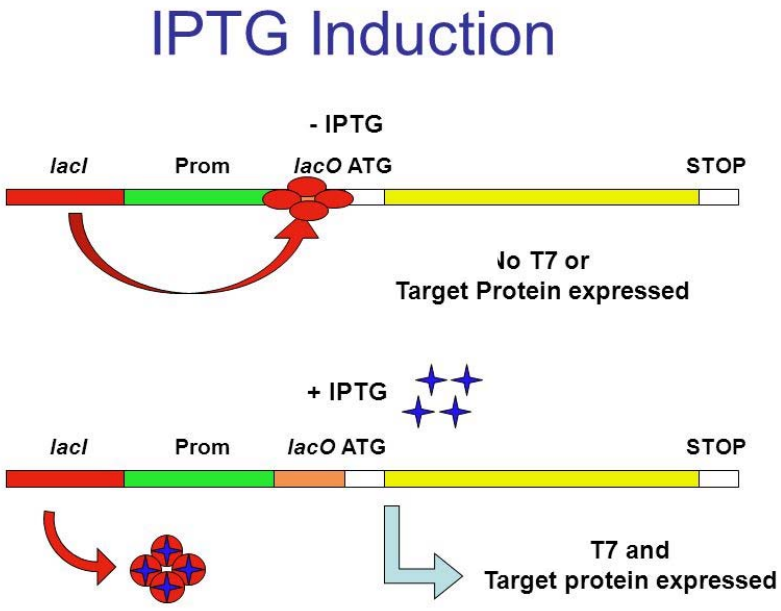

Figure 5: pHluorin gene expression under control of *lac* operon and induction with IPTG. The *tac* promotor has the same working principal as *lac* promotor. Figure above: without addition of IPTG the regulator gene is expressed and the repressor protein is synthesized with binding sites for inducer and the operator region. The repressor protein binds to the operator region, covering part of the promoter region where RNA polymerase attaches. RNA polymerase cannot bind to the promoter region so the target gene is not transcribed to mRNA and cannot be later translated into the protein. **Figure below:** after addition of IPTG, the inducer binds to the other site on the repressor protein, causing the repressor protein to change shape and dissociate from the operator region. The promoter region is now unblocked so RNA polymerase can bind to it and initiate transcription, and the target protein can be expressed **(Sweeney, 2014)**.

Die approbierte gedruckte Originalversion dieser Diplomarbeit ist an der TU Wien Bibliothek verfügbar.
The approved original version of this thesis is available in print at TU Wien Bibliothek.
TU Bibliothek Your knowledge hub WIEN

3.4 Genetically encoded pH-sensitive fluorescent sensors

The development of engineered fluorescent proteins (FPs) started with the discovery by Shimomura and colleagues of the green fluorescent protein (GFP), which causes the natural green bioluminescence of the Pacific Ocean jellyfish *Aequorea Victoria* (Shimomura O, 1962). However, the value of GFP was only fully realized some 30 years later when Chalfie and co-workers isolated GFP cDNA (Germond, 2016). Color variants exhibiting various emission spectra have been engineered by means of direct mutagenesis (Tsien, 1998; Nifosí R, 2007). Nowadays, FPs are extensively used in the fields of biochemistry, biotechnology, and cell and development biology (Germond, 2016). The genetically encoded (GE) sensors have been developed from FPs which enables visualization and quantification of various intracellular physiological events in living cells, tissues, and/or whole organisms. Genetically encoded sensors have also been developed to probe the variations of pH or changes in the chemical concentrations of specific ions (Germond, 2016).

Intracellular pH can be measured by flow cytometry in a generally complex procedure. Fluorescence properties (intensity, emission and excitation spectrum) of several probes vary depending on the hydrogen ion (H^+) concentration of their environment, because hydrogen ion binding changes the electronic structure of the probe (Haugland RP, 1996). Maximum response of the probe occurs for pH values near its pK_a with the sensitivity of around 0.1–0.2 pH units (Araniti, 2018). On the other hand, the genetically encoded fluorescent pH-sensitive sensors (GFP mutants) with a range of pK_a values, such as Cameleon (Miyawaki A, 1999), pHluorin (Miesenbock G, 1998) or pHusion (Gjetting SK, 2012) offer information about pH dynamics without dye loading or sample manipulation.

Cameleons are genetically-encoded fluorescent indicators for Ca^{2+} based on green fluorescent protein variants and calmodulin (CaM). As they can be targeted genetically, Cameleons offer the possibility for monitoring Ca^{2+} in whole organisms, tissues, organelles, and submicroscopic environments in which measurements were previously impossible (Miyawaki A, 1999).

The other non-invasive intracellular pH sensor is pHusion, which is especially designed for apoplastic pH measurements, and works as a ratiometric pH sensor (Gjetting SK, 2012). It was constitutively expressed in *Arabidopsis* and targeted for expression in either the cytosol or the apoplast including intracellular compartments. pHusion consists of the tandem concatenation of enhanced green fluorescent protein (EGFP) and monomeric red fluorescent protein (mRFP1).

Genetically encoded ratiometric fluorescent pH-sensitive sensor pHluorin was used during this study. This pH-sensitive mutant of green fluorescent protein was developed to measure absolute pH by structure-directed combinatorial mutagenesis (Anderson, 1988; Südhof, 1995). Ratiometric pH indicators were developed with dual excitation (D_{ex}) and dual emission mode (D_{em}), because the absolute pH value cannot be estimated from changes in the fluorescence, due to dependence of fluorescence intensity not only on the pH value, but also on other factors, including, the expression level of the gene and photobleaching (Germond, 2016). This genetically encoded sensor exhibit bimodal excitation and/or emission spectra with pH-dependent changes in excitation/emission and, consequently, they can be used to quantify the absolute pH value from the spectral properties (Germond, 2016). Ratiometric pHluorin contains the original mutation S202H plus E132D, S147E, N149L, N164I, K166Q, I167V, R168H and L220F (Miesenbock G, 1998), what causes the antiparallel reaction at excitation peaks of 396 nm and 474 nm. Upon a pH change, the excitation efficiency at 396 nm increases and the excitation intensity at 474 nm decreases when the pH is shifting from 6 to 8.3 (Figure 6). This means that the pH value can be estimated by calculating the ratio of the fluorescence intensities at excitation peaks of 396 nm and 474 nm, respectively.

Die approbierte gedruckte Originalversion dieser Diplomarbeit ist an der TU Wien Bibliothek verfügbar.
The approved original version of this thesis is available in print at TU Wien Bibliothek.

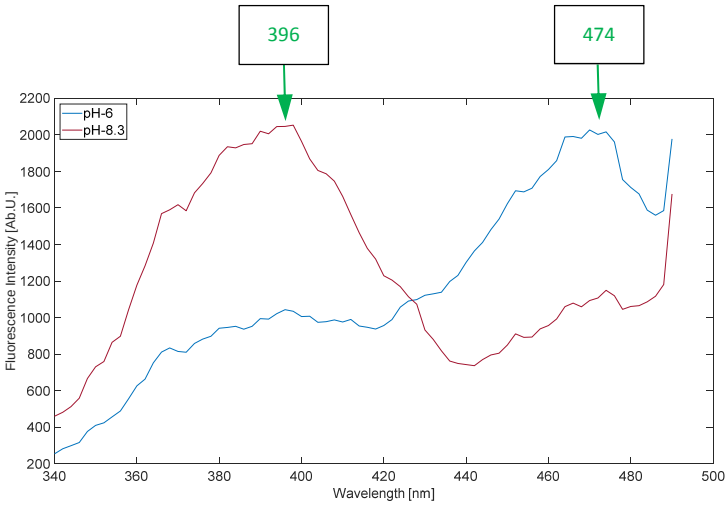

Figure 6: Fluorescence intensity signal [A] versus wavelength [nm] of expressed pHluorin sensor in *Corynebacterium glutamicum* with OD_{600} 1 at pH 6.0 and 8.3.

pH affects the equilibrium between protonated and deprotonated forms of these fluorescent proteins appearing as good pH sensors to detect changes in intracellular pH (Araniti, 2018).

3.5 Membrane stress inducers

In this study membrane stress inducers were used in the first order for building calibration equation for intracellular pH calculation. Therefore, two membrane disturbance chemicals were applied: cetyl trimethyl ammonium bromide (CTAB) and Nigericin, in order to equilibrate external and internal pH values.

Nigericin is a linear molecule with heterocyclic oxygen-containing rings together with a hydroxyl group. This molecule is mobile in its protonated non-complexed form, so that the ionophore can catalyze the overall electroneutral exchange of K^+ for H^+. Nigericin can abolish ΔpH across a membrane and the ionophore equalizes the K^+ and H^+ concentration gradients, with the final ion gradients depending on the experimental conditions (Nicholls, 2013). Thus, the intracellular pH can be "clamped" using high [K^+] buffers of known pH in combination with the K^+/H^+ ionophore Nigericin. This forces the pH of cells and individual organelles to equilibrate with the pH of the surrounding environment (i.e., the calibration buffer) (Galluzzi, 2017).

CTAB is a quaternary ammonium surfactant. It is used to dissolve cell membranes, which consist of hydrophilic and lipophilic end-groups, since they interact with both polar and nonpolar end-groups. (Azmat, et al., 2012). The positive charge of the CTAB molecule allows denaturing these molecules (Clarke, 2009). This results in permeable membrane for H^+, leading to an identical pH outside and inside of the cells.

The other stress inducers applied during this study were Penicillin G and Tween 40, which were used in order to induce extracellular glutamate production. Glutamate overproduction by *Corynebacterium glutamicum* is triggered by treatment with fatty acid ester surfactants such as polyoxyethylene sorbitan monopalmitate (Tween 40) (Takinami K, 1965) and β-lactam antibiotics such as penicillin (Nara T, 1964). Metabolic change at the branch point of 2-oxoglutarate in the tricarboxylic acid cycle (TCA) is important for glutamate production due to the reduced activity of the 2-oxoglutarate dehydrogenase complex (ODHC) (Kawahara Y, 1997; Shigu H, 1971) and is highly associated with changes in metabolic flow from the citric acid cycle (CAC), also known as the TCA cycle, to glutamate production (Shimizu H, 2003; Kim, 2010).

Die approbierte gedruckte Originalversion dieser Diplomarbeit ist an der TU Wien Bibliothek verfügbar.
The approved original version of this thesis is available in print at TU Wien Bibliothek.

Glutamate efflux represents the interplay of several components including exporter, cytoplasmic membrane, peptidoglycan and mycolic acid layer (Eggeling, 2001). Due to this interaction of a variety of cell wall components, the addition of penicillin leads to the accumulation of about one third as much glutamate in comparison to the use of i.e. biotin limitation (Kimura E. Y., 1999). However, there is no conclusive model that can explain glutamate excretion and the variety of induction conditions at the molecular level. All biochemical data on the mechanism of translocation of L-glutamate indicates excretion via an active, specific L-glutamate export system, since the translocation is amino acid specific and independent from membrane potential, this can be possible with the help of a chemical concentration gradient, and correlated with the energy balance of the cells (Gutmann, 1992; Hoischen, 1990).

3.6 Statistical methods for pHlourin calibration

During this work statistical methods were applied for generation of calibration models for pH estimation based on pHluorin spectra. Regression analysis is a form of predictive modelling technique which investigates the relationship between a dependent and independent variable (Pant, 2019). Therefore, first, polynomic regression was tested in order to find the best fit for pHluorin calibration. Afterwards, linear function with later multiple linear regression (MLR) model were evaluated. Boltzmann sigmoidal fit, according to Zhou, 2014, was also applied to the dataset to calculate calibration equation.

Linear regression is a basic and commonly used type of predictive analysis which usually works on continuous data (Pant, 2019). A simple linear regression makes predictions about one variable based on the information that is known about another variable. Linear regression can only be used when one has two continuous variables — an independent variable and a dependent variable. The independent variable is the parameter that is used to calculate the dependent variable or outcome (Kenton, 2019). It is a linear approach to modeling the relationship between a dependent variable and one independent variable. Simple linear regression equation (Equation 1) is presented below:

Equation 1

$$\boldsymbol{Y_i = ß_o + ß_1 * x_i + \varepsilon}$$

Here, the Y_i is a dependent variable, the β_1 is the parameter - population slope coefficient (also called weight), β_o is the population y-intercept, x_i is independent variable and ε_i is the random error term whose role is to add bias. The Equation 1 is the linear equation that needs to be obtained with the minimum error (Pant, 2019).

For more than one independent variable, the process is called Multiple Linear Regression (MLR) (Freedman, 2009). MLR is a statistical technique that uses several explanatory variables to predict the outcome of a response variable. The goal of multiple linear regression is to model the linear relationship between the explanatory (independent) variables and response (dependent) variable (Kenton, 2019). The formula for MLR is presented below in Equation 2:

Equation 2

$$\boldsymbol{Y_i = ß_o + ß_1 * x_{i1} + ß_2 * x_{i2} + \cdots + ß_p * x_{ip} + \varepsilon}$$

where, for *i*=*n* observations:
$\mathbf{Y_i}$ = dependent variable
$\mathbf{x_i}$ = explanatory variables
$\mathbf{ß_0}$ = y-intercept (constant term)

Die approbierte gedruckte Originalversion dieser Diplomarbeit ist an der TU Wien Bibliothek verfügbar.
The approved original version of this thesis is available in print at TU Wien Bibliothek.
TU Bibliothek Your knowledge hub WIEN

ß$_p$ = slope coefficients for each explanatory variable
ε = the model's error term (also known as the residuals)

The multiple regression model is based on the following assumptions (Lohninger, 2019):

- The correlation between y and x_i is linear in the parameters
- The error terms ε are normally distributed with a mean of 0
- The variance of the error terms does not depend on x (homoscedastic)
- The error terms are independent from one another (no autocorrelation)
- The predictors x_i are predetermined and are not random variables
- The values of the predictors x_{ij} have no errors
- The predictors are linearly independent from one another

The coefficient of determination (**R-squared**) is a statistical metric that is used to measure how much of the variation in outcome can be explained by the variation in the independent variables. R^2 always increases as more predictors are added to the MLR model even though the predictors may not be related to the outcome variable. R^2 can only be between 0 and 1, where 0 indicates that the outcome cannot be predicted by any of the independent variables and 1 indicates that the outcome can be predicted without error from the independent variables (Kenton, 2019).

Table 2: Advantages and disadvantages/problems of MLR (Lohninger, 2019)

Advantages	Disadvantages
- A simple method, easy to understand	- Correlated descriptors result in imprecise regression coefficients
- Fast calculation	- Prerequisites for a correct application of MLR are often not fully met in practical settings
- Mature mathematical method	

Polynomial regression is a form of regression analysis in which the relationship between the independent variable x and the dependent variable Y is modelled as an n^{th} degree polynomial in x. Polynomial regression fits a nonlinear relationship between the value of x and the corresponding conditional mean of Y. The general equation of a polynomial regression is shown below:

Equation 3

$$Y_i = ß_o + ß_1 * x + ß_2 * x^2 + \cdots + ß_n * x^n + \varepsilon$$

where:
Y_i = predicted outcome value for the polynomial model
x_i = explanatory variables
ß$_0$ = y-intercept (constant term)
ß$_m$ = regression coefficients for each n degree
ε = residual error

General principles of polynomial regression (statsdirect.com):

- Fitted model is more reliable when it is built on large numbers of observations.
- No extrapolation beyond the limits of observed values.
- Values for the predictor (x) should not be too large as they will cause overflow with higher degree polynomials.

Die approbierte gedruckte Originalversion dieser Diplomarbeit ist an der TU Wien Bibliothek verfügbar.
The approved original version of this thesis is available in print at TU Wien Bibliothek.
TU Bibliothek Your knowledge hub WIEN

Table 3: Advantages and disadvantages of polynomial regression (Pant, 2019)

Advantages	Disadvantages
- provides the best approximation of the relationship between the dependent and independent variable	- overfitting, due to high parameter errors
- a broad range of function, which can be fitted	- the presence of one or two outliers in the data can seriously affect the results of the nonlinear analysis
- can fit a wide range of curvature	- there are fewer model validation tools for the detection of outliers in nonlinear regression than there are for linear regression

Boltzmann sigmoid function is a mathematical function having a characteristic "S"-shaped curve or sigmoid curve. It is often used to describe the various physical and chemical transitions and belong within the scope of the so-called “transition function” (Zhou, 2014). The mathematical expression of Boltzmann Sigmoid is as follows (Equation 4):

Equation 4

$$y(t) = A + \frac{B}{1+exp(-(t-C)/D)} \qquad \text{(Zhou, 2014)}$$

where *t* is the external perturbation variable. A typical Boltzmann Sigmoid curve is shown in Figure 7. *A* is the lower limit of the Boltzmann Sigmoid curve and *A + B* represents the upper limit. *C* corresponds with the abscissa value of the half-intensity (vertical axis) of the curve and is usually called the center. *D* represents the intensity change rate of the curve. As shown in Figure 7, the slope of the tangent is proportional to *1/D* (Zhou, 2014).

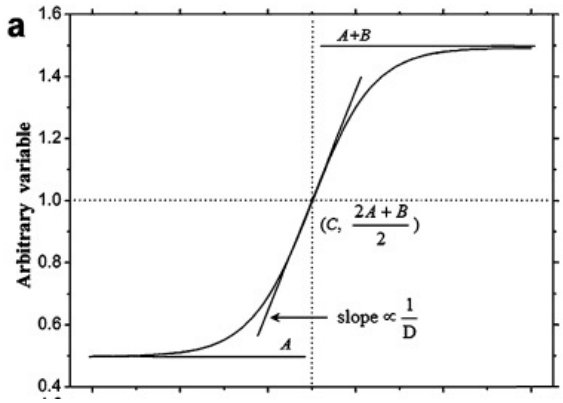

Figure 7: “S” shape curve of Boltzmann sigmoid function (Zhou, 2014).

A sigmoid function is a bounded differentiable, real function, that is defined for all real input values and that has a positive derivative everywhere. It shows a sufficient degree of smoothness and is also a suitable extension of the soft limiting nonlinearities (Han, 1995). Advantages and disadvantages are presented in Table 4.

Die approbierte gedruckte Originalversion dieser Diplomarbeit ist an der TU Wien Bibliothek verfügbar.
The approved original version of this thesis is available in print at TU Wien Bibliothek.

Table 4: Advantages and disadvantages of Boltzmann sigmoidal fit

Advantages	Disadvantages
- Nonlinear relationship can be evaluated - Parameters can be representative of physiology - Maximum value cannot be exceed	- Potential for overparameterization - Not all parameters can be identified

Die approbierte gedruckte Originalversion dieser Diplomarbeit ist an der TU Wien Bibliothek verfügbar.
The approved original version of this thesis is available in print at TU Wien Bibliothek.

4 Materials and Methods

4.1 Materials

4.1.1 Bacterial strain and plasmid

In this study was used modified strain of *Corynebacterium glutamicum*, which was provided by University of Ulm and Technical University of Denmark. The background wild type strain number was ATCC13032, which was modified by addition of pEKEx2_*pHluorin* plasmid. Recombinant strain holds kanamycin resistance (*Kan*R), *tac* promotor (P*tac*), *lac* repressor (*lacI*q) and *pHluorin* gene under control of *tac* promotor. Expression of the *pHluorin* gene was induced with IPTG at different concentrations as an inducer molecule.

4.1.2 Chemicals

Used media and solutions are listed alphabetically.

2 TY medium

Table 5: 2TY medium components

Chemical	Concentration	Company	Article number
Tryptone (Ingredient) for microbiology	16 g/L	AppliChem, Germany	103682.121
Yeast extract	10 g/L	Carl Roth, Germany	2363.5
Sodium chloride	5 g/L	Carl Roth, Germany	3957.2
For 2TY agar plates			
Agar, Bacteriological European Type (Ingredient) for microbiology	18 g/L	AppliChem, Germany	402302.121

The components were dissolved in Milli Q water and autoclaved. For the strain cultivation 50 µg/mL kanamycin sulfate was added to the medium after cooling.

Acid and base

Table 6: Acid and base components

Chemical	Concentration	Company	Article number
Acid			
Ammonia solution 25 %	13.3 M	Carl Roth, Germany	5460.2
Base			
Phosphoric acid 85 %	14.6 M	Carl Roth, Germany	9079.3

Acid and base were diluted with Mili Q water and used for bioreactor cultivation.

Die approbierte gedruckte Originalversion dieser Diplomarbeit ist an der TU Wien Bibliothek verfügbar.
The approved original version of this thesis is available in print at TU Wien Bibliothek.

CGXII medium:

Table 7: CGXII medium components

Chemical	Concentration	Company	Article number
Dipotassium hydrogen phosphate	1 g/L	Carl Roth, Germany	P749.3
Potassium dihydrogen phosphate	1 g/L	Carl Roth, Germany	3904.3
Ammonium sulfate	10 g/L	Carl Roth, Germany	9218.2
Urea	5 g/L	Carl Roth, Germany	6979.4
MOPS	21 g/L	Carl Roth, Germany	X999.3
pH was adjusted to 7 with 5M KOH			
Autoclaving → filter sterilized solutions added (0.22 µm):			
Magnesium sulfate heptahydrate	0.25 g/L	Carl Roth, Germany	8283.3
Calcium chloride dihydrate	0.01 g/L	Carl Roth, Germany	5239.3
Biotin	0.2 mg/L	Carl Roth, Germany	3822.3
Trace element solution (1000x)	1 mL/L	specified below	

All the components were dissolved in Mili Q water. When CGXII medium was used for batch and fed-batch cultivations with pH control, urea and MOPS were not added.

Additionally, 50 µg/L kanamycin and filter sterilized (0.2 µm) glucose solution (concentrations are specified separately for each experiment in the following sections) were added to the medium. Also, IPTG solution was used for induction of the plasmid encoded gene expression (concentrations are specified in the sections below).

In bioreactor cultivations, polypropylene glycol 2000 was added as antifoam to the medium with a concentration of 0.5 mL/L.

Table 8: Carbon source and antifoam

Chemical	Concentration	Company	Article number
D(+) glucose monohydrate	350 g/L	Carl Roth, Germany	6887.5
Polypropylene glycol 2000	0.5 mL/L	Sigma Aldrich, Spain	81380

CTAB solution

Table 9: CTAB solution

Chemical	Concentration	Company	Article number
Cetyltrimethylammoniumbromide	0.05 g/L	Carl Roth, Germany	9161.1
Ethanol	-	Carl Roth, Germany	P076.1

CTAB was dissolved in ethanol and, afterwards, was sterile filtered (0.22 µm).

IPTG solution (1000x)

Table 10: IPTG solution

Chemical	Concentration	Company	Article number
IPTG	1 mol/L	Carl Roth, Germany	2316.4

IPTG was dissolved in Mili Q water and was sterile filtered (0.22 µm).

Die approbierte gedruckte Originalversion dieser Diplomarbeit ist an der TU Wien Bibliothek verfügbar.
The approved original version of this thesis is available in print at TU Wien Bibliothek.
TU Bibliothek Your knowledge hub WIEN

Kanamycin solution (1000x)

Table 11: Antibiotic component

Chemical	Concentration	Company	Article number
Kanamycin sulfate	50 mg/mL	Carl Roth, Germany	T832.2

Kanamycin sulfate was dissolved in Mili Q water and was sterile filtered (0.22 µm).

Nigericin solution

Table 12: Nigericin solution

Chemical	Concentration	Company	Article number
Nigericin	10 µM	Sigma Aldrich, Israel	N7143

Nigericin was dissolved in ethanol and sterile filtered through 0.22 µm filter.

Penicillin G solution

Table 13: Penicillin solution

Chemical	Concentration	Company	Article number
Penicillin G sodium salt	750 U/L	Sigma-Aldrich, China	P3032-100MU

Penicillin G was dissolved in Mili Q water and sterile filtered through 0.22 µm filter.

pH buffer

Table 14: stock solution of pH buffers

Chemical	Concentration	Company	Article number
Dipotassium hydrogen phosphate	0.5 M	Carl Roth, Germany	P749.3
Potassium dihydrogen phosphate	0.5 M	Carl Roth, Germany	3904.3

Both of the components were dissolved in the Mili Q water separately and sterilized by autoclaving. Detailed description of volumes taken for buffer (with different pH values) preparation are described in attachment Table 35.

PBS buffer:

Table 15: PBS buffer components

Chemical	Concentration	Company	Article number
Disodium hydrogen phosphate dehydrate	1.8 g/L	Carl Roth, Germany	T877.1
Potassium chloride	0.2 g/L	Carl Roth, Germany	HN02.3
Potassium dihydrogen phosphate	0.24 g/L	Carl Roth, Germany	3904.3
Sodium chloride	8 g/L	Carl Roth, Germany	3957.2

All the components were dissolved in Mili Q water and sterilized by autoclaving.

Die approbierte gedruckte Originalversion dieser Diplomarbeit ist an der TU Wien Bibliothek verfügbar.
The approved original version of this thesis is available in print at TU Wien Bibliothek.
TU Bibliothek Your knowledge hub WIEN

Trace element solution (1000x):

Table 16: Trace element solution components

Chemical	Concentration	Company	Article number
Iron(II) sulfate heptahydrate	16.4 mg/L	Carl Roth, Germany	P015.2
Manganese sulfate monohydrate	10 mg/L	Carl Roth, Germany	7347.1
Copper(II) sulfate pentahydrate	0.2 mg/L	Carl Roth, Germany	8175.1
Zinc sulfate heptahydrate	1 mg/L	Carl Roth, Germany	T884.1
Nickel(II) chloride hexahydrate	0.02 mg/L	De Haën, Germany	31462

All the components were dissolved in Mili Q water, pH was adjusted to 1 by addition of 32% (v/v) hydrochloric acid and the solution was sterile filtered (0.22 µm).

Table 17: pH adjustment chemical

Chemical	Concentration	Company	Article number
Hydrochloric acid 32%	16.4 mg/L	Carl Roth, Germany	X896.1

Tween 40 solution

Table 18: Tween 40 specifications

Chemical	Concentration	Company	Article number
Tween 40	2 g/L	Carl Roth, Germany	8240

Tween 40 was sterilized by autoclaving.

4.1.3 Equipment

See attachment - Table 34: Equipment list.

4.2 Cultivation methods

4.2.1 Strain maintenance and pre-culture preparation

Strain *Corynebacterium glutamicum,* carrying pEKEx2_*pHluorin* plasmid was stored as cryopreserved stock in -80°C freezer. Cultures were plated out on a 2TY agar plate with 50 µg/mL kanamycin as antibiotic source and incubated for approximately 24 hours at 30 °C in the incubator. Afterwards, single colony was transferred to 5 mL 2TY medium and incubated in rotary shaker at 30°C and 250 rpm. After 10 hours of incubation, the culture was transferred into 50 mL of CGXII medium with 50 µg/mL kanamycin and 0.5 mM IPTG (if not specified) with glucose as carbon source. The substrate concentration varied according to the specified experiment. For bioreactor cultivation, 150 mL of CGXII medium with 10 g/L glucose was used. The culture on the CGXII medium was incubated for 12-14 hours at 30°C and 250 rpm and, afterwards, transferred to 50 mL falcon tubes for washing of the cells. The tubes were centrifuged with the speed of 3240 g for 10 minutes at 4°C. The supernatant was discarded and the pellet resuspended in fresh CGXII medium without addition of antibiotics and IPTG. The resuspended culture was used afterwards as inoculum for further cultivations.

4.2.2 Microtiter plate cultivation

High-throughput screening was made in µClear® 96 Well Cell Culture Microplate in biological triplicates. The plate had black wall color with transparent bottom film for optical density measurement. The cultivation was made in Tecan Infinite 200, where the fluorescence was measured at excitation wavelength rates 394 nm, 396 nm, 398 nm, 400 nm, 468 nm, 470 nm, 472 nm, 474 nm,

Die approbierte gedruckte Originalversion dieser Diplomarbeit ist an der TU Wien Bibliothek verfügbar.
The approved original version of this thesis is available in print at TU Wien Bibliothek.
TU Bibliothek Your knowledge hub WIEN

476 nm (where two peaks could be observed) and emission wavelength 520 nm, at the gain 80. Absorption measurement was conducted at 600 nm. Each measurement was repeated every 20.1 min, after short shaking (duration: 10 s, mode: orbital, amplitude: 3 mm, frequency: 44.3 rpm) and 20 min incubation at 30°C in-between, which were programmed and automated in Tecan. The whole cultivation took approximately 25 hours.

In this experiment, tuning of inducer as well as sensor response on the stress conditions was tested. Therefore, different parameters were applied.

First set: complete induction with IPTG. Therefore, in the pre-culture (with 5 g/L glucose) 0.5 mM IPTG was added. As main culture, 100 µL of the resuspended pre-culture was mixed with 100 µL CGXII medium, containing 3 g/L glucose and 50 µg/mL kanamycin and different amounts of IPTG. IPTG concentrations applied were in the range from 0 µM to 10 mM.

Second set: the pre-culture was not induced, whereas main culture was induced with IPTG. In this case, pre-culture components were the same as in the first experimental set except of the presence of IPTG. Main culture as well as IPTG concentrations were the same as described above.

Third set: stress response. This experiment was conducted with the same pre-culture parameters as the first set. In the main culture defined concentration of 1 mM IPTG was added to each sample. As additional cell stress, Penicillin G at different concentrations was used. The following concentrations of Penicillin G were applied: 150 U/L, 300 U/L, 500 U/L, 750 U/L and 1150 U/L.

4.2.3 Shake flask cultivation

Shake flask cultivation was made to investigate pHluorin fluorescence sensor response under stress and non-stress conditions in batch cultivation. For this, pre-culture with 5 g/L glucose was followed by main culture, which consisted of 100 mL CGXII medium, 50 µg/mL kanamycin, 1 mM IPTG and 7 g/L glucose. The main culture was inoculated to an optical density (OD_{600}) of 0.5 and cultivated on a rotary shaker at 30°C and 250 rpm for 25 hour. The sample was taken every 2 hour (accept of the night time) with a volume of 3 mL.

Table 19: Shake flask experiment description

Condition 1	Condition 2	Condition 3
Tween 40 (2 g/L)	Control	Penicillin G (750 U/L)

Each experiment was made in biological duplicates. As stress conditions, Tween 40 and Penicillin G were chosen. The induction with these chemicals was performed after four hours of cultivation.

4.2.4 Cultivation in bioreactor

Cultivation in bioreactor was carried out in order to tune the pHluorin inducer as well as to analyze the correlation of pH gradient with other process parameters.

The resuspended culture, as described in 4.2.1, was inoculated to batch medium to an OD of 1. After the glucose was consumed, the batch phase was over and the fed-batch was started with the exponential feed, which contained CGXII medium, 350 g/L glucose and had open-loop controlled µ of 0.06 1/h.

Tuning of the IPTG inducer was made in DasGip bioreactor system. The four reactors have a working volume of 1.5 L. Agitation rate during the experiments was from 400 rpm to 1200 rpm, aeration – 0.7 vvm with oxygen supplementation, where 21% was air and up to 40% oxygen was provided. pO_2

Die approbierte gedruckte Originalversion dieser Diplomarbeit ist an der TU Wien Bibliothek verfügbar.
The approved original version of this thesis is available in print at TU Wien Bibliothek.

signal was controlled, using stirrer speed and oxygen supplementation. Substrate uptake rate was held constant with open-loop control.

During the whole cultivation the process parameters were controlled at following set points: pH at 7, temperature at 30°C and 30% of dissolved oxygen.

Table 20: Tuning of inducer. Concentrations of IPTG used during bioreactor cultivation.

N° bioreactor	1	2	3	4	5
Pre-culture: IPTG concentrations	Not induced	Not induced	200 µM	200 µM	500 µM
Main culture: IPTG concentrations	Not induced	20 µM	20 µM	200 µM	1000 µM

For examination of correlation of pH gradient with other process parameters, two DasGip bioreactors and two Labfors 5 bioreactors with a volume of 3.5 L and double 6-blade disc stirrer were used. Along with offline analytics (described in 4.3), online signals were recorded, i.e. pH and pO_2 in the medium, the amount of vessel and feed volume by the use of balances. In case of 3.5-L -Labfors bioreactor systems, online devices were connected and data recorded by use of the process information management system Lucullus (Applikon Biotechnology, USA). The inoculation procedure as well as process parameter features were the same as described above. More detailed description of each experiment can be found in Table 21.

Table 21: Batch and fed-batch cultivations conducted in DasGip bioreactor system.

N° bioreactor	6	7
Pre-culture: IPTG concentrations	500 µM	500 µM
Main culture: IPTG concentrations	1000 µM	1000 µM
Deflection	- Carbon source starvation - External pH change	- External pH change

Deflection of both bioreactors was applied in fed-batch phase. For reactor 6 – carbon starvation was made after 27 h of cultivation for 6 hours and pH change (from 7 to 6 and back to 7) – after 49 h of cultivation for 11 hours. Reactor 7 had only one deflection, namely pH change from 6 to 7 and back to 7, for 9 hours after 17 h of cultivation. More detailed description of the experiments conducted can be found in 5.4.

Cultivations, described in Table 22 were made only in batch phase. Reactor 8 and 9 underwent deflection in batch phase. Reactor 8 had a pH change from 7 to 6 after 7.2 hours of cultivation and back to 7 after 15 hours of cultivation. Reactor 9 had a Penicillin G addition as a stress condition after 10 hours of cultivation.

Die approbierte gedruckte Originalversion dieser Diplomarbeit ist an der TU Wien Bibliothek verfügbar.
The approved original version of this thesis is available in print at TU Wien Bibliothek.

Table 22: Batch cultivations conducted in 3.5-L-Labfors reactor.

N° bioreactor	8	9
Pre-culture: IPTG concentrations	200 µM	200 µM
Main culture: IPTG concentrations	20 µM	20 µM
Deflection	- External pH shift	- Stress condition using Penicillin G

Samples were taken for analytics according to 4.3.1, 4.3.2, 4.3.3 and 4.3.4.

4.3 Analytical methods

4.3.1 Dry cell weight determination

Dry cell weight was determined in triplicates in order to analyze biomass formation. Therefore, 1.8 mL of the sample, taken directly from the bioreactor, were transferred to a pre-dried and pre-weighted 2-mL-tube and centrifuged at 11180 g for 10 minutes at 4 °C. Afterwards, part of the supernatant was collected for other analyses (see 4.3.3 and 4.3.4) and the rest was discarded. The pellet was washed with 1.8 mL PBS buffer and centrifuged again, using the same parameters. Later, the supernatant was discarded and the pellet was dried in a drying cupboard at 110 °C for at least 72 hours. Quantification of the dried cell mass was made with the usage of analytical balance and therefore concentration of the biomass could be calculated.

4.3.2 Optical density measurement

Optical density was measured to determine biomass formation. In this case, the sample, taken directly from the bioreactor, was analyzed in photometer at 600 nm. As background PBS buffer was used. The linear range of the photometer is from OD_{600} 0.2 to 0.8. Therefore, if OD value measured exceeded this range, the dilution with PBS buffer was conducted. Each measurement was made in triplicates.

4.3.3 Substrate and metabolite analytics

The determination of glucose, glutamate, lactate and ammonium concentrations were made via enzymatic photometric assay with the use of Cedex Bio HT Analyzer. Therefore, glucose was determined using hexokinase, glutamate – glutamate oxidase, lactate with the use of lactate oxidase and NH_3 using glutamate dehydrogenase. For this, the 400 µL of the supernatant after the first centrifugation, as described in 4.3.1, was taken and placed in the analyzer.

4.3.4 Fluorescence analysis of pHluorin

Fluorescence analysis of pHluorin protein was carried out in order to calculate intracellular pH. The fluorescence measurement was made in black 96-Well microplate at excitation wavelength range 340 – 490 nm with 2 nm step size and emission wavelength 520 nm with the gain 80, top reading mode, number of reads – 25, 0 µs settle time, 20 µs integration time and 0 µs lag time, at 30°C. Z-position was at 20000 µm.

200 µL of the sample was taken during cultivation and measured directly. During bioreactor cultivation, 200 µL of supernatant after the first centrifugation, as described in 4.3.1, was measured to check the abundance of the sensor in the surrounding culture medium.

Intracellular pH of each sample was calculated with the help of calibration equation, which is described in 4.3.5.

Die approbierte gedruckte Originalversion dieser Diplomarbeit ist an der TU Wien Bibliothek verfügbar.
The approved original version of this thesis is available in print at TU Wien Bibliothek.
TU Bibliothek Your knowledge hub WIEN

For the measurement of extracellular signal, samples were centrifuged at 11180 g for 10 minutes at 4 °C. The supernatant was detected in Tecan, using the same parameters described above.

4.3.5 pHluorin sensor calibration

In order to calculate intracellular pH, calibration of the pHluorin sensor in the black 96 well microplate and µClear® 96 well cell culture microplate was carried out. For this, buffer solutions at different pH values were prepared. Buffer components used were potassium dihydrogen phosphate and dipotassium hydrogen phosphate. They were mixed at different concentrations according to the Table 35 in attachment. The amount mixed was calculated using the following formula:

Equation 5

$$pH = pK + \log\left(\frac{proton\ acceptor}{proton\ donor}\right)$$

Calibration (black 96 well microplate and µClear® 96 well cell culture microplate): pre-culture composition was as described in 4.2.1 with 10 g/L glucose; main culture contained 100 mL CGXII medium, 30 g/L glucose, 50 µg/mL kanamycin, 1 mM IPTG and resuspended pre-culture with adjusted OD of 1. Cultivation took approximately 4 hours. Afterwards, 500 µL of the culture were centrifuged at 3240 g for 10 minutes at 4°C, supernatant was discarded and the pellet was resuspended in 2 mL of the corresponding buffer. To each solution, either 20 µL Nigericin or 20 µL CTAB was added and incubated in dark for 6 min or 1 hour respectively. This was followed by fluorescence measurement with above described parameters (section 4.3.4). Calibration experiments were made in triplicates.

Calibration at different optical densities (black 96 well microplate): pre-culture composition was as described in 4.2.1 with 5 g/L glucose; main culture contained 100 mL CGXII medium, 15 g/L glucose, 50 µg/mL kanamycin, 1 mM IPTG and resuspended pre-culture with adjusted OD of 1. Main culture cultivation took approximately 12 hours. Afterwards, the whole volume was centrifuged at the same parameters as described above, supernatant was discarded and pellet was resuspended in CGXII medium. OD_{600} was adjusted to 1, 10, 25 and 50, centrifuged again and, eventually, pellet was resuspended in the correspondent pH buffer with addition of either Nigericin or CTAB. In this case, new pH buffer solutions (see Table 36 in attachment) were prepared in order to expand pH range of calibration. To confirm the stability of the pH value in the buffer after addition of the cells and chemicals for cell disturbance, pH values were measured again. They can be also found in attachment in Table 36. For further calculation, the pH values measured after calibration procedure were taken.

Calculation of intracellular pH: first, fluorescence ratio was calculated out of two maxima peaks - **396/474** (Figure 8) (Miesenböck G, 1998). Then, it was plotted against pH values and calibration equation was derived with the help of either linear, polynomic or sigmoidal fit in MATLAB (see 5.1).

Die approbierte gedruckte Originalversion dieser Diplomarbeit ist an der TU Wien Bibliothek verfügbar.
The approved original version of this thesis is available in print at TU Wien Bibliothek.

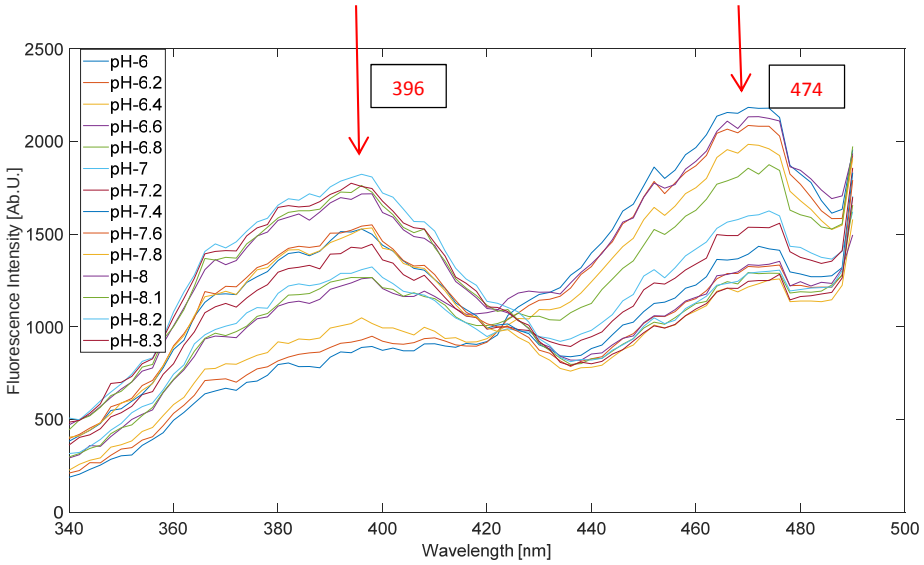

Figure 8: Fluorescence intensity signal versus wavelength of expressed pHluorin sensor in *Corynebacterium glutamicum* with OD_{600} of 1 at different pH values.

Die approbierte gedruckte Originalversion dieser Diplomarbeit ist an der TU Wien Bibliothek verfügbar.
The approved original version of this thesis is available in print at TU Wien Bibliothek.

5 Results and Discussion

5.1 Fluorescence sensor calibration and validation

Fluorescence sensor calibration was carried out at different optical densities by the means of Nigericin and CTAB. From the generated data, regression models were built in order to find a good fit. To verify the model statistical methods were applied. The results of polynomic, Boltzmann sigmoidal and linear regression can be observed in the following sections. All evaluations and plots were constructed using the software MATLAB R2018a from MathWorks.

5.1.1 Calibration by means of CTAB

5.1.1.1 Polynomic function (CTAB)

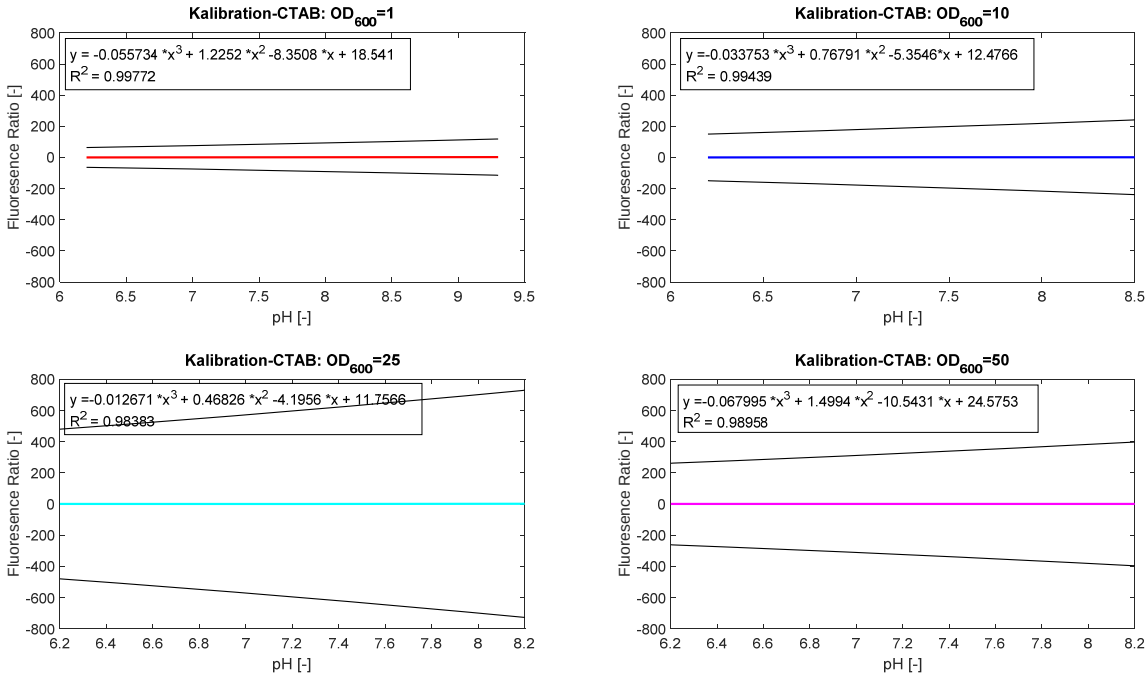

Figure 9: Polynomic fit with the use of CTAB for the cells with optical densities 1, 10, 25 and 50. As black lines relevant confidence intervals (95 % level of significance) are presented.

In Figure 9 the data was regressed using a polynomic function with a maximum order of 3. The Figure shows calibrations for optical density (OD) at 600 nm of 1, 10, 25 and 50 which are positioned in the top left, top right, bottom left and bottom right respectively. The OD_{600} correlates and is proportional to the cell concentration. In addition to the data with the regressed line each diagram contains the relevant confidence intervals with a level of significance 95%.

The confidence interval of the polynomic curve is considerably wider than the range in which the fitting occurred. This prevents the recognition of the classical features of the polynomic curve. The uncertainty of the quadratic and cubic term leads to these large intervals. The biggest intervals and highest uncertainty occur with cell concentrations represented by the optical density of 25, whereas the smallest (concerning polynomic function with CTAB) intervals and uncertainty occur with low cell concentrations represented by OD_{600} 1. Summarizing, confidence intervals and the corresponding uncertainty of the regression coefficients are generally high and also increase with the cell concentration. The R-squared value for biomass concentrations can be seen in the Table 23.

Die approbierte gedruckte Originalversion dieser Diplomarbeit ist an der TU Wien Bibliothek verfügbar.
The approved original version of this thesis is available in print at TU Wien Bibliothek.
TU Bibliothek Your knowledge hub WIEN

Table 23: R^2 value for the polynomic regression model of third order for different OD_{600} and biomass concentrations

Optical Density at 600 nm [A]	Biomass Concentration [g/L]	R^2 Value [-]
1	0.407	0.998
10	4.071	0.994
25	10.177	0.984
50	20.355	0.989

Using these R^2 values as the basis of comparison the best polynomial fit can be identified as the calibration with a cell concentration represented by an OD_{600} of 1.

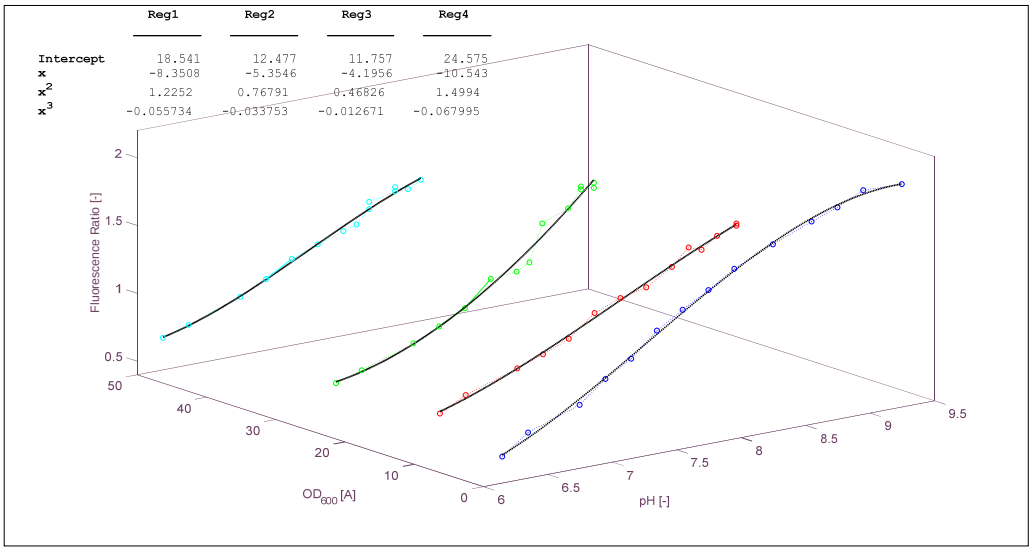

Figure 10: 3D model of polynomic fit with the use of CTAB for the cells with optical densities 1, 10, 25 and 50.

In Figure 10 a three-dimensional plot showing the fitted polynomic functions to the raw data with an order of 3 is shown for better visualization. Reg 1, 2, 3 and 4 represent the regression coefficients for the different models representing the optical densities 1, 10, 25 and 50 respectively. The results of t-statistics, p-values, and root mean squared error (RMSE) for polynomic fits with an order 3 and 2 can be seen in Figure 11 and Figure 12 respectively.

```
Linear regression model:
    y ~ 1 + x1^2 + x1*x2 + x1^3 + (x1^2):x2

Estimated Coefficients:
                   Estimate        SE        tStat       pValue
                   ________    ________    ________    ________

    (Intercept)      20.805      11.971       1.738    0.088491
    x1              -9.0984      4.7278      -1.9245    0.060115
    x2             0.076922    0.090385     0.85105     0.39888
    x1^2             1.3089     0.61751      2.1197    0.039119
    x1:x2          -0.020268    0.025058    -0.80883     0.42252
    x1^3           -0.058929    0.026679     -2.2088    0.031893
    x1^2:x2       0.0012767    0.001726      0.7397     0.46301


Number of observations: 56, Error degrees of freedom: 49
Root Mean Squared Error: 0.088
R-squared: 0.955,  Adjusted R-Squared 0.949
F-statistic vs. constant model: 172, p-value = 3.91e-31
```

Figure 11: Statistical results, calculated in MATLAB of polynomic fits with an order 3.

Die approbierte gedruckte Originalversion dieser Diplomarbeit ist an der TU Wien Bibliothek verfügbar.
The approved original version of this thesis is available in print at TU Wien Bibliothek.

```
Linear regression model:
    y ~ 1 + x1^2 + x1*x2

Estimated Coefficients:
                    Estimate        SE         tStat       pValue
                    ________    _________    ________    _________

    (Intercept)       -3.7429      1.3198     -2.8359    0.0065381
    x1                0.85402     0.34605      2.4679     0.016985
    x2              0.0039763   0.0081894     0.48554      0.62937
    x1^2            -0.023578    0.022494     -1.0482      0.29949
    x1:x2          -0.00086246   0.0010983    -0.78527      0.43593


Number of observations: 56, Error degrees of freedom: 51
Root Mean Squared Error: 0.0964
R-squared: 0.943,  Adjusted R-Squared 0.939
F-statistic vs. constant model: 212, p-value = 4.16e-31
```

Figure 12: Statistical results, calculated in MATLAB of polynomic fits with an order 2.

In the case of polynomic fit with an order of 2, x^2 value is not relevant, due to the p-value that is higher than the level of significance of 0.05 (95% certainty). Polynomic fit with an order of 3 has x^3 p-value of 0.032, which is below 0.05, meaning that this regression coefficient is relevant to the model. The model itself can be considered as representative, due to high F-value of 172 and square regression coefficient of 0.955. No interaction terms were considered for the development of this model.

5.1.1.2 Sigmoidal function (CTAB)

The next regression model applied was the Boltzmann sigmoidal function according to Zhou, 2014. The regressed curves for the different cell concentrations with their respective OD_{600} and confidence intervals are shown in Figure 13. The OD_{600} are 1 on the top left, 10 on the top right, 25 on the bottom left and 50 on the bottom right.

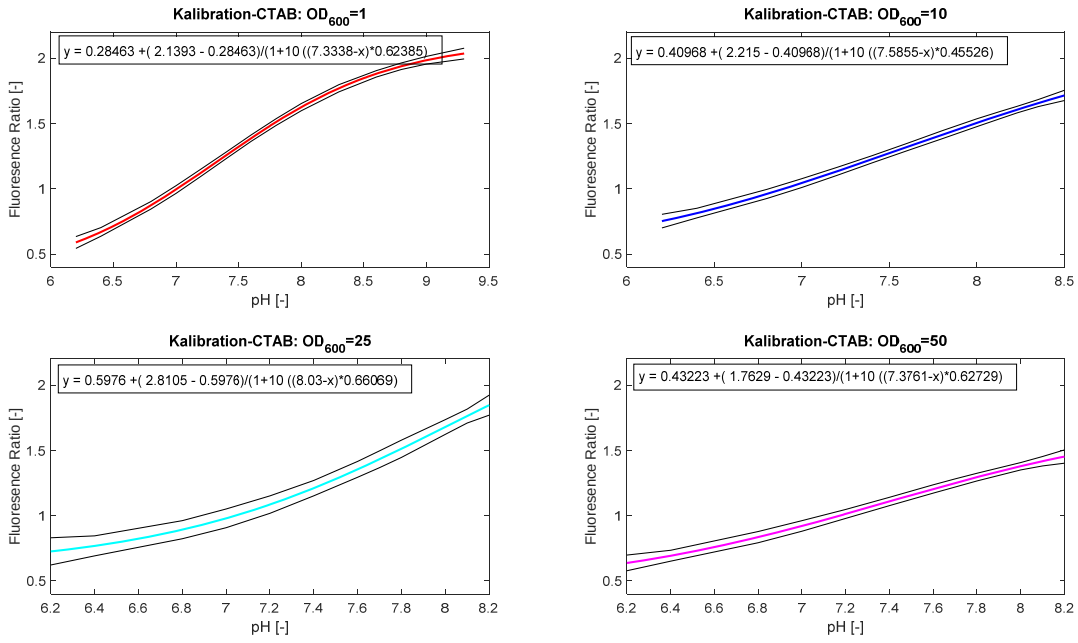

Figure 13: Boltzmann sigmoidal fit with the use of CTAB for the cells with optical densities 1, 10, 25 and 50. As black lines relevant confidence intervals (95 % level of significance) are presented.

For this fitting method the Boltzmann sigmoidal curve equation was applied:

Die approbierte gedruckte Originalversion dieser Diplomarbeit ist an der TU Wien Bibliothek verfügbar.
The approved original version of this thesis is available in print at TU Wien Bibliothek.

Equation 6

$$y = x_{min} + \frac{(x_{max} - x_{min})}{(1 + 10^{((x_{50\%} - x) * x_{slope})})}$$

x_{min} ….. minimum y value that can be reached
x_{max} ….. maximum y value that can be reached
$x_{50\%}$ ….. y value at which the 50% of maximum can be reached
x_{slope} ….. slope at which the curve increases in the exponent

The sigmoidal function was calculated in MATLAB with the help of the sigm_fit script (by R. P., Copyright (c) 2016). This script estimates a total of four parameters.

Boltzmann sigmoidal function shows smaller confidence intervals compared to the polynomic function. In Figure 13 with the observation can be seen that fluorescence ratio does not exceed 2.8 while the polynomic calibration function yields +/- 800. These more sensible values suggest that this fitting method gives more reliable results.

Figure 14 shows a three-dimensional plot of the regressed sigmoidal functions from the raw data for different optical densities and therefore different cell concentrations. Reg 1, 2, 3 and 4 represent the regression coefficients for optical densities of 1, 10, 25 and 50 respectively. Parameters x_{min}, x_{max}, x_{50} and x_{slope} are the values that are substituted in the Equation 6 to build calibration equations.

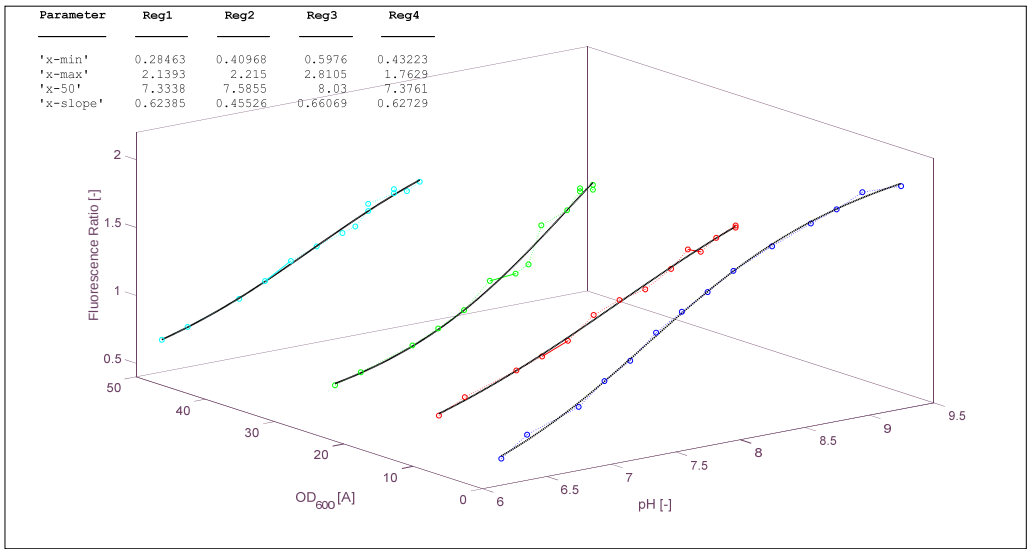

Figure 14: 3D model of Boltzmann sigmoidal fit with the use of CTAB for the cells with optical densities 1, 10, 25 and 50.

5.1.1.3 Linear function (CTAB)

Linear regression in one variable, in this case the pH, was conducted. The confidence intervals and the regression models for different OD_{600}/cell concentrations are shown in Figure 15. The OD_{600} for 1, 10, 25 and 50 are shown on the top left, top right, bottom left and bottom right respectively in the Figure 15. A multiple linear regression (MLR) model was developed in order to include the cell concentration/optical density as a variable. This was done in order to predict the curve trend of the cells with other cell density apart of the ones described in this thesis.

Die approbierte gedruckte Originalversion dieser Diplomarbeit ist an der TU Wien Bibliothek verfügbar.
The approved original version of this thesis is available in print at TU Wien Bibliothek.

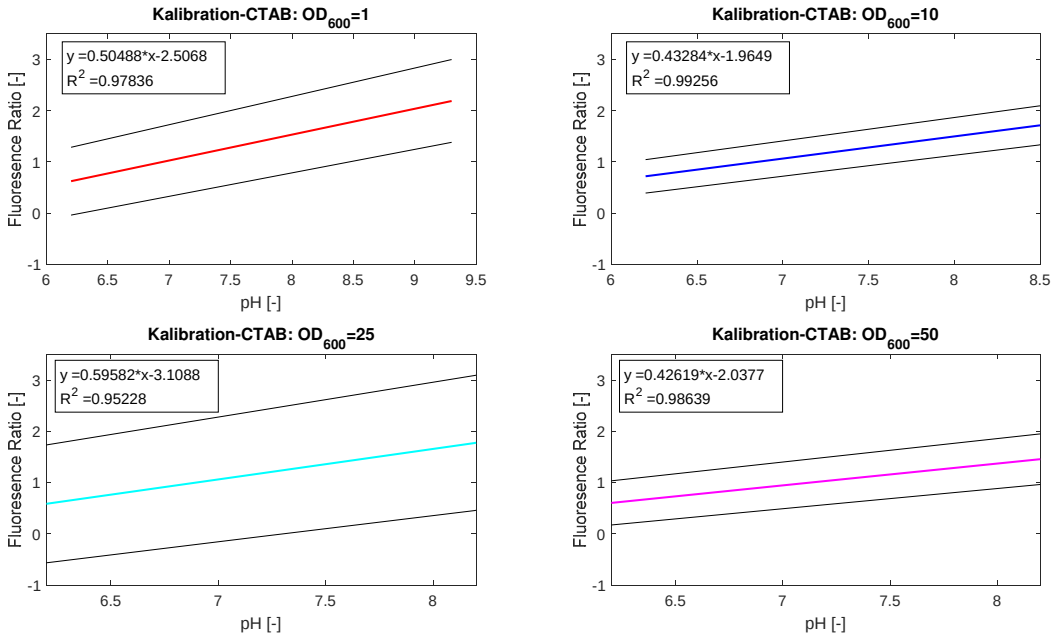

Figure 15: Linear fit with the use of CTAB for the cells with optical densities 1, 10, 25 and 50. As black lines relevant confidence intervals (95 % level of significance) are presented.

In the case of the linear fit, the confidence intervals do not exceed a fluorescence ratio of 3 in the observed range, which is smaller than in the case of the polynomic fit but higher than in the case of the Boltzmann sigmoidal function. It can be also recognized that the widest confidence interval occurs with cells concentration represented by an optical density of 25, whereas the smallest interval occurs with cell concentrations with an optical density of 10. The R^2 values of the different regression models are shown in Table 24.

Table 24: R^2 values of the regression models for different OD_{600} values and therefore different cell concentrations [g/L]

Optical Density at 600 nm [A]	Cell concentration [g/L]	R^2 Value [-]
1	0.407	0.978
10	4.071	0.992
25	10.177	0.952
50	20.355	0.986

Die approbierte gedruckte Originalversion dieser Diplomarbeit ist an der TU Wien Bibliothek verfügbar.
The approved original version of this thesis is available in print at TU Wien Bibliothek.

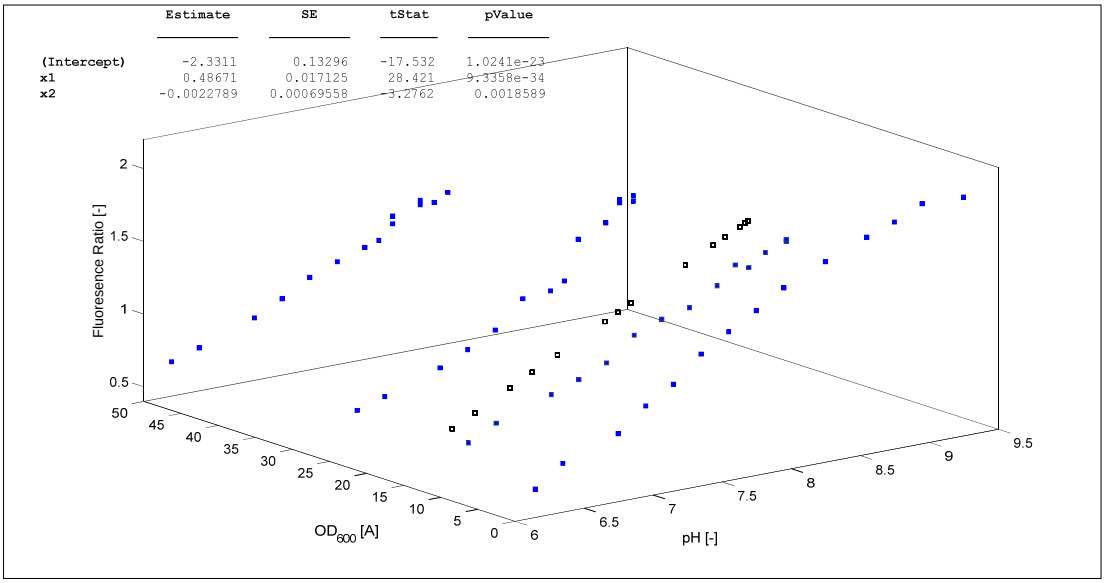

Figure 16: MLR model of the cells with optical densities 1, 10, 25 and 50 (with the use of CTAB). Blue squares correspond to experimental data, whereas black squares represent simulated data.

In Figure 16 a multiple linear model (MLR) with regression coefficients x1 representing the variable pH and x2 representing the variable OD was applied. The t-statistics and p-value for the regression model are shown in the table in the top left of the figure. All p-values of 7.943×10^{-49} and 0.0019 for x1 and x2 correspondently are below the level of significance of 0.05 (95% certainty), which suggests that the regression coefficients x1 and x2, who represent the pH and OD respectively, as well as the y intercept are relevant to the model. As dependent variable fluorescence ratio was chosen, whereas as independent variables– OD_{600} and pH were chosen. In order to predict and estimated fluorescence ratios for a cell concentration represented by an OD_{600} of 15, the MLR model was applied and a fluorescence ratio was calculated. Estimated fluorescence ratio values for the cells with optical density 15 for different pH values are shown as black squares. Blue points represent measured fluorescence ratios of OD 1, 10, 25 and 50 correspondently. In order to check cross-correlation of the two variables (OD and pH) - variance inflation factor (VIF) was determined. The calculated VIF value was 1.019, which is far below 10, meaning that no cross-correlations can be assumed and the model can be applied.

5.1.2 Calibration by means of Nigericin

The same statistical fitting methods were applied to the Nigericin dataset in order to select the best suitable membrane disturbing compound.

Die approbierte gedruckte Originalversion dieser Diplomarbeit ist an der TU Wien Bibliothek verfügbar.
The approved original version of this thesis is available in print at TU Wien Bibliothek.

5.1.2.1 Polynomic function (Nigericin)

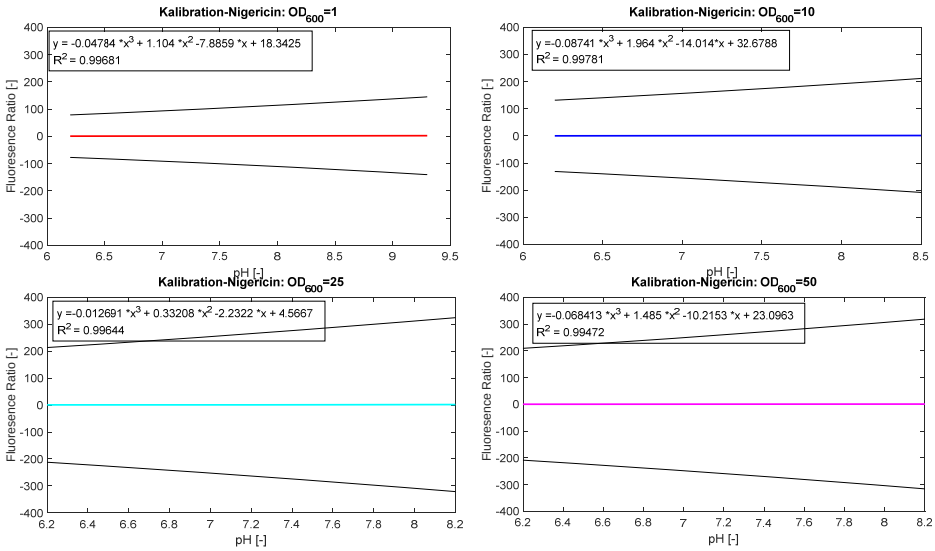

Figure 17: Polynomic fit with the use of Nigericin for the cells with optical densities 1, 10, 25 and 50. As black lines relevant confidence intervals (95 % level of significance) are presented.

Confidence intervals of polynomic regression with an order of 3 for OD_{600} 1, 10, 25 and 50 in case of Nigericin are smaller by a factor of two (fluorescence ratio +/- 400) than in case of CTAB (fluorescence ratio +/- 800), but still wide enough not to be able to recognize the features of the polynomic curve. Confidence intervals increase with the cell concentration as well. R^2 values for the different biomass concentrations can be seen in Table 25.

Table 25: R^2 value for the curves regressed using a polynomic model of order 3 for Nigericin

Optical Density at 600 nm [A]	Cell concentration [g/L]	R^2 Value [-]
1	0.407	0.997
10	4.071	0.998
25	10.177	0.996
50	20.355	0.995

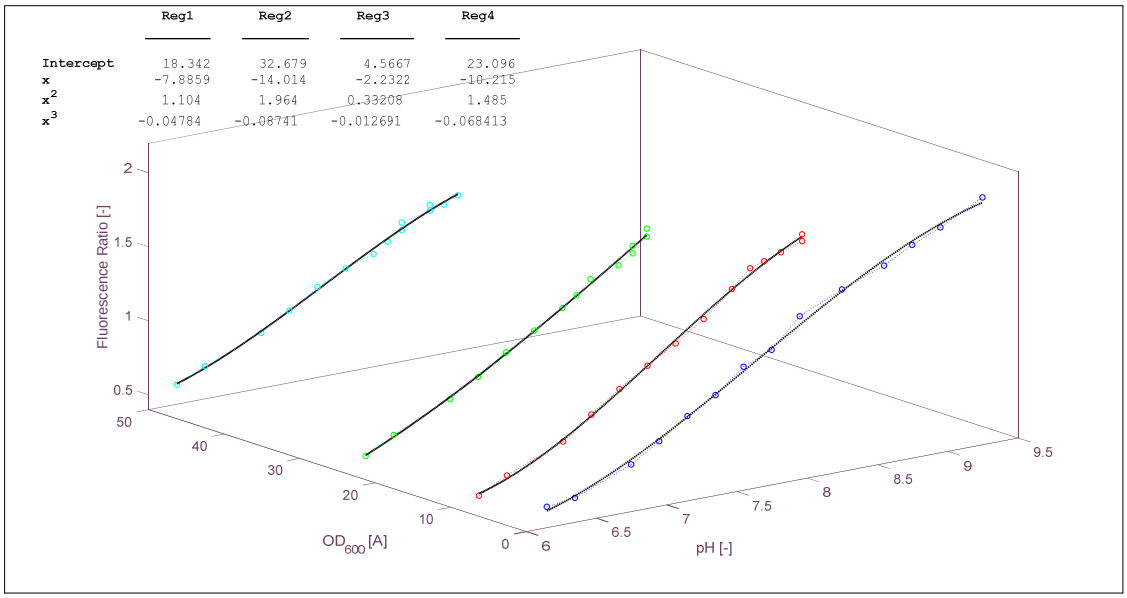

Figure 18: 3D model of polynomic fit with the use of Nigericin for the cells with optical densities 1, 10, 25 and 50.

Die approbierte gedruckte Originalversion dieser Diplomarbeit ist an der TU Wien Bibliothek verfügbar.
The approved original version of this thesis is available in print at TU Wien Bibliothek.
TU Bibliothek Your knowledge hub WIEN

In Figure 18 a three-dimensional plot of the polynomic functions with an order of 3 is shown. Reg 1, 2, 3 and 4 represent the regression coefficients of OD 1, 10, 25 and 50 respectively. The results of t-statistics, p-values, and root mean squared error (RMSE) for polynomic fits with an order 2 and 3 can be seen in Figure 19 and Figure 20 respectively.

```
Linear regression model:
    y ~ 1 + x1^2 + x1*x2

Estimated Coefficients:
                    Estimate        SE         tStat       pValue
                    ________    __________    _______    __________

    (Intercept)       -3.875       0.73439    -5.2765    2.7158e-06
    x1                0.78015       0.19255     4.0517    0.00017367
    x2              0.0085606     0.0045567     1.8787      0.066011
    x1^2             -0.014412      0.012516    -1.1515       0.25489
    x1:x2            -0.0011525    0.00061111    -1.8859      0.065005


Number of observations: 56, Error degrees of freedom: 51
Root Mean Squared Error: 0.0536
R-squared: 0.985,  Adjusted R-Squared 0.984
F-statistic vs. constant model: 823, p-value = 1.22e-45
```

Figure 19: Statistical results, calculated in MATLAB of polynomic fits with an order 2.

```
Linear regression model:
    y ~ 1 + x1^2 + x1*x2 + x1^3 + (x1^2):x2

Estimated Coefficients:
                    Estimate        SE         tStat       pValue
                    ________    __________    _______    __________

    (Intercept)       25.411       5.4537     4.6594    2.4607e-05
    x1               -10.953       2.1539    -5.0851    5.7738e-06
    x2             -0.021756     0.041178    -0.52834       0.59965
    x1^2              1.5381      0.28133     5.4673    1.5306e-06
    x1:x2           0.0080279     0.011416    0.70321       0.48525
    x1^3             -0.067863     0.012154    -5.5834    1.0191e-06
    x1^2:x2        -0.00068541    0.00078634    -0.87165       0.38765


Number of observations: 56, Error degrees of freedom: 49
Root Mean Squared Error: 0.0401
R-squared: 0.992,  Adjusted R-Squared 0.991
F-statistic vs. constant model: 990, p-value = 2.46e-49
```

Figure 20: Statistical results, calculated in MATLAB of polynomic fits with an order 3.

It can be seen, that in polynomic fit with an order of 2, x^2 value is not relevant as was the case with CTAB, due to the p-value of 0.255, which is higher than the level of significance of 0.05 (95% certainty). Polynomic fit with an order of 3 has x^3 p-value of 1.019×10^{-6}, which is far below 0.05, meaning that this regression coefficient is relevant to the model. The model itself can be considered as valid, due to high F-value of 990 and square regression coefficient of 0.992. These values are relevantly higher as in case of CTAB.

Die approbierte gedruckte Originalversion dieser Diplomarbeit ist an der TU Wien Bibliothek verfügbar.
The approved original version of this thesis is available in print at TU Wien Bibliothek.

5.1.2.2 Sigmoidal function (Nigericin)

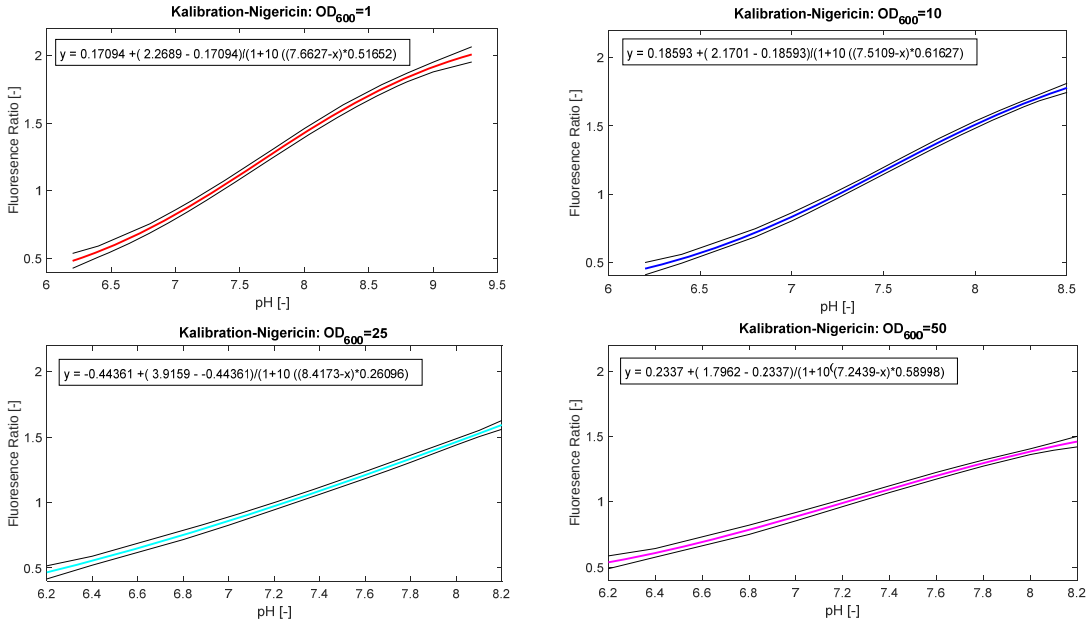

Figure 21: Boltzmann sigmoidal fit with the use of Nigericin for the cells with optical densities 1, 10, 25 and 50. As black lines relevant confidence intervals (95 % level of significance) are presented.

Boltzmann sigmoidal function was calculated with the sigmoidal curve equation as seen in Equation 6. In the case of Nigericin the confidence intervals are also smaller compared to the polynomic regression model. In Figure 21 the fluorescence ratio does not exceed 2.2, which makes this fitting method more reliable than the polynomic one.

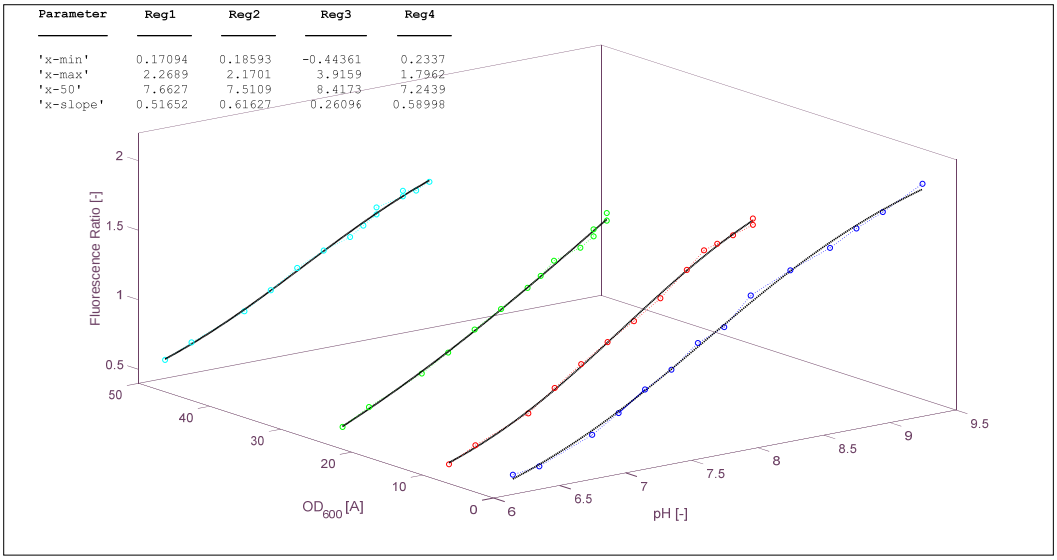

Figure 22: 3D model of Boltzmann sigmoidal fit with the use of Nigericin for the cells with optical densities 1, 10, 25 and 50.

Figure 22 shows a three-dimensional plot of the sigmoidal functions of the fluorescence ratio with different optical densities. Reg 1, 2, 3 and 4 represent the regression coefficients for optical densities 1, 10, 25 and 50 respectively. Parameters x_{min}, x_{max}, x_{50} and x_{slope} are the values that are substituted in the Equation 6 to calculate the calibration equations.

Die approbierte gedruckte Originalversion dieser Diplomarbeit ist an der TU Wien Bibliothek verfügbar.
The approved original version of this thesis is available in print at TU Wien Bibliothek.
TU Bibliothek Your knowledge hub WIEN

5.1.2.3 Linear function (Nigericin)

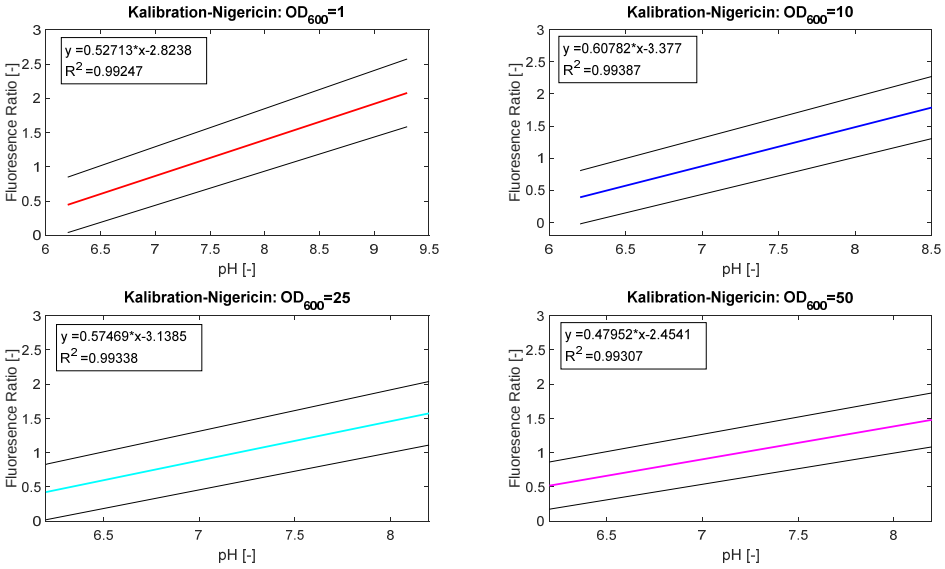

Figure 23: Linear fit with the use of Nigericin for the cells with optical densities 1, 10, 25 and 50. As black lines relevant confidence intervals (95 % level of significance) are presented.

In case of the linear regression models, the confidence intervals do not exceed a fluorescence ratio of 3 in the calibration range, as was the case with CTAB. Confidence intervals and R^2 values for the different optical densities only show neglectably small differences, this feature can be quantitatively observed in the R^2 value in Table 26.

Table 26: R^2 value for the curves regressed using a linear model for Nigericin

Optical Density at 600 nm [A]	Biomass Concentration [g/L]	R^2 Value [-]
1	0.407	0.992
10	4.071	0.994
25	10.177	0.993
50	20.355	0.993

Die approbierte gedruckte Originalversion dieser Diplomarbeit ist an der TU Wien Bibliothek verfügbar.
The approved original version of this thesis is available in print at TU Wien Bibliothek.

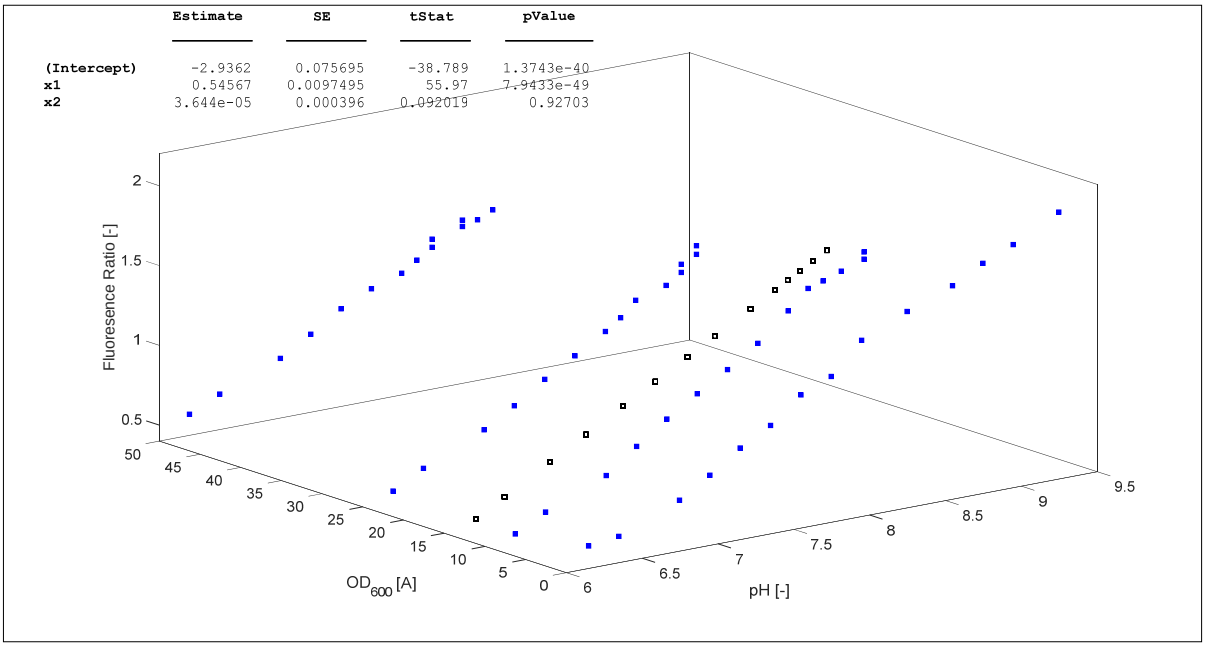

Figure 24: MLR model of the cells with optical densities 1, 10, 25 and 50 (with the use of Nigericin). Blue squares correspond to experimental data, whereas black squares represent simulated data.

In Figure 24 a multiple linear regression model (MLR) with regression coefficients x1 representing the variable pH and x2 representing the variable OD is depicted. In addition, the t-statistics and p-value for the regression model are shown. The p-value of 7.943×10^{-49} for x1 is below the level of significance of 0.05 (95% certainty). However, the variable x2 has a level of significance of 0.927 and therefore is considerably higher than the level of significance of 0.05. This suggests that only the regression coefficient x1 which represents the pH and the y intercept are relevant to the model, meaning that the influence of biomass concentration is statistically insignificant if calibrations are based on Nigericin data set. As dependent variable fluorescence ratio was chosen, whereas as independent variables – OD_{600} and pH variables were selected. Estimated fluorescence ratios for OD 15 were also calculated to test the MLR model. Estimated fluorescence ratio values for the cells with optical density 15 are shown as black squares for different pH set points. Blue points represent measured fluorescence ratios of OD 1, 10, 25 and 50 correspondently. In order to check for cross-correlation between the two variables OD and pH - variance inflation factor (VIF) was calculated. The Calculated VIF value was 1.019, which is below 10. This indicates that the model does not include cross-correlations and can be applied.

5.1.3 Sensor validation at different optical density levels

To compose a sensor validation at different optical density levels, MLR model as well as cross-validation of measured pH vs estimated pH was applied. This comparison was made to test if OD values influence fluorescence ratios and therefore intracellular pH.

Application of MLR model in 5.1.1.3 and 5.1.2.3 showed, that in case of CTAB, biomass concentration does have an influence on the model, whereas in case of Nigericin, OD variable do not appear to be relevant to the model. To have a better understanding cross-validation was applied. The estimated pH values with the OD value of 10, 25 and 50 were plotted against measured pH values for OD of 10, 25 and 50 respectively. The estimated pH values were calculated with the help of calibration equation of OD_{600}=1 from Nigericin dataset, using linear, polynomic and sigmoidal fits (Figure 25, Figure 26 and Figure 27). The results are shown below.

Die approbierte gedruckte Originalversion dieser Diplomarbeit ist an der TU Wien Bibliothek verfügbar.
The approved original version of this thesis is available in print at TU Wien Bibliothek.

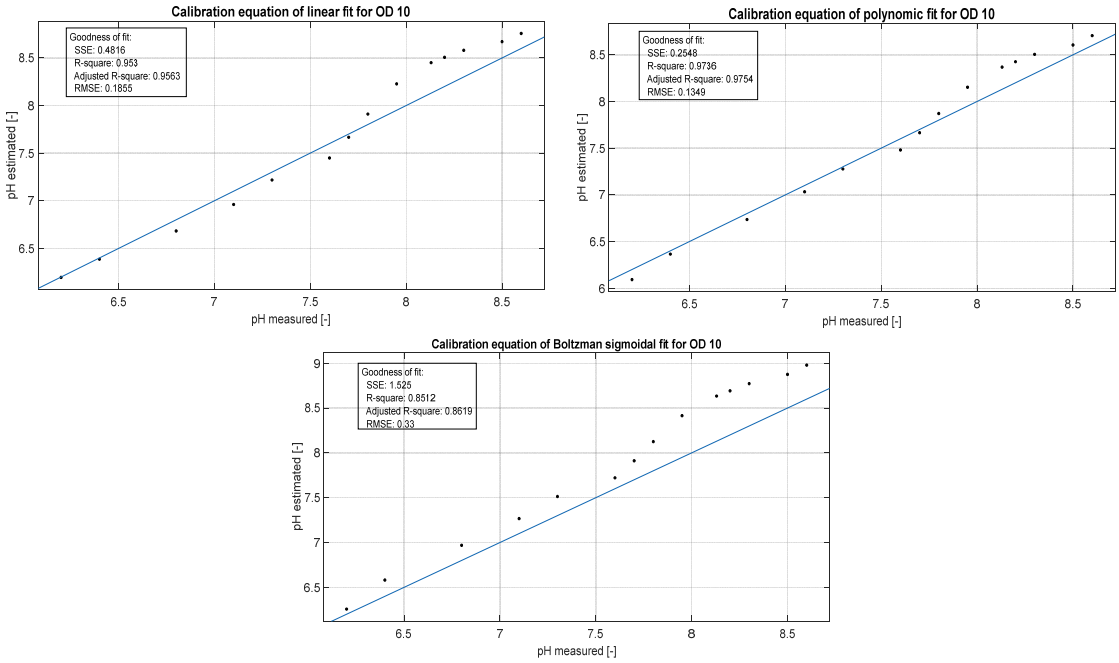

Figure 25: Cross-validation of OD variable. pH estimation for OD 10, using calibration equation of linear, polynomic and Boltzmann sigmoidal fitting of OD 1 calibration data set. Measured pH of OD 10.

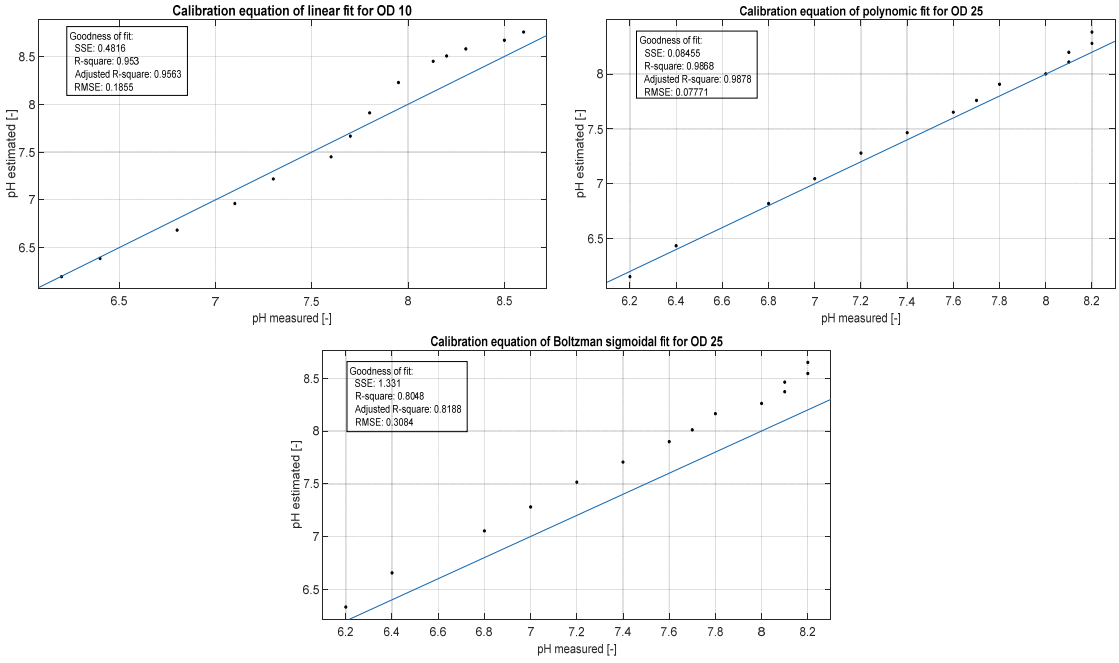

Figure 26: Cross-validation of OD variable. pH estimation for OD 25, using calibration equation of linear, polynomic and Boltzmann sigmoidal fitting of OD 1 calibration data set. Measured pH of OD 25.

Die approbierte gedruckte Originalversion dieser Diplomarbeit ist an der TU Wien Bibliothek verfügbar.
The approved original version of this thesis is available in print at TU Wien Bibliothek.

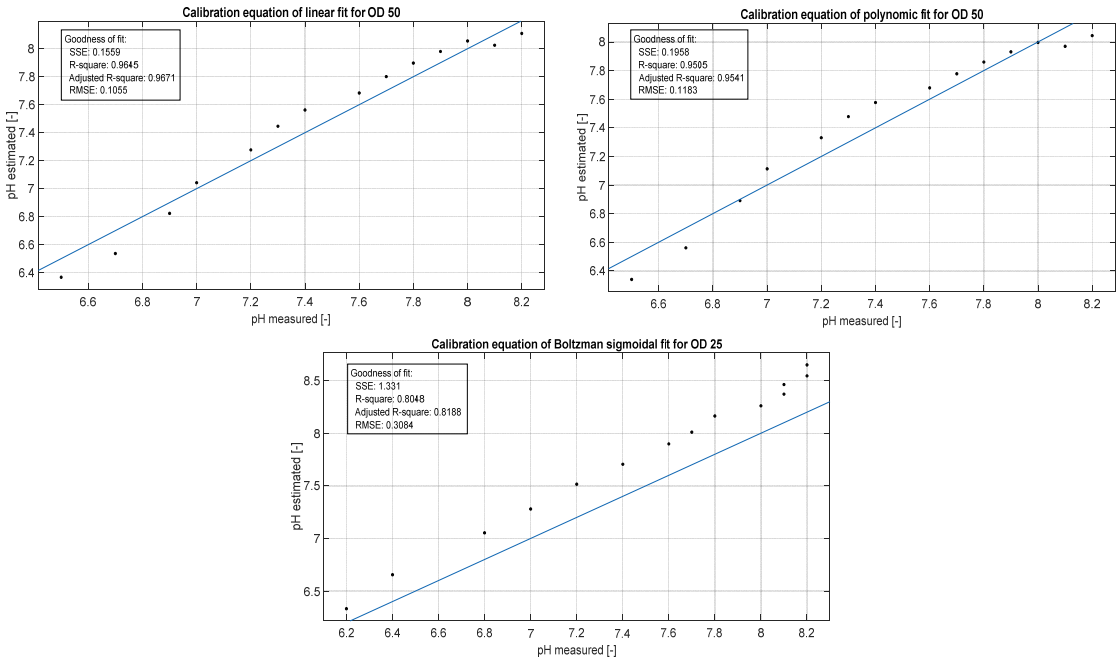

Figure 27: Cross-validation of OD variable. pH estimation for OD 50, using calibration equation of linear, polynomic and Boltzmann sigmoidal fitting of OD 1 calibration data set. Measured pH of OD 50.

Linear functions for correlation of measured vs. predicted values applied had a slope 1 and a y intercept of zero. Thereby, the cross-validation results of different fitting methods can be compared based on R^2 and Root Mean Square Error (RMSE) of the measured vs. predicted correlation function.

R^2 values and RMSE of OD values 10, 25 and 50 of the calibration equation for corresponded fitting method can be seen in the Table 27, Table 28 and Table 29 respectively.

Table 27: R^2 and RMSE for fitting methods applied for OD 10

Fitting method	R^2	RMSE
Linear	0.953	0.185
Polynomic	0.974	0.123
Boltzmann sigmoidal	0.851	0.131

Table 28: R^2 and RMSE for fitting methods applied for OD 25

Fitting method	R^2	RMSE
Linear	0.993	0.143
Polynomic	0.987	0.131
Boltzmann sigmoidal	0.805	0.179

Table 29: R^2 and RMSE for fitting method applied for OD 50

Fitting method	R^2	RMSE
Linear	0.964	0.129
Polynomic	0.950	1.033
Boltzmann sigmoidal	0.953	0.523

Cross-validation was applied also for calibration equations based on OD_{600}=10, OD_{600}=25 and OD_{600}=50 from Nigericin dataset, using linear, polynomial and sigmoidal fits. Therefore estimated pH

Die approbierte gedruckte Originalversion dieser Diplomarbeit ist an der TU Wien Bibliothek verfügbar.
The approved original version of this thesis is available in print at TU Wien Bibliothek.
TU Bibliothek Your knowledge hub WIEN

values with the OD value of 1, 10, 25 or 50 correspondently were plotted against measured pH values for OD of 1, 10, 25 and 50 respectively. The root mean square error of each plot was calculated. The results are presented in the form of diagram, comparing calibration equations based on different OD values and regression types, what can be seen in Figure 28.

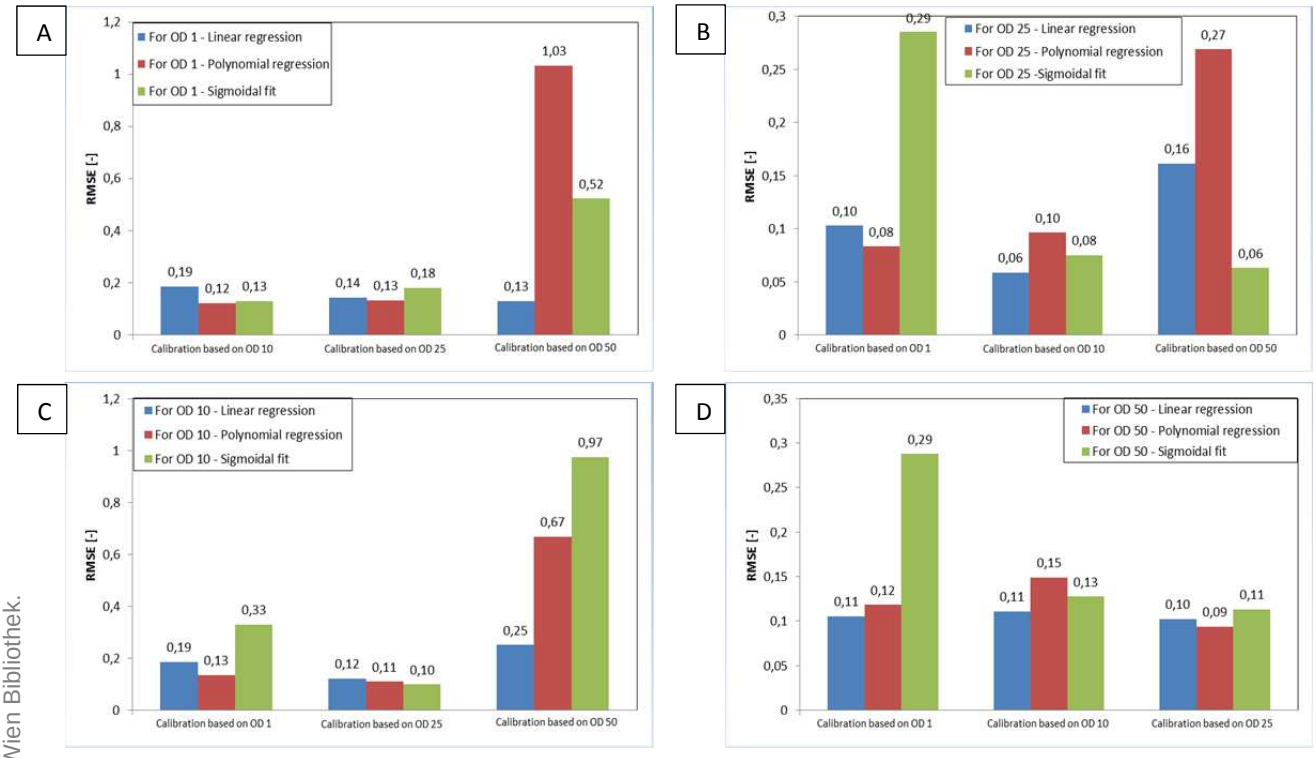

Figure 28: Root Mean Square Errors of calibration equations of linear regression, polynomial regression and sigmoidal fit based on: calibration of OD 10, 25, 50 for OD 1 (A), calibration of OD 1, 25, 50 for OD 10 (B), calibration of OD 1, 10, 50 for OD 25 (C), calibration of OD 1, 10, 25 for OD 50 (D).

According to Figure 25, Figure 26, Figure 27, Figure 28 and Table 27, Table 28, Table 29 can be said that linear regression has the highest values for R^2 as well as low and less fluctuating root mean square errors across different OD estimated values in comparison to other fitting methods.

5.1.4 CTAB/Nigericin and pH range validation

As it was already mentioned in 5.1.3, following statistical analysis and fitting models, calibration procedure, worked better when Nigericin was used. For better visualization, in Figure 29 sigmoidal fitting curves with confidence intervals of CTAB and Nigericin datasets are presented.

Die approbierte gedruckte Originalversion dieser Diplomarbeit ist an der TU Wien Bibliothek verfügbar.
The approved original version of this thesis is available in print at TU Wien Bibliothek.
TU Bibliothek Your knowledge hub WIEN

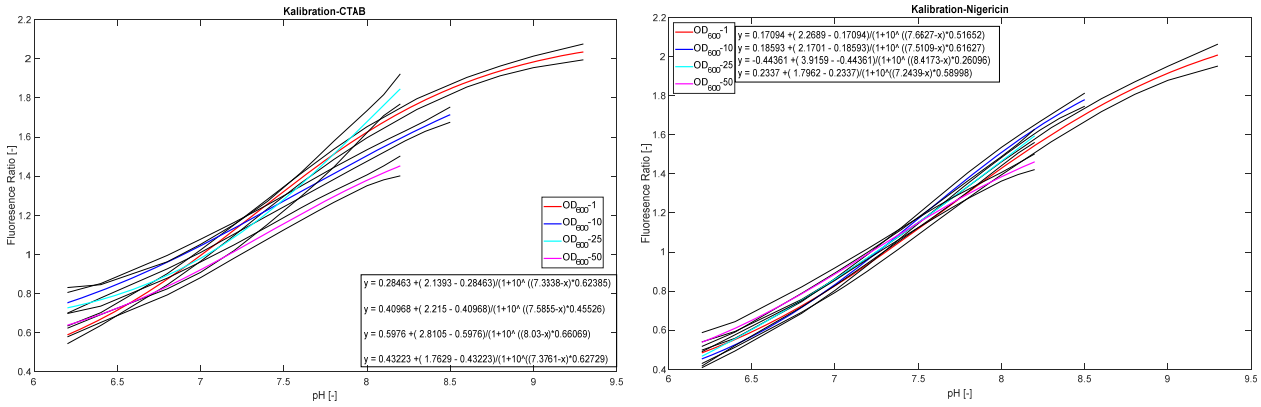

Figure 29: Sigmoidal fitting of CTAB (left) and Nigericin (right) dataset with OD 1, 10, 25 and 50. Red line represents OD=1, blue line – OD=10, turquoise line represents OD=25 and pink line represents OD=50. Black lines from both sides represent confidence intervals for each OD.

In Figure 29 can be seen that the Boltzmann sigmoidal curves and confidence intervals of OD 1, 10, 25 and 50 are located close to each other, especially in the pH range of 6.8 - 8.0, where the hypothetical pH optimum for *Corynebacterium glutamicum* is, corresponding to the reported physiological range of intracellular pH of *C.glutamicum* by Ochrombel, 2011. In CTAB dataset curves are more spread from each other. That confirms that calibration data based on Nigericin treatment should be used for intracellular pH evaluation.

In Figure 30 fluorescence ratios plotted against pH values are shown. Error bars represent biological triplicates. It can be observed that error bars in the neutral pH range are smaller than in the acidic or basic range. Besides of possible adverse physical effects on the sensor signal at the borders of the physiological pH range, this can be caused by the regression modelling itself. The behaviour of confidence intervals of estimated values obtained by linear regression models is expected to be hyperbolic.

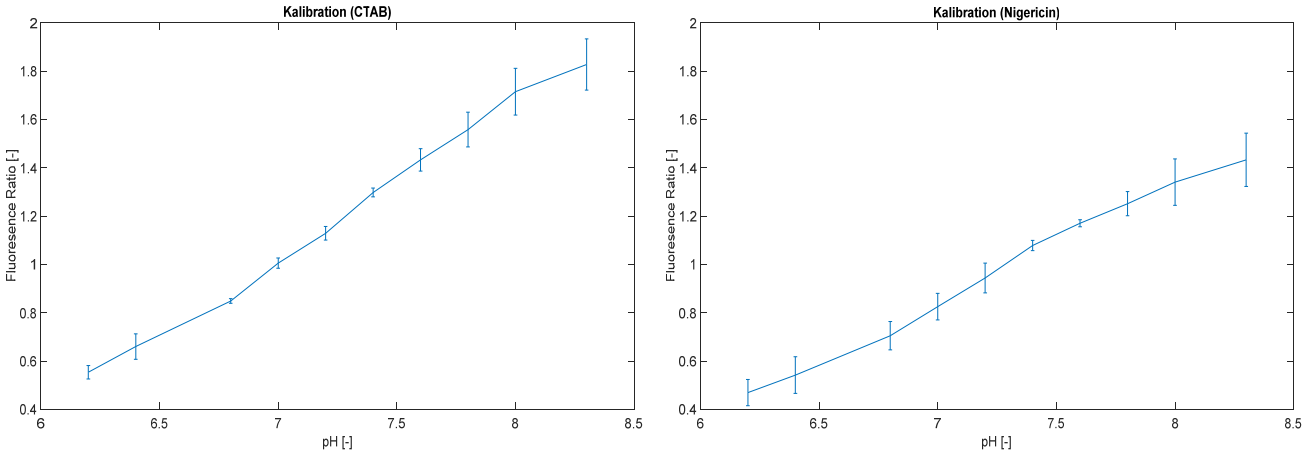

Figure 30: Plot fluorescence ratios against pH for CTAB (right) and Nigericin (left) datasets with error bars (triplicate measurement).

To summarize, as a membrane disturbing chemical for calibration Nigericin should be used. The essential and novel result is that the biomass concentration does not influence the fluorescence ratio, which means that the samples can be taken directly from the bioreactor or shake flask and measured without prior dilution steps thereby eliminating a possible source of error. With respect to the best applicable calibration equation – the equation, obtained via linear regression method should be considered for intracellular pH evaluations, due to low root mean square errors, high values for R^2 and low uncertainty corresponding to confidence intervals.

Die approbierte gedruckte Originalversion dieser Diplomarbeit ist an der TU Wien Bibliothek verfügbar.
The approved original version of this thesis is available in print at TU Wien Bibliothek.
TU Bibliothek Your knowledge hub WIEN

5.2 Dynamics of intracellular pH and cell growth during batch cultivations in shake flasks

Shake flask cultivations were conducted to examine the dynamics of intracellular pH under stress conditions in order to induce extracellular glutamate production. As membrane stress inducers, Tween 40 and Penicillin G were used, according to Eggeling, 2001.

In Figure 31 biomass concentration (Cell Dry Weight (CDW)) in g/L can be observed. Each experiment was made in biological duplicates. Blue lines represent addition of Tween 40, whereas red lines represent control runs, without addition of any stress inducing chemicals. Green lines symbolize addition of Penicillin G. The curve trends are not identical. This fact can be explained as additional stress parameters influencing the cells, which cannot be verified, due to uncontrolled nature of the shake flask cultivation or a stochastic culture response after identical Penicillin G addition.

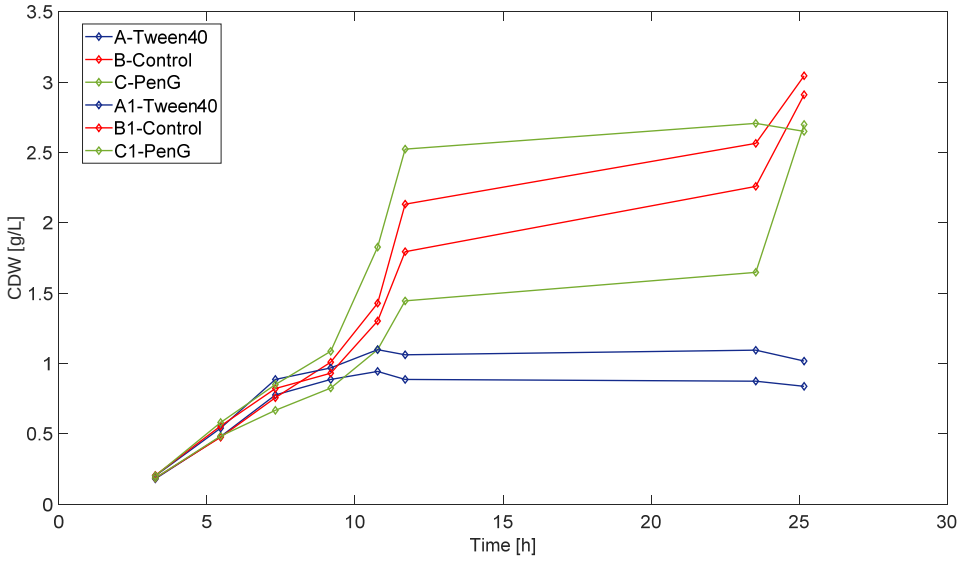

Figure 31: Biomass concentration of shake flask cultivation: blue lines– addition of Tween 40, red lines – control run without any stress addition, green lines – addition of Penicillin G.

In Figure 32 intracellular pH trend (left) and pH gradient trend (right) is presented. Intracellular pH (pH_i) was calculated based on linear regression model of Nigericin calibration data out of fluorescence ratios determined by fluorescence sensor measurement. Three curves are shown: addition of Tween 40, Penicillin G and no stress conditions (control run). All curves behave similarly and decrease rapidly to a pH of 8.7 and slowly increase up to pH 9.9 which is outside of the initial calibration range. Concerning delta pH, which was calculated by subtraction intracellular pH from extracellular pH (measured at-line with the means of pH-probe), the curves trends are increasing at the same rate to the final value of -0.4.

Die approbierte gedruckte Originalversion dieser Diplomarbeit ist an der TU Wien Bibliothek verfügbar.
The approved original version of this thesis is available in print at TU Wien Bibliothek.

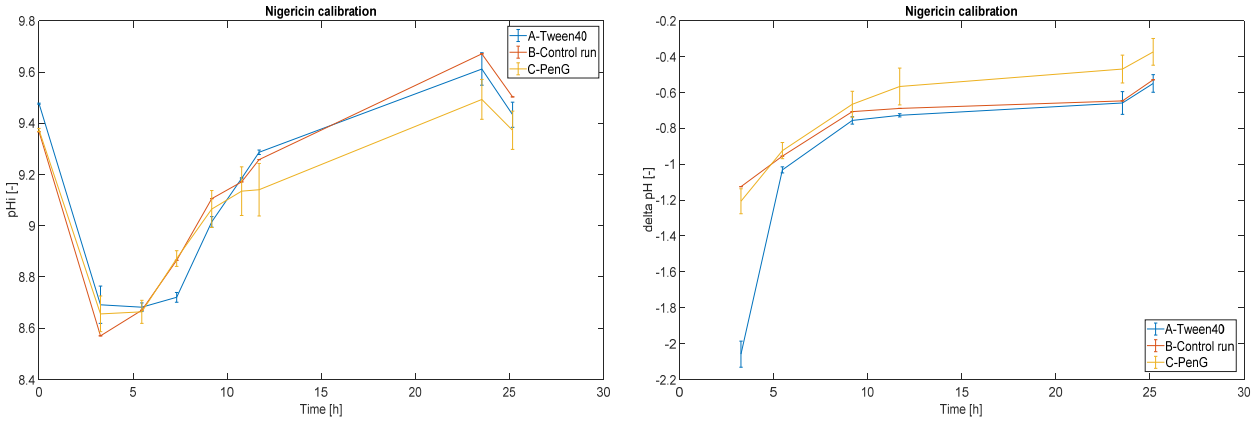

Figure 32: Left: intracellular pH versus cultivation time of three experiments in biological duplicates. Right: pH gradient versus cultivation time of three experiments in biological duplicates.

The highest glutamate amount produced was reached in shake flask cultivation with an addition of Penicillin G with concentration of 222 mg/L, whereas maximum glutamate concentration produced after addition of Tween 40 was 193 mg/L (see 5.5.2). However, only small amount of glutamate was produced, comparing the results of Eggeling, 2001. The reason of what could be genetically modification of the strain and its focus on pHluorin production.

Summarizing, shake flask cultivation data did not deliver reliable results, concerning intracellular pH and pH gradient trends, due to the uncontrolled nature of the whole cultivation process. The other reason could be high fluorescence sensor induction via the use of IPTG, which is already causing a stress condition for cells and can influence theirs pH homeostasis. This will be further analysed and discussed in the following sections.

Die approbierte gedruckte Originalversion dieser Diplomarbeit ist an der TU Wien Bibliothek verfügbar.
The approved original version of this thesis is available in print at TU Wien Bibliothek.

5.3 Tuning of sensor protein expression levels by high-throughput screening

Experiments in shake flasks with external stress factors showed the importance of investigating the sensor protein expression levels, in order to reduce cell stress during the cultivation and to prevent reduction of specific growth rate. Furthermore, relation of glutamate induction und intracellular pH dynamics was investigated. Tuning of pHluorin expression levels was conducted by means of high-throughput screening in µClear microtiter plates. This screening method gives the possibility to measure online optical density and fluorescence at defined wavelengths of cells. Wittmann, 2004 described that microtiter-plate cultivations are suitable for detailed comparative metabolic network analysis at a miniaturized scale, because of the possibility of many parallel experiments, what makes these cultivations very useful for high-throughput applications. The overview of the experiments conducted for inducer tuning and its dependence on external stress addition can be found in Table 30.

Table 30: Cultivation parameters used for 3 different experiments during high-throughput screening

Experinent N°	**1**	**2**	**3**
Pre-culture	Not induced	Induced with 0.5 mM IPTG	Induced with 0.5 mM IPTG
Main culture:			
IPTG	1) Not induced 2) 10 µM IPTG 3) 200 µM IPTG 4) 500 µM IPTG 5) 1000 µM IPTG 6) 10000 µM IPTG	1) Not induced 2) 10 µM IPTG 3) 200 µM IPTG 4) 500 µM IPTG 5) 1000 µM IPTG 6) 10000 µM IPTG	Induced with 0.5 mM IPTG
Penicillin G	-	-	1) Not induced 2) 150 U/L PenG 3) 300 U/L PenG 4) 500 U/L PenG 5) 750 U/L PenG 6) 1150 U/L PenG

The results of optical density measurements of six experiments, whereas each was made in biological triplicates, at different IPTG concentrations with induced and non-induced pre-culture can be found in Figure 33 and Figure 34.

Die approbierte gedruckte Originalversion dieser Diplomarbeit ist an der TU Wien Bibliothek verfügbar.
The approved original version of this thesis is available in print at TU Wien Bibliothek.

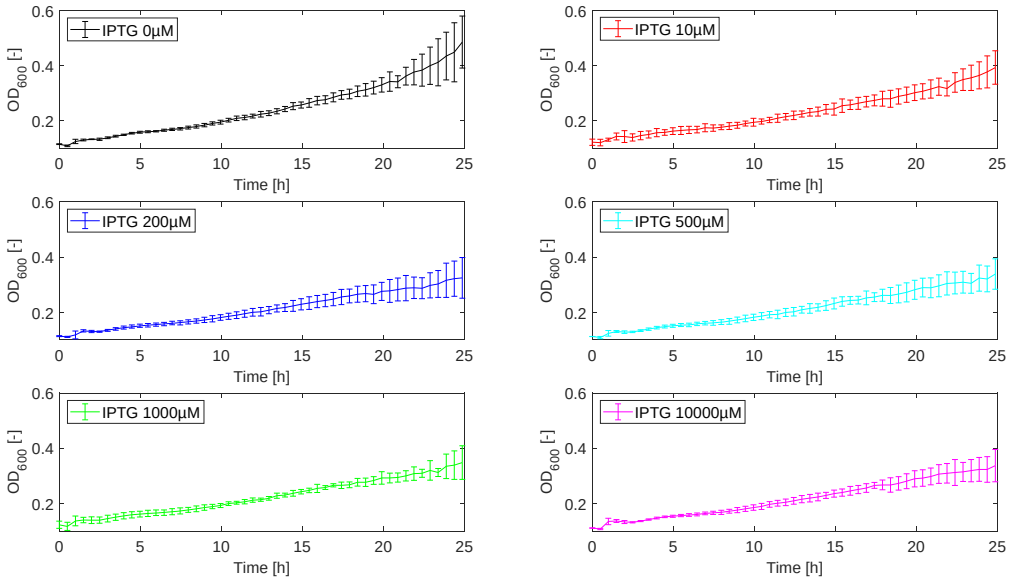

Figure 33: Optical density at 600 nm versus time in hours of IPTG concentration tuning with non-induced pre-culture at different inducer concentrations.

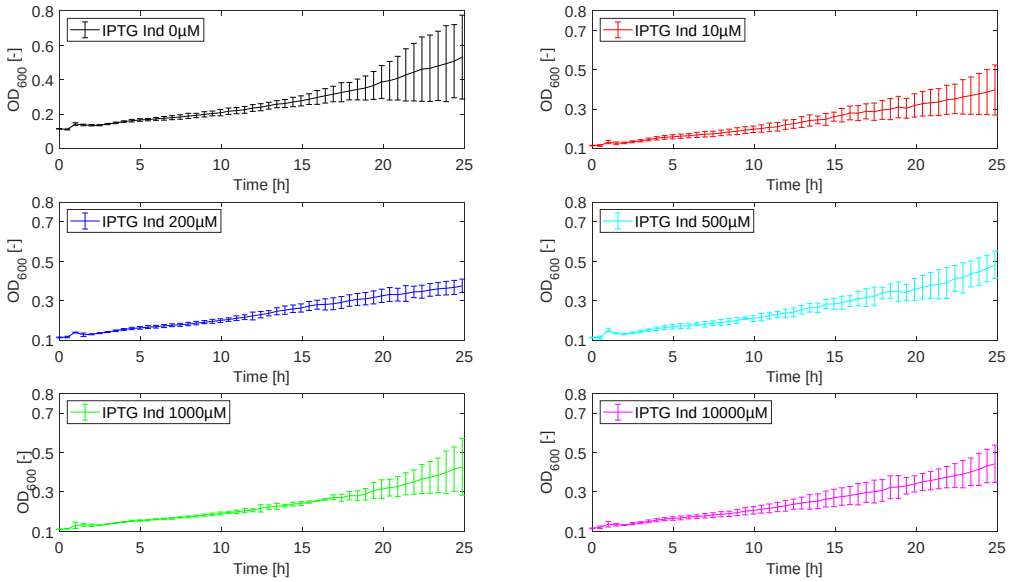

Figure 34: Optical density at 600 nm versus time in hours of IPTG concentration tuning with induced pre-culture at different inducer concentrations.

Figure 33 and Figure 34 and shows IPTG concentrations in the range of 0 µM to 10 mM, with which *Corynebacterium glutamicum* cells were induced. In the case of induced pre-culture in Figure 34, 0.5 mM IPTG was added to the cultivation media. Pre-culture was induced in order to ensure that cells produce enough sensor protein for fluorescence signal evaluation already at the time point of microtiter plate inoculation. Final optical density during this cultivation is around 0.7. In Figure 33 experiments with non-induced pre-culture are shown. In this case optical density maximum is around 0.55. Error deviations of three biological replicates in of non-induced samples are the highest, possible due to the absence of any stress application and the nature of uncontrolled conditions.

Below are presented six graphs with inducer tuning of induced (Figure 35) and six graphs with non-induced (Figure 36) pre-cultures, where intracellular pH versus cultivation time is shown. Here it can be noticed that error deviations in the case of non-induced pre/main-culture are in general smaller

Die approbierte gedruckte Originalversion dieser Diplomarbeit ist an der TU Wien Bibliothek verfügbar.
The approved original version of this thesis is available in print at TU Wien Bibliothek.
TU Bibliothek Your knowledge hub WIEN

than in the case of with 0.5 mM IPTG induced pre-culture and non-induced main culture. This could be explained by a change in metabolic state when the culture is transferred in an inducer free main culture environment, due to inducer absence. Intracellular pH in Figure 35 as well as in Figure 36 is decreasing: in set of non-induced pre-cultures from pH 8.8 to 6.8 and in set of induced pre-cultures from pH 8.2 to 6.8 correspondently. The difficulty of this method is that external pH cannot be measured and therefore pH gradient cannot be evaluated, which does not yield information about pH homeostasis.

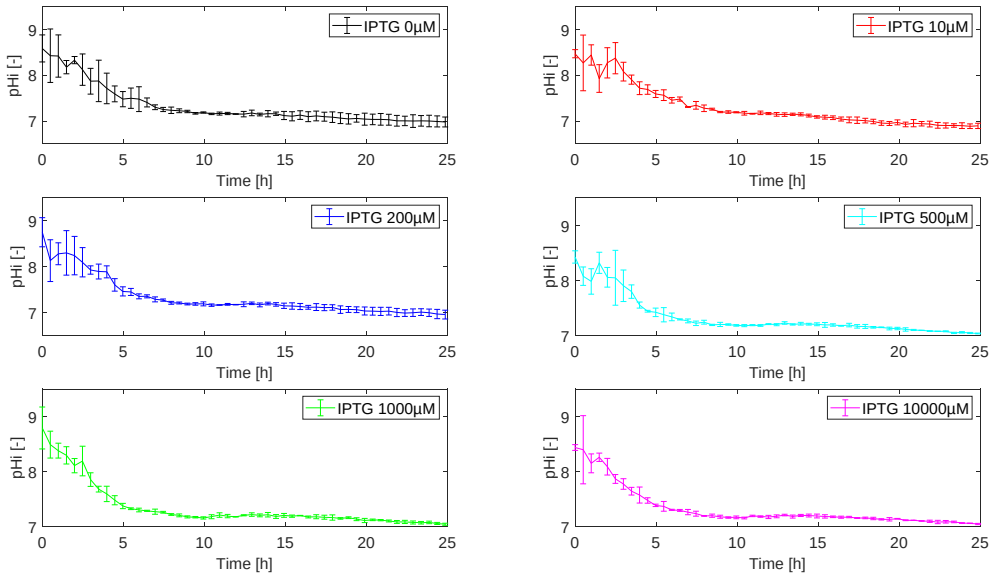

Figure 35: Intracellular pH (pHi) versus time in hours of IPTG concentration tuning with non-induced pre-culture at different inducer concentrations.

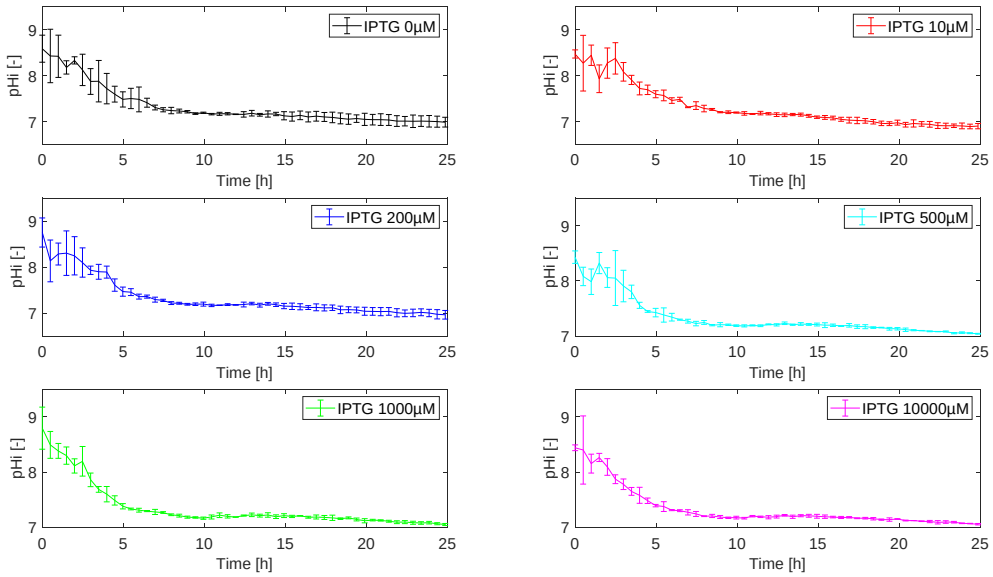

Figure 36: Intracellular pH (pHi) versus time in hours of IPTG concentration tuning with induced pre-culture at different inducer concentrations.

For determination of sufficient inducer concentration in order to estimate intracellular pH, biomass specific sensor production amount was calculated by dividing fluorescence intensity through biomass concentration (CDW), which is shown in Figure 37.

Die approbierte gedruckte Originalversion dieser Diplomarbeit ist an der TU Wien Bibliothek verfügbar.
The approved original version of this thesis is available in print at TU Wien Bibliothek.
TU Bibliothek Your knowledge hub WIEN

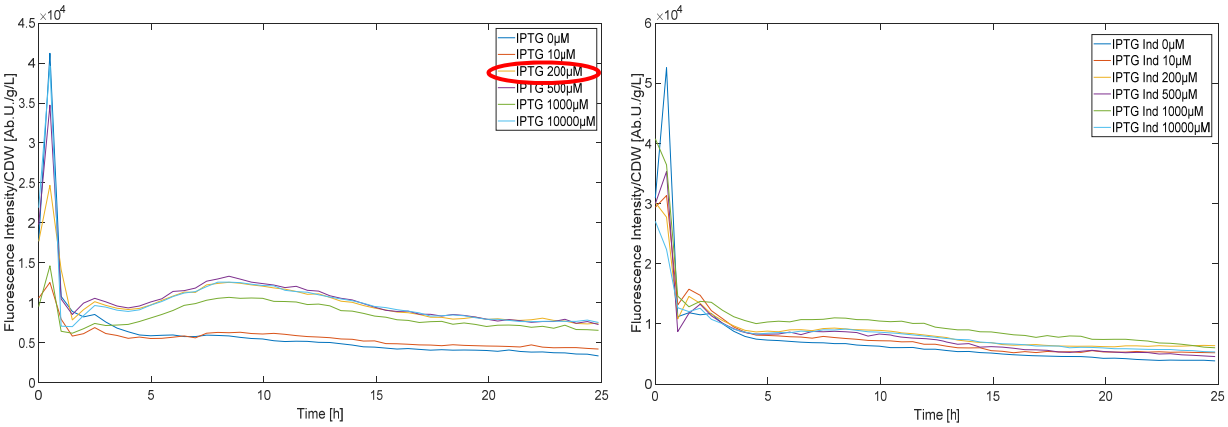

Figure 37: Fluorescence sensor amount versus time in h. Left: IPTG concentration tuning with non-induced pre-culture at different inducer concentrations. Right: IPTG concentration tuning with induced pre-culture at different inducer concentrations.

The effect of different IPTG concentrations on sensor production dynamics can be better recognized in the experimental set of non-induced pre-culture. Therefore, concerning cultivation with non-induced pre-culture in Figure 37, the highest production of pHluorin sensor is at following IPTG concentrations: 10 mM, 0.5 mM and 200 µM. As the goal was to find the lowest inducer concentration, which is needed to be added for sufficient sensor expression, 200 µM IPTG addition is the most compatible option.

In Figure 38, Figure 39 and Figure 40 are presented the graphs, which correspond to the experimental set, where pre-culture and main culture was induced with 0.5 mM IPTG with addition of Penicillin G in the range of 150 U/L – 1150 U/L. This range of concentrations was applied in order to investigate behavior of intracellular pH and the differences of cell growth inhibition after applying stress conditions. Optimal Penicillin G concentration reported in literature to induce glutamate expression is 750 U/L (Schultz, 2007).

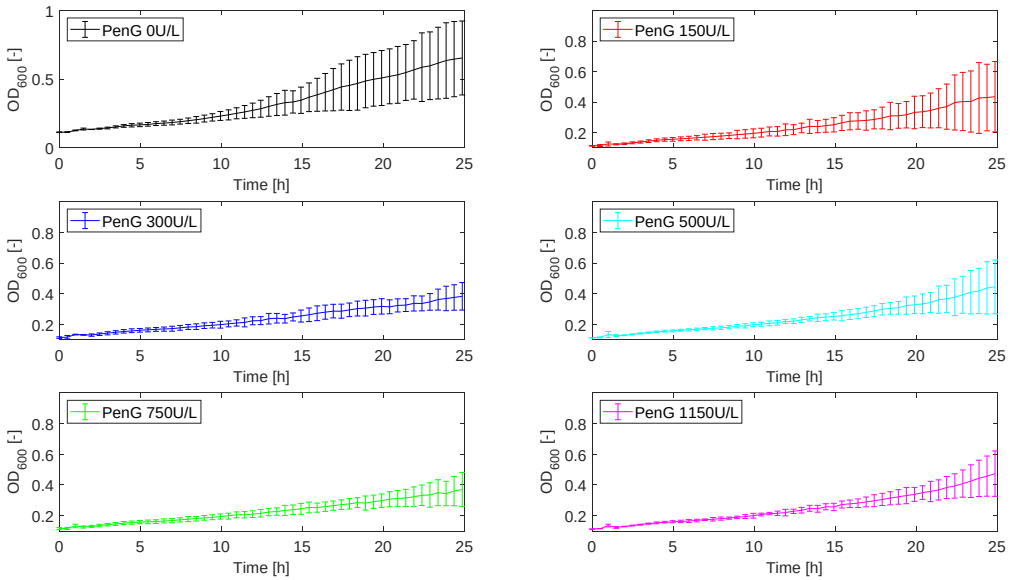

Figure 38: Optical density at 600 nm versus time in hours of experimental set with induced pre- and main culture (0.5 mM IPTG) and addition of different concentrations of Penicillin G in the range of 150 U/L – 1150 U/L.

Die approbierte gedruckte Originalversion dieser Diplomarbeit ist an der TU Wien Bibliothek verfügbar.
The approved original version of this thesis is available in print at TU Wien Bibliothek.
TU Bibliothek Your knowledge hub WIEN

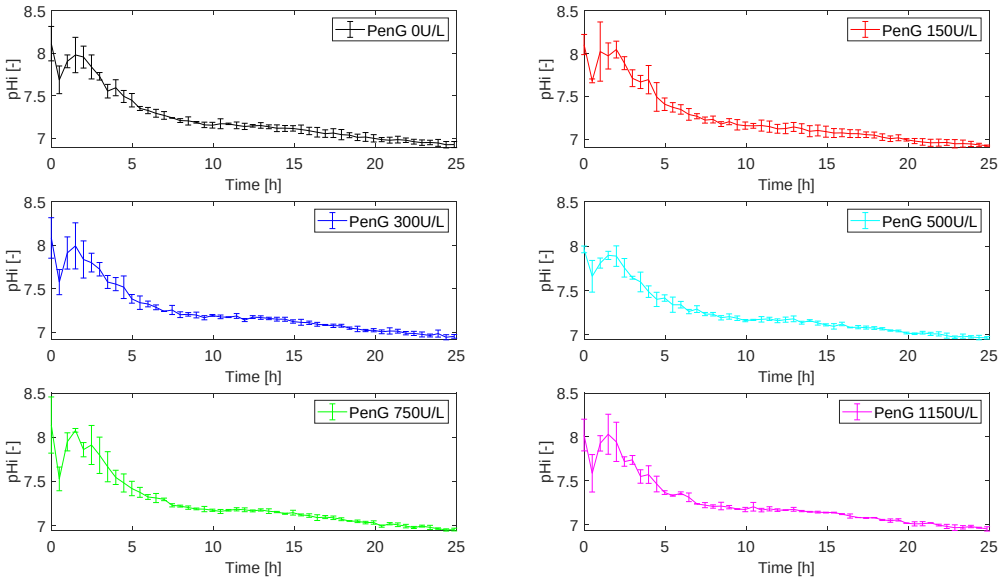

Figure 39: Intracellular pH versus time in hours of experimental set with induced pre- and main culture (0.5 mM IPTG) and addition of different concentrations of Penicillin G in the range of 150 U/L – 1150 U/L.

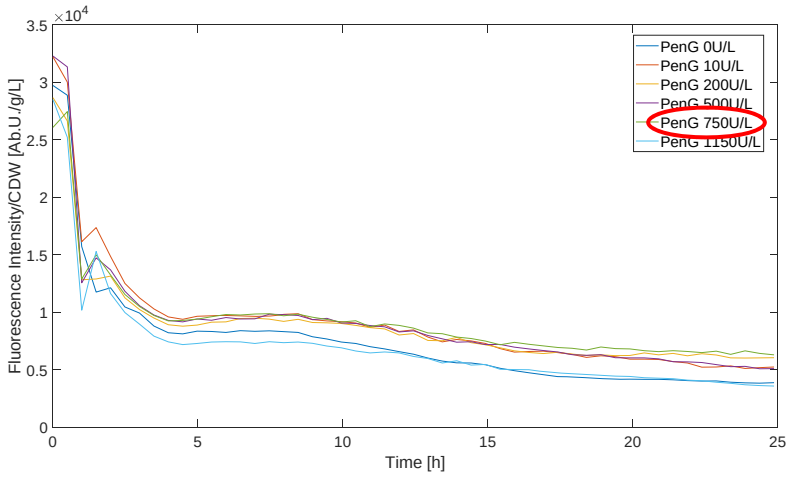

Figure 40: Biomass specific fluorescence amount versus time in hours of experimental set with induced pre- and main culture (0.5 mM IPTG) and addition of different concentrations of Penicillin G in the range of 150 U/L – 1150 U/L.

Figure 38 represents six graphs of optical density, measured at 600 nm, at different concentrations of Penicillin G added, whereas Figure 39 shows six graphs of intracellular pH, calculated with the help of fluorescence ratios (396/474), and Figure 40 represents the amount of pHluorin, calculated by division of fluorescence intensity through biomass concentration. The highest error deviations in the graph with optical density versus time are in the case of induced pre- and main cultures without any membrane stress induction, due to the absence of membrane disturbance. However, the smallest error deviations can be noticed in the case of addition of 300 U/L and 750 U/L, what means that these Penicillin G concentrations reduces growth rate at similar amounts. Concerning intracellular pH trend in Figure 39, the similar decrease at all applied Penicillin G amounts with approximately identically error bars can be observed. Figure 40 shows the highest biomass specific fluorescent amount at PenG concentrations of 750 U/L. This concentration was applied later for further investigation of the influence of Penicillin G on the production of pHluorin sensor, which was also described for glutamate production in *Corynebacterium glutamicum* by Schultz, 2007.

Die approbierte gedruckte Originalversion dieser Diplomarbeit ist an der TU Wien Bibliothek verfügbar.
The approved original version of this thesis is available in print at TU Wien Bibliothek.
TU Bibliothek Your knowledge hub WIEN

5.4 Tuning of sensor protein expression levels in batch and fed-batch bioreactor cultivations

As it was described in 5.2 and 5.3, no clear conclusion can be made concerning optimal inducer amount for fluorescence sensor expression, due to uncontrolled cultivation conditions during a microplate screening. However, 200 µM IPTG concentration can be taken as upper limit derivable received from high throughput screening. Therefore, for further investigations, five batch and fed-batch bioreactor cultivations were conducted. The overview of them can be observed in Table 31.

Table 31: Cultivation parameters used during five batch and fed-batch cultivations

Bioreactor N°	**1**	**2**	**3**	**4**	**5**
Pre-culture	Not induced	Not induced	Induced with IPTG	Induced with IPTG	Induced with IPTG
Main culture (Batch & Fed-Batch processes)	Not induced	Induced 20 µM IPTG	Induced 20 µM IPTG	Induced 200 µM IPTG	Induced 1 mM IPTG

5.4.1 Intracellular sensor signal

In order to investigate the effects after addition of different inducer concentrations during pre-culture, batch and fed-batch cultivations, fluorescence intensity, intracellular pH, pH gradient, biomass specific sensor signal expression and sensor production rate were calculated, using the calibration equation of linear regression fit.

In Figure 41 fluorescence signal intensities that correspond to production of pHluorin are shown.

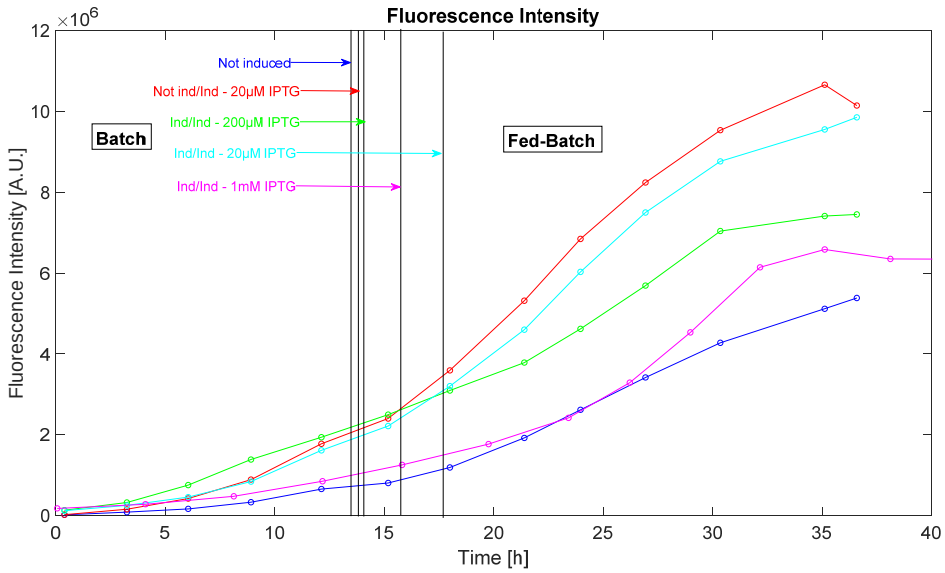

Figure 41: Fluorescence intensity of non-induced cultivation, non-induced pre-culture and induced (20 µM IPTG) main culture cultivation, induced pre- and main culture (200 µM) cultivation, induced pre- and main culture (20 µM) cultivation, induced pre- and main culture (1 mM) cultivation.

Figure 41 shows curve trends of five experiments during batch and fed-batch processes. End of batch phase is indicated by vertical black lines. Batch phase of each process was ended at different time points, when the glucose in the media was consumed completely. With completion of the batch phase the fed-batch with exponential feeding was initialized. It can be observed that fluorescence

Die approbierte gedruckte Originalversion dieser Diplomarbeit ist an der TU Wien Bibliothek verfügbar.
The approved original version of this thesis is available in print at TU Wien Bibliothek.
TU Bibliothek Your knowledge hub WIEN

intensity of the sensor is constantly increasing until a stationary level is reached. The highest fluorescence intensity reached was by addition of 20 µM IPTG.

In Figure 42 calculated intracellular pH (pH_i) and fluorescence spectra at selected process times are presented.

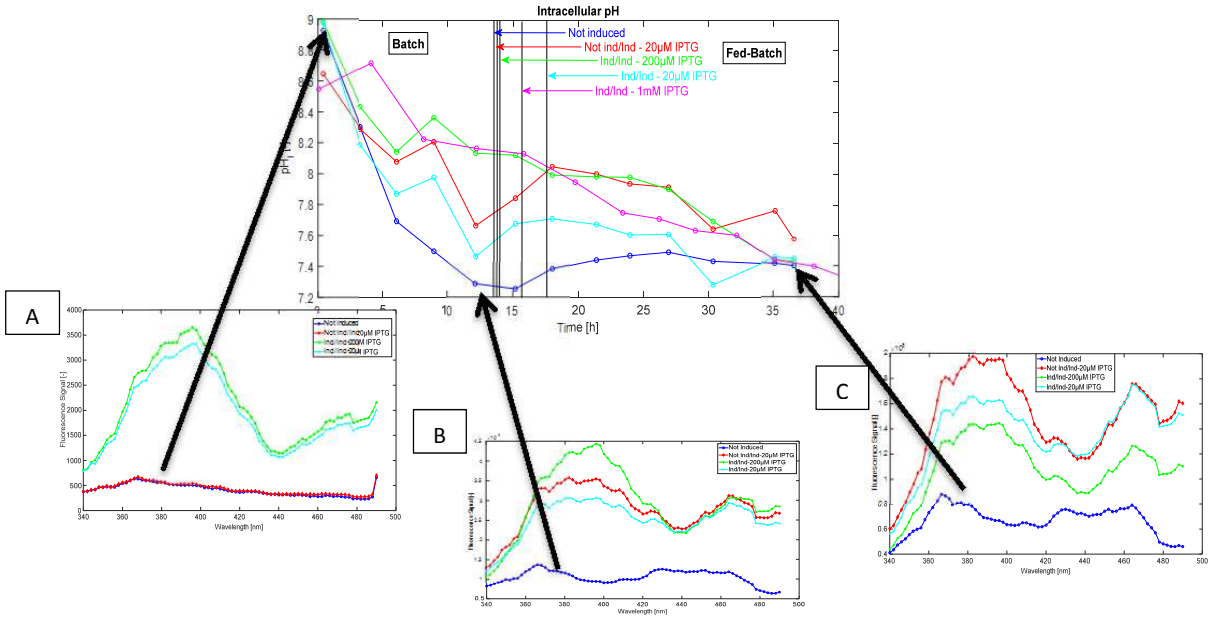

Figure 42: Intracellular pH of not-induced cultivation, non-induced pre-culture and induced (20 µM IPTG) main culture cultivation, induced pre- and main culture (200 µM) cultivation, induced pre- and main culture (20 µM) cultivation, induced pre- and main culture (1 mM) cultivation. A represents graph of fluorescence signals of the first batch samples, B shows fluorescence signals of the last batch samples and C represents fluorescence signals of the last fed-batch samples.

As it can be observed in Figure 42, at the beginning of batch process, measured pH values exceed the calibration pH range. A possible explanation could be the uncontrolled conditions during pre-culture cultivation. The expected value at the end of pre-culture was expected to be slightly above 7, due to adjusted pH 7 for cultivation medium. During batch and fed-batch cultivations, the external pH set point was also 7. As it can be observed, the intracellular pH trend goes down, in order to possibly reach pH homeostasis. Fluorescence spectra at different process time points show that fluorescence intensity increased with the time for all cultivations. The spectra labeled as "A" shows two un-induced samples. However they represent high intracellular pH value even though possibly only auto-fluorescence signal could be observed. In the spectra labeled with "B", at the end of the batch phase, fluorescence signal of the sensor under addition of inducer increases, whenever, this was not the case for the non-induced bioreactor run. However, the spectra marked with "C", at the end of fed-batch phase, does show the fluorescence signal of the un-induced sample along with induced bioreactor cultivations. The assumptive argumentation of it could be a possible leakage of *tac*-promoter, which can cause protein production without IPTG induction.

In Figure 43 pH gradient is presented. The pH gradient was calculated out of external pH (controlled parameter with set up 7) and intracellular pH.

Die approbierte gedruckte Originalversion dieser Diplomarbeit ist an der TU Wien Bibliothek verfügbar.
The approved original version of this thesis is available in print at TU Wien Bibliothek.
TU Bibliothek Your knowledge hub WIEN

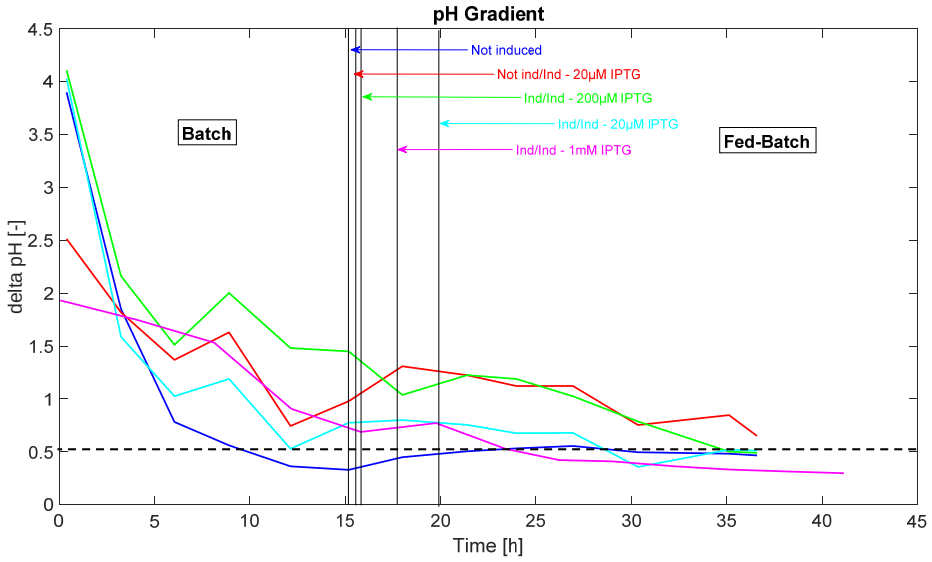

Figure 43: pH gradient calculated out of intracellular and extracellular pH. The results are presented for non-induced cultivation, non-induced pre-culture and induced (20 µM IPTG) main culture cultivation, induced pre- and main culture (200 µM) cultivation, induced pre- and main culture (20 µM) cultivation, induced pre- and main culture (1 mM) cultivation.

In Figure 43 the first sampling results can be neglected, according to a possible explanation of uncontrolled conditions during pre-culture cultivation. The trend remains decreasing to the hypothetical pH-optimum value of 0.5, however, going later below it when the cells in culture start to lose their viability, like in the case of induction with 1 mM IPTG (due applied high induction concentration). The value of 0.5 was considered as optimum, according to reported authentic intracellular and extracellular pH values by Ochrombel, 2011. However, further investigations about pH-optimum value of recombinant *Corynebacterium glutamicum* need to be conducted.

In order to calculate biomass specific fluorescence amount, fluorescence intensity was divided through cell dry weight. The results are presented in Figure 44.

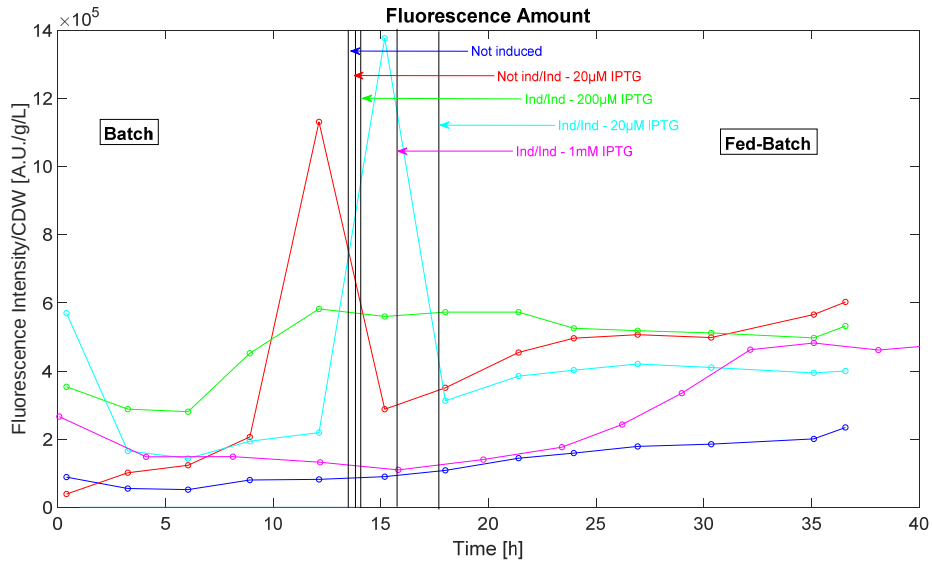

Figure 44: Biomass specific fluorescence amount of non-induced cultivation, non-induced pre-culture and induced (20 µM IPTG) main culture cultivation, induced pre- and main culture (200 µM) cultivation, induced pre- and main culture (20 µM) cultivation, induced pre- and main culture (1 mM) cultivation.

Die approbierte gedruckte Originalversion dieser Diplomarbeit ist an der TU Wien Bibliothek verfügbar.
The approved original version of this thesis is available in print at TU Wien Bibliothek.
TU Bibliothek Your knowledge hub WIEN

Figure 44 shows that cultivation induced with 200 µM IPTG possesses the highest fluorescence amount. However, two cultivations with 20 µM IPTG induction show a peak of biomass specific fluorescence amount at 12 h (red line) and 15 h (turquoise line). This event can be related to batch phase end and could be caused by ongoing translation and delayed chromophore maturation of already translated sensor protein (Balleza, 2018).

Figure 45 shows the fluorescence production rate - q_p, which shows similar results as fluorescence amount trends in Figure 44. Equation 7 and Equation 8 were applied for production rate calculation:

Equation 7

$$r_p = \frac{\Delta\, Fluorescence\ Intensity}{\Delta t}$$

Equation 8

$$q_p = \frac{r_p}{X_{mean}}$$

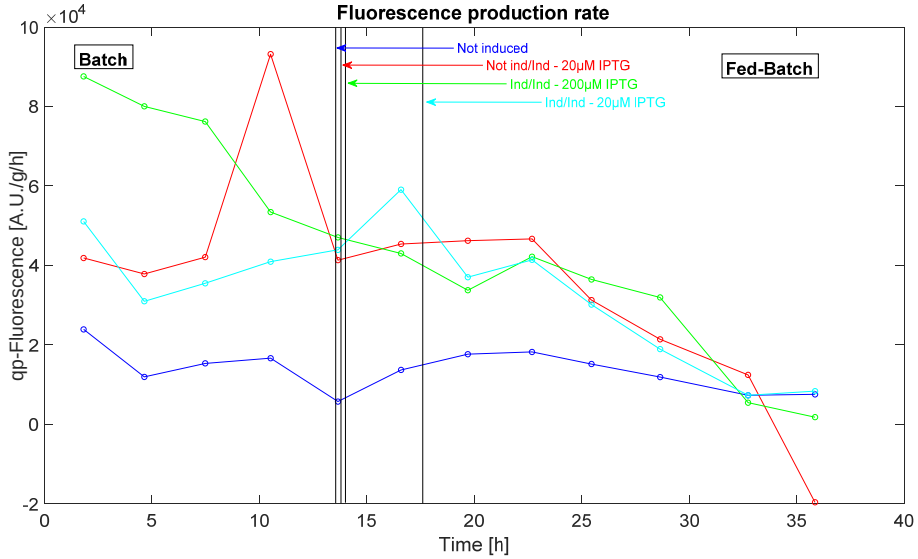

Figure 45: Fluorescence production rate of non-induced cultivation, non-induced pre-culture and induced (20 µM IPTG) main culture cultivation, induced pre- and main culture (200 µM) cultivation, induced pre- and main culture (20 µM) cultivation.

Fluorescence production rate trends remain decreasing for all cultivations. Figure 45 shows the highest value for the bioreactor run with 20 µM IPTG induced main culture and un-induced pre-culture. Comparing with Figure 44, the highest peak of biomass specific fluorescence amount occurred in the cultivation with 20 µM IPTG induced main culture and induced pre-culture. The possible reason of peak occurrence could be the end of the batch phase, when cells were undergoing substrate limitation. However, cultivation induced with 200 µM IPTG shows the highest initial fluorescence amount in Figure 44 along with highest fluorescence production rate in Figure 45 (excluding two peaks at the end of batch). Nevertheless, trends of production efficiency of induced bioreactor cultivations declined fast, showing the lowering of fluorescence production rate. Concerning non-induced cultivation, q_p response can be observed, despite the absence of the inducer.

Die approbierte gedruckte Originalversion dieser Diplomarbeit ist an der TU Wien Bibliothek verfügbar.
The approved original version of this thesis is available in print at TU Wien Bibliothek.

In Figure 46 the interrelationship between fluorescence amount and IPTG concentration added during batch cultivations can be observed.

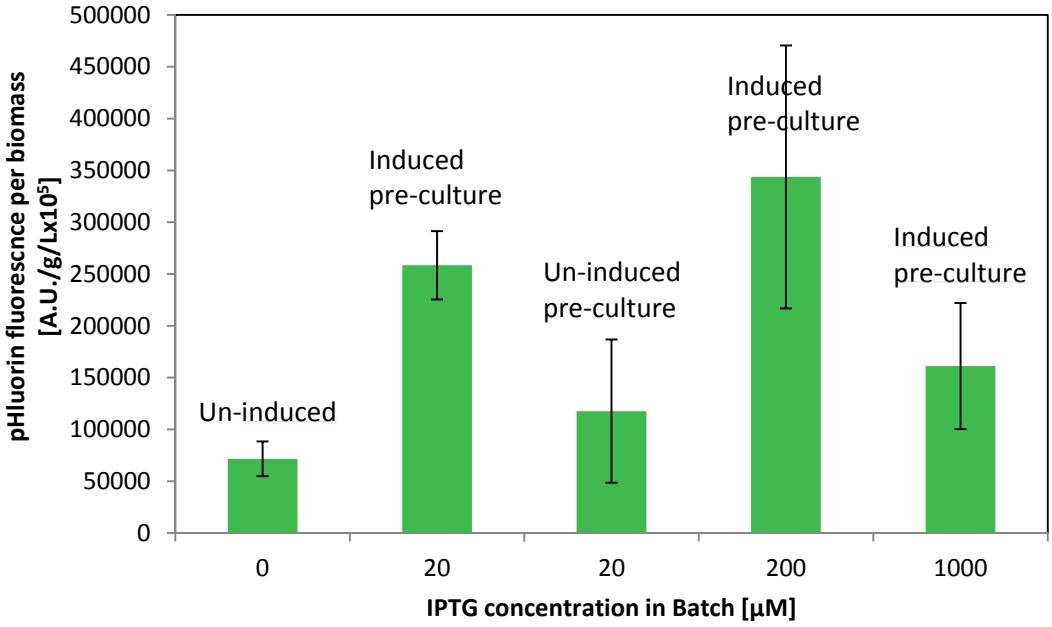

Figure 46: Interrelationship between pHluorin fluorescence per biomass and IPTG concentration added during batch cultivations. Errors bars represent variability in fluorescence level during the entire process time course.

Error bars in Figure 46 were calculated with the help of standard deviation of all fluorescence measurement points, representing variability over the whole process. The smallest error bar represents the cultivation induced with 20 µM IPTG in main culture and induced pre-culture, showing the most beneficial cultivation with poor variability during the process. In Figure 46 is demonstrating that the highest fluorescence amount is reached with induced pre-culture and induced main culture at 200 µM IPTG. However, induced main culture with 1 mM showed smaller fluorescence sensor amount than the one induced with 200 µM, or the cultivation induced with 20 µM IPTG. This novel fact can indicate that application of higher inducer concentration does not give a stronger sensor signal per biomass, but can cause additional stress which inhibits efficient protein production. Not induced cultivation also shows fluorescence signal, due to possible leakage of *tac*-promotor and auto-fluorescence. Not induced pre-culture and with 20 µM IPTG induced main culture reveal poor fluorescence amount production and high variability of sensor signal per biomass. Therefore these results demonstrate that higher fluorescence amount can be reached with induced pre-culture and soft IPTG induction levels.

In Figure 47 shows maximum growth rate (μ_{max}) in dependence of different IPTG induction conditions.

Die approbierte gedruckte Originalversion dieser Diplomarbeit ist an der TU Wien Bibliothek verfügbar.
The approved original version of this thesis is available in print at TU Wien Bibliothek.

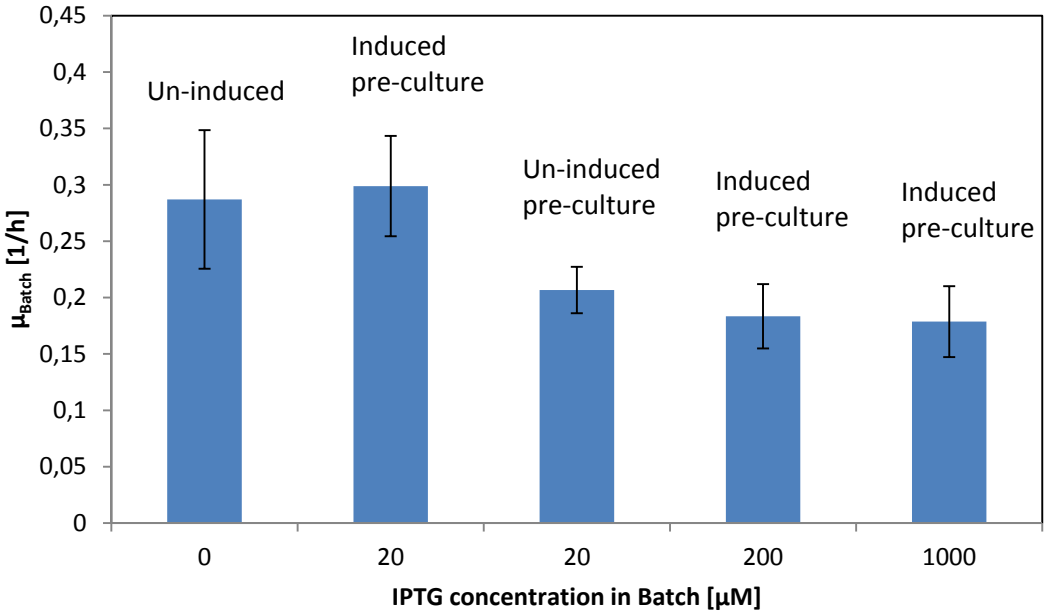

Figure 47: Maximum growth rate (μ_{max}) in dependence of different IPTG induction conditions. Error bars based on error propagation of measurement errors.

In Figure 47 can be recognized that induced pre-culture and with 20 µM IPTG induced main culture demonstrate the highest maximum growth rate during batch phase. Bioreactor cultivation without any induction shows relatively high growth rate. This was expected, due to the absence of stress condition like inducer addition. Non-induced pre-culture and with 20 µM IPTG induced main culture cultivation in comparison to the cultivation with induced pre-culture represents lower maximum growth rate, determining that induced pre-culture is more beneficial for growth rate and pHluorin production. Induced pre-cultures and with 200 µM /1 mM IPTG induced batch cultivations show similarly low maximum growth rate. This result met the expectations, because of high inducer concentration addition and production of fluorescence sensor protein. Conclusively, 20 µM IPTG concentration is sufficient to provide adequate fluorescent signal, minimizing the metabolic load on the strain.

5.4.2 Extracellular sensor signal

Extracellular sensor signal was measured in the form of supernatant after sample centrifugation. The results of pHluorin fluorescence intensity, biomass specific fluorescence amount and fluorescence production rate concerning the external signal are presented below.

Figure 48 shows fluorescence intensity of the signal in the supernatant. It can be recognized that intensity is increasing with the time. The same could be observed in Figure 41, but in a difference of magnitude, meaning that less sensor signal was present extracellular.

Die approbierte gedruckte Originalversion dieser Diplomarbeit ist an der TU Wien Bibliothek verfügbar.
The approved original version of this thesis is available in print at TU Wien Bibliothek.

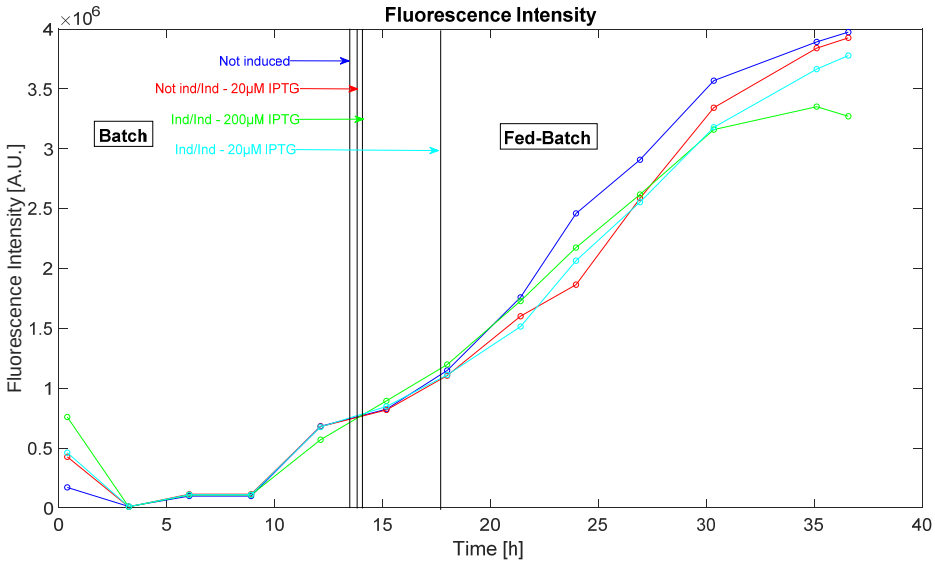

Figure 48: Fluorescence intensity of extracellular sensor of non-induced cultivation, non-induced pre-culture and induced (20 µM IPTG) main culture cultivation, induced pre- and main culture (200 µM) cultivation, induced pre- and main culture (20 µM) cultivation.

Figure 49 and Figure 50 show fluorescence amount in the supernatant available and fluorescence production rate respectively. Both trends of biomass specific fluorescence amount and q_p remain similar to intracellular sensor signal (5.4.1), however in a smaller scale.

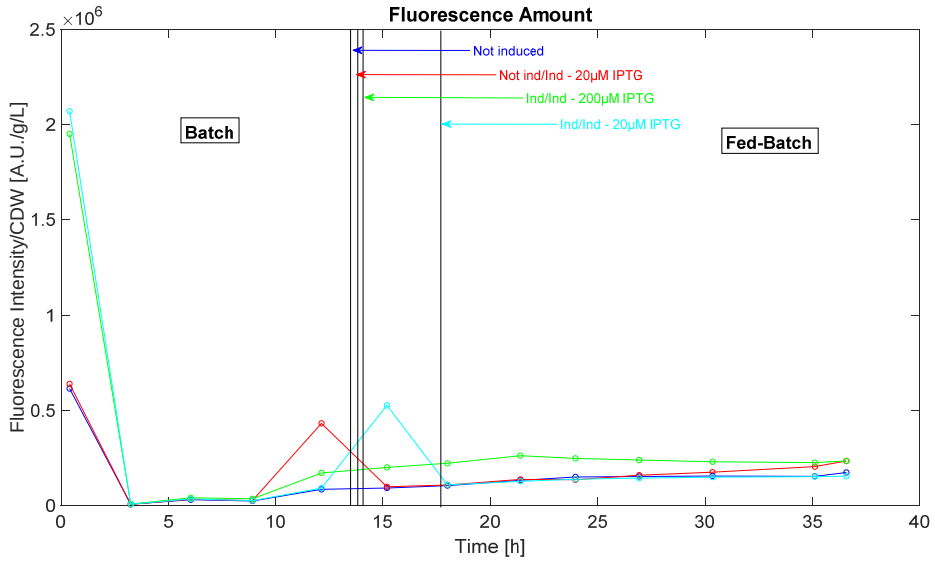

Figure 49: Biomass specific fluorescence amount of non-induced cultivation, non-induced pre-culture and induced (20 µM IPTG) main culture cultivation, induced pre- and main culture (200 µM) cultivation, induced pre- and main culture (20 µM) cultivation.

Die approbierte gedruckte Originalversion dieser Diplomarbeit ist an der TU Wien Bibliothek verfügbar.
The approved original version of this thesis is available in print at TU Wien Bibliothek.

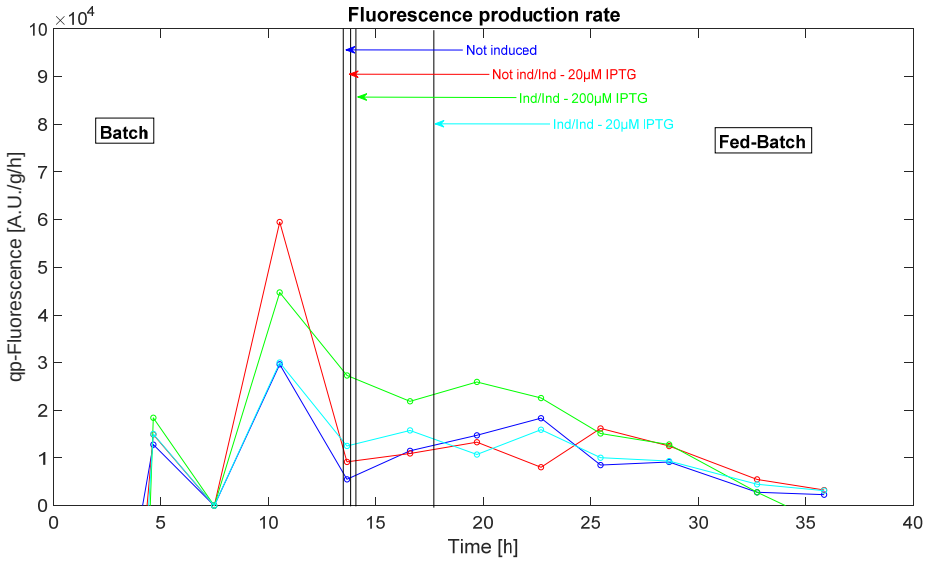

Figure 50: Fluorescence production rate of non-induced cultivation, non-induced pre-culture and induced (20 µM IPTG) main culture cultivation, induced pre- and main culture (200 µM) cultivation, induced pre- and main culture (20 µM) cultivation.

In a conclusion can be said that fluorescence signal can be detected extracellularly. Additionally to potential pHluorin leakage into the medium during the process, supernatant sample preparation and centrifuging could possibly lead to the cell breakage. According to the obtained results, lower fluorescence signal in the supernatant in comparison to intracellular fluorescence signal could be observed, what was also investigated by Delvigne, 2011.

5.4.3 Relation of carbon dioxide evolution rate and pH gradient

The following Figure 51 represents interrelations of carbon dioxide evolution rate and pH gradient.

Die approbierte gedruckte Originalversion dieser Diplomarbeit ist an der TU Wien Bibliothek verfügbar.
The approved original version of this thesis is available in print at TU Wien Bibliothek.

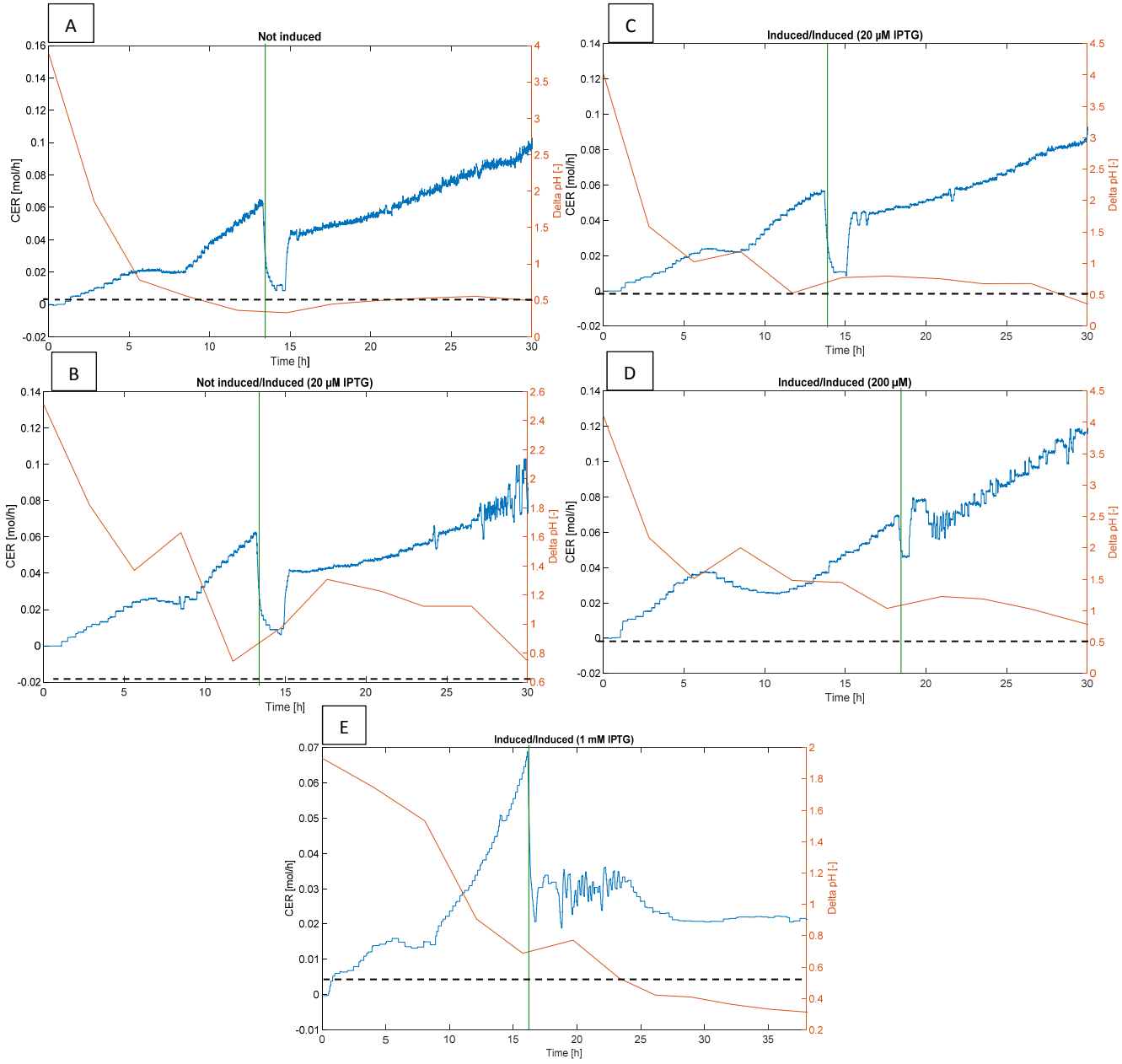

Figure 51: Relation ΔpH to Carbon Dioxide Evolution Rate (CER) against time of non-induced cultivation (A), non-induced pre-culture and induced (20 µM IPTG) main culture cultivation (B), induced pre- and main culture (20 µM) cultivation (C), induced pre- and main culture (200 µM) cultivation (D), induced pre- and main culture (1 mM) cultivation (E). Green lines separate batch and fed-batch phases.

In Figure 51 dashed lines represent hypothetical pH optimum of approximately 0.5 based on finding of Ochrombel, 2011. The graph labeled "A" shows un-induced process. In this case calculation of pH gradient becomes more challenging, due to the lack of inducer, which leads to a lack of pHluorin sensor strength at the initial phase of the batch process. However, at the start of fed-batch leakiness of the promoter already resulted in sufficient sensor signal for pH estimation. Therefore, pH gradient could reach optimum, because inducer as additional stress condition was not applied. The graph labeled as "B" represents non-induced pre-culture and with 20 µM IPTG induced main culture. Here can be seen that by the end of the batch phase with proceeding substrate limitation, pH gradient goes down and at around 12 hours of cultivation starts to increase again. However, carbon dioxide evolution rate was increasing, while having sufficient carbon source for growing, and drops down, when undergoes carbon limitation. The drop of ΔpH happens prior the one of CER, earlier indicating the change in metabolic flux. After end of the batch phase and later exponential addition of glucose, CER stabilizes and goes up again. Concerning pH gradient, it increases upon start of fed batch process

Die approbierte gedruckte Originalversion dieser Diplomarbeit ist an der TU Wien Bibliothek verfügbar.
The approved original version of this thesis is available in print at TU Wien Bibliothek.
TU Bibliothek Your knowledge hub WIEN

conditions, representing a changed environment for cells, and decreases to achieve again the balance between extracellular and intracellular pH. The graph labeled “C” represents induced pre-culture and with 20 µM induced main culture cultivation. In this case the same trend of CER (growing up) and pH gradient (being dropped) by the end of the batch phase as in previously described cultivation can be observed. However, the trend of pH gradient goes up and afterwards down, reaching a pH gradient close to 0.5, what occurs a lot smoother than in the case of non-induced pre-culture. The same can be said about carbon dioxide evolution rate trend, underlining sufficiently reduced metabolic load for a stable cultivation process. This effect demonstrates again the positive effect of induced pre-culture. In the graph marked “D”, the relation of pH gradient and CER in induced pre-culture and with 200 µM IPTG induced main culture cultivation can be observed. The batch process of this cultivation has taken longer as shown in Figure 47, during which two remarkable interrelations of CER and ΔpH can be identified: at around 6 hours of batch cultivation, carbon dioxide evolution rate decreases which caused an increase and later a decrease of the pH gradient; the same can be also observed by the end of the batch phase. Bioreactor cultivation with 200 µM IPTG addition shows that cells can undergo applied inducer concentration without decrease in carbon dioxide evolution rate. However, small amount of inducer is more beneficial for better cell viability. The graph labeled “E” describes induced pre-culture and with 1 mM IPTG induced main culture cultivation. Similar as in the above described cultivations interrelations of pH gradient and CER can be observed. It can be noticed that CER signal after end of the batch phase cannot go up again and starts to decrease. pH gradient maintains developed conditions, however the drop occurs and the trend goes below hypothetical pH optimum. This bioreactor cultivation shows that 1 mM IPTG concentration is too intense for the cells to maintain appeared stress condition.

Consequently, according to Figure 51 and Figure 47, representing correlation between μ_{max} and biomass specific fluorescence amount, induced pre-culture and addition of 20 µM IPTG during main culture remains the optimized condition to produce sufficient pHluorin amount while minimizing the applied cellular stress.

5.4.4 Correlation of substrate uptake rate and pH gradient

In order to monitor process variables during bioreactor cultivation with the help of intracellular pH, correlation between them need to be obtained. Therefore, dependence of substrate uptake rate on pH gradient was investigated. The results are presented below.

Die approbierte gedruckte Originalversion dieser Diplomarbeit ist an der TU Wien Bibliothek verfügbar.
The approved original version of this thesis is available in print at TU Wien Bibliothek.

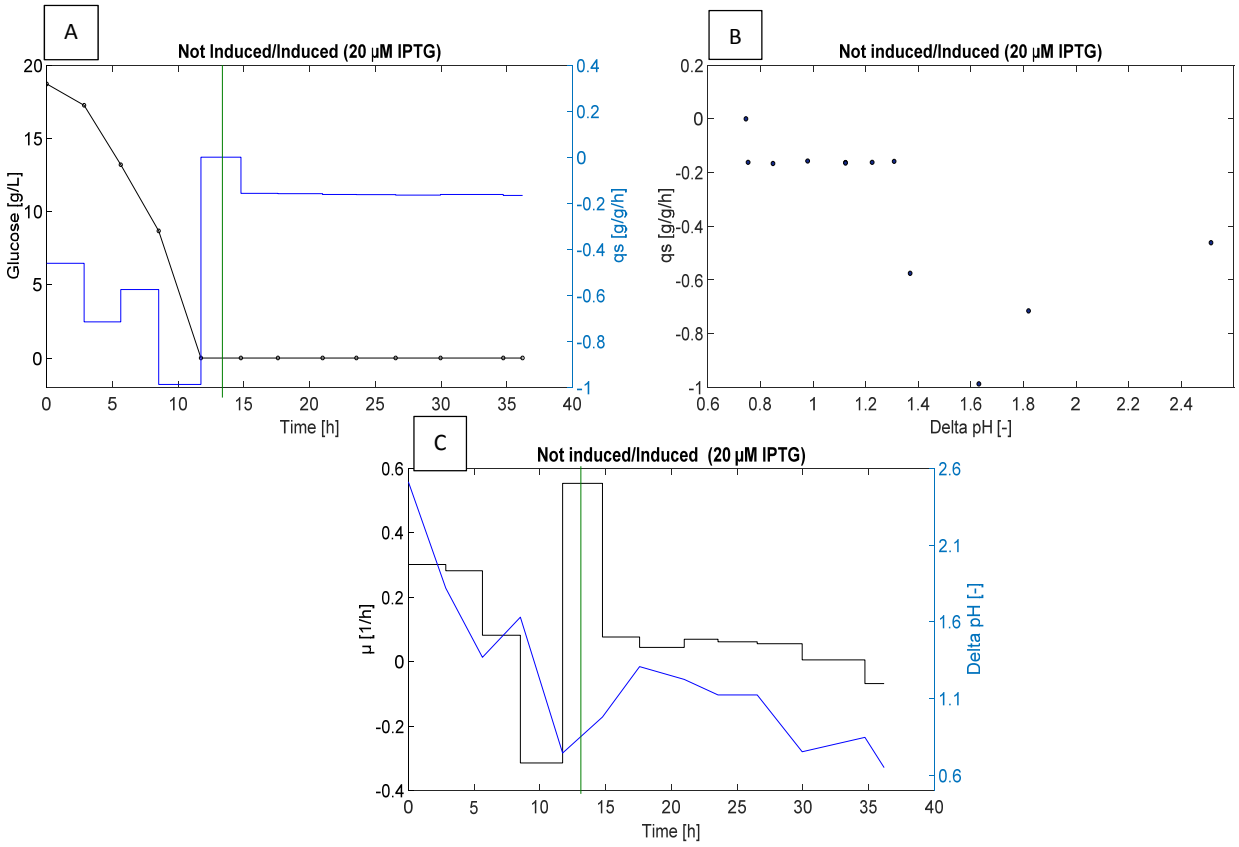

Figure 52: Plot A: substrate uptake rate and glucose concentration against time; Plot B: substrate uptake rate against pH gradient; Plot C: growth rate and pH gradient against time of non-induced pre-culture and with 20 µM IPTG induced main culture cultivation. Green lines separate batch and fed-batch phases.

Figure 52 shows the correlation of q_s with delta pH (B), in addition to trends of glucose consumption and substrate uptake rate versus time (A), and growth rate with ΔpH versus time (C). This bioreactor cultivation had un-induced pre-culture and with 20 µM IPTG induced main culture. From the plot labeled with "A" constant glucose concentration and substrate uptake rate in the fed batch phase can be recognized, without any glucose accumulation. On the scatter plot marked "B", correlation in form of straight line in the ΔpH region of 0.7-1.4 can be observed. With delta pH increment, the data becomes more chaotic, which can be tied to the instability of the cells, when they leave the optimum pH range. The plot labeled "C" shows the trend of pH gradient and growth rate. Correlation in this case was complicated to conduct, due to noise present in the data.

In Figure 53 the correlation of q_s rate and ΔpH of the cultivation with induced pre-culture and induced main culture (200 µM IPTG) is presented. Moreover trends of glucose concentration, substrate uptake rate, growth rate and pH gradient versus time during the cultivation can be found.

Die approbierte gedruckte Originalversion dieser Diplomarbeit ist an der TU Wien Bibliothek verfügbar.
The approved original version of this thesis is available in print at TU Wien Bibliothek.

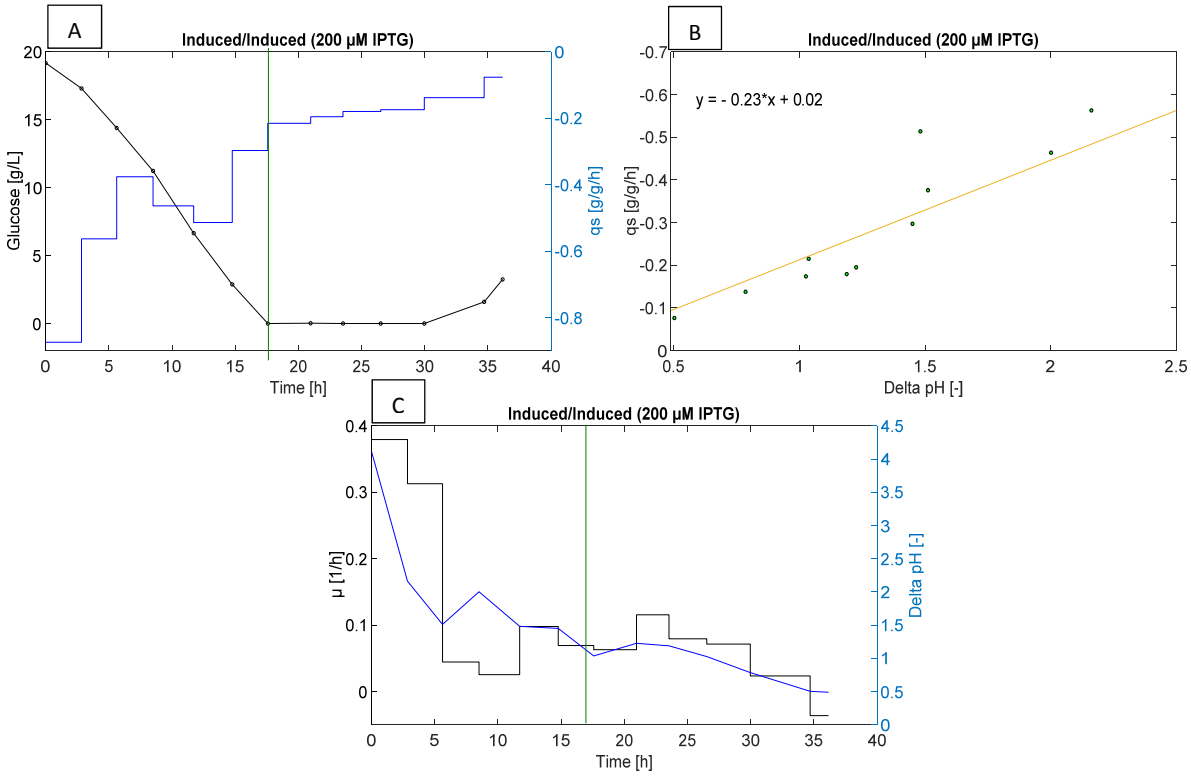

Figure 53: Plot A: Substrate uptake rate and glucose concentration against time; Plot B: substrate uptake rate against pH gradient; Plot C: growth rate and pH gradient against time of induced pre-culture and with 200 µM IPTG induced main culture cultivation. Green lines separate batch and fed-batch phases.

In this cultivation decreasing substrate uptake rate can be recognized ("B") along with glucose accumulation in the graph labeled with "A". The reason of this effect could be high concentration of inducer, leading to culture instability. Nevertheless, linear correlation of ΔpH and q_s can be observed. Moreover, it can be seen that growth rate decreases faster as in the case of 20 µM IPTG induction.

Consequently, further experiments were needed to be conducted in order to investigate the existence and type of the correlation of substrate uptake rate and pH gradient under induction conditions with reduced metabolic load.

Die approbierte gedruckte Originalversion dieser Diplomarbeit ist an der TU Wien Bibliothek verfügbar.
The approved original version of this thesis is available in print at TU Wien Bibliothek.

5.5 Dynamics of pH_i during carbon starvation, external pH changes and Penicillin G addition

Dynamics of pH gradient under external stress conditions: carbon limitation, pH shift and Penicillin G addition were investigated. Therefore, two batch & fed-batch and two batch bioreactor cultivations were conducted in order to determine the existence of relation/correlation between ΔpH and process parameters. The addition of Penicillin G was conducted in order to investigate sensor response and glutamate production of modified *Corynebacterium glutamicum* strain. An overview of cultivations parameters can be found in Table 32.

Table 32: Cultivation parameters used for investigating pH dynamics during carbon starvation, external pH changes and stress addition

Bioreactor N°	1	2	3	4
Pre-culture		**Induced**		
Batch phase	Induction 1 mM IPTG **No extra stress**	Induction 1 mM IPTG **No extra stress**	Induction 20 µM IPTG **pH change (from 7 to 6 and back)**	Induction 20 µM IPTG **Peincillin G addition**
Fed-Batch phase	Induction 1mM **Substrate limitation; pH change (7 to 6)**	Induction 1mM **pH change (from 7 to 6 and back)**		

5.5.1 Batch & Fed-Batch cultivations

During these induced bioreactor cultivations, response of pH gradient on external stress was investigated. Therefore, CER and pH gradient were calculated and compared in order to find interrelations. Results are presented in Figure 54 and Figure 55.

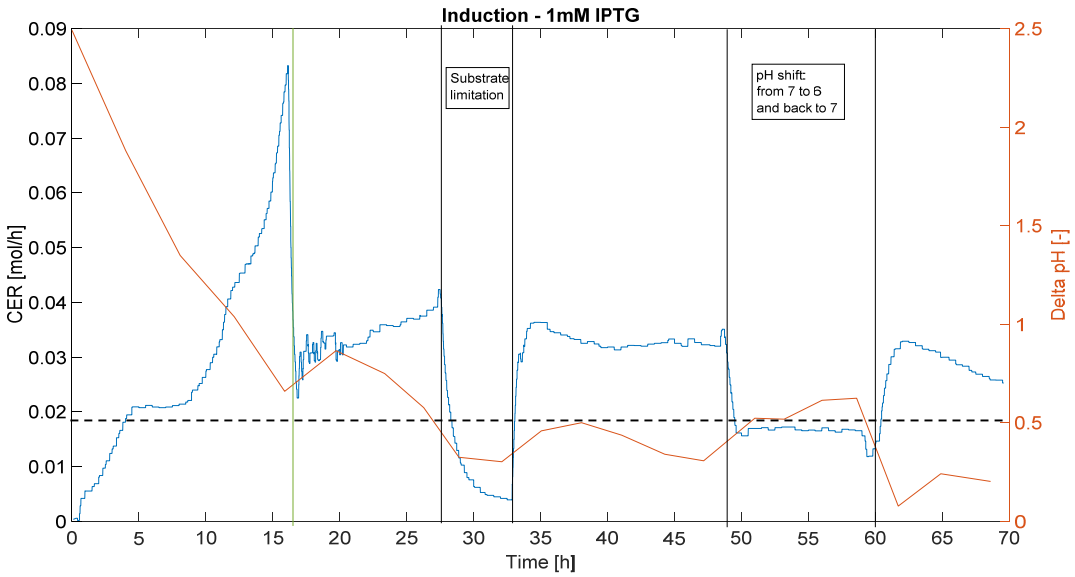

Figure 54: Relation ΔpH to Carbon Dioxide Evolution Rate (CER) against time of induced cultivation (1 mM IPTG) with substrate limitation and pH shift (from 6 to 7 and return). The green line divides batch from fed-batch phase. Dashed line represents hypothetical pH optimum.

Die approbierte gedruckte Originalversion dieser Diplomarbeit ist an der TU Wien Bibliothek verfügbar.
The approved original version of this thesis is available in print at TU Wien Bibliothek.

In Figure 54, relation between carbon dioxide evolution rate and pH gradient can be observed. CER grows during the whole batch phase and rapidly falls when cells meet carbon limitation. At the same time, delta pH decreases to reach the hypothetical optima, but shortly before batch phase end increases in order to handle newly occurred environment. After starting exponential glucose feeding, CER starts to increase. Reaching substrate starvation, CER decreases rapidly and pH gradient drops off below the hypothetical pH optimum. After addition of glucose to the media, delta pH increases, shortly coming to the value of 0.5, but dropping off again, at the same time with not exponential growth of carbon dioxide evolution rate indicating low metabolic activity. This was a result of high inducer concentration, substrate limitation and the inability of the cells to maintain the pH homeostasis. The next deviation conducted was pH shift (from 7 to 6), which occurred at around 48 h of cultivation, where response of CER and ΔpH, can be noticed. After returning to pH 7, cells couldn't come back to the previous state, which can be traced by the linear decrease of CER as well as final lowering of delta pH approaching zero, indicating decrease of the cell viability and eventually termination of the cultivation.

Bioreactor cultivation with batch and fed-batch phases was conducted in order to investigate sensor response, applying only one stress parameter – pH shift. The result is presented in Figure 55.

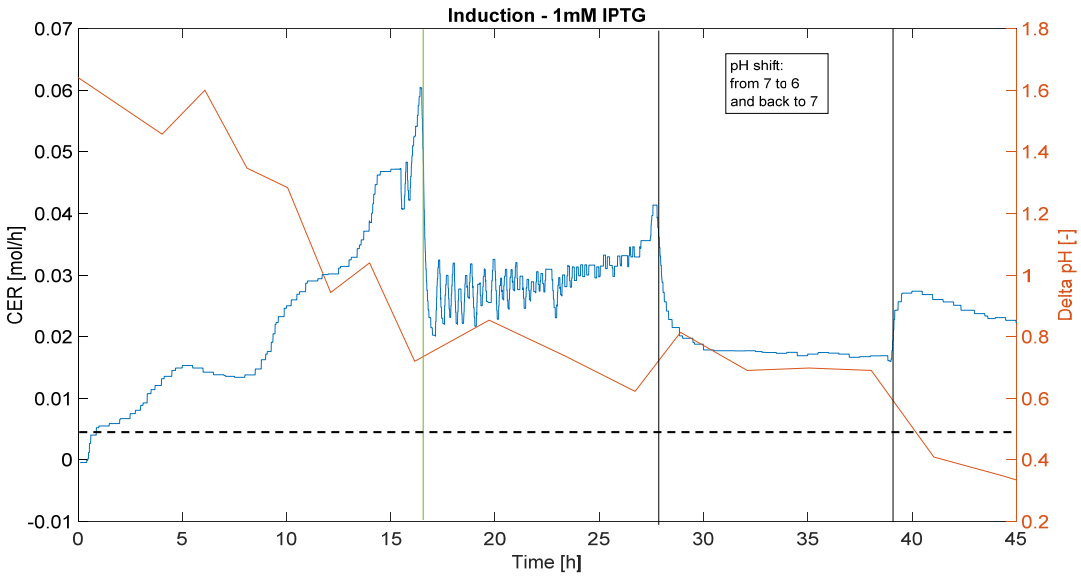

Figure 55: Relation ΔpH to Carbon Dioxide Evolution Rate (CER) against time of induced cultivation (1 mM IPTG) with pH shift (from 6 to 7 and return). The green line divides batch from fed-batch phase. Dashed line represents pH optimum.

Figure 55 presents relation of CER and ΔpH versus process time. Since this bioreactor cultivation was induced with 1 mM IPTG, cells went through additional stress, which can be traced by the trend of the carbon dioxide evolution rate. Response on external pH change during the process can be noticed. As it can be seen, CER signal first decreased, while undergoing pH shift, stayed constant, and later increased when returning to previous pH set up. Delta pH in its turn increased to the value of 0.8 and rapidly decreased to 0.7, where stayed constant for some period of time. After returning to the previous pH of 7, ΔpH dropped off, being below pH optimum. At the same time, CER decreased exponentially indicating the process end, as a breakdown of culture activity. The obtained results affirm that the effect of pH deviation can be traced by means of ΔpH and CER. This cultivation run confirms one more time that application of high inducer concentration leads to the inability of the cells to maintain the pH homeostasis, what leads to decrease of the cells viability.

Die approbierte gedruckte Originalversion dieser Diplomarbeit ist an der TU Wien Bibliothek verfügbar.
The approved original version of this thesis is available in print at TU Wien Bibliothek.
TU Bibliothek Your knowledge hub WIEN

5.5.2 Batch cultivations

In order to give a better understanding of batch cultivations with pH shift and Penicillin G addition, overview of process parameters during the bioreactor runs are presented in Figure 56 and Figure 57 respectively.

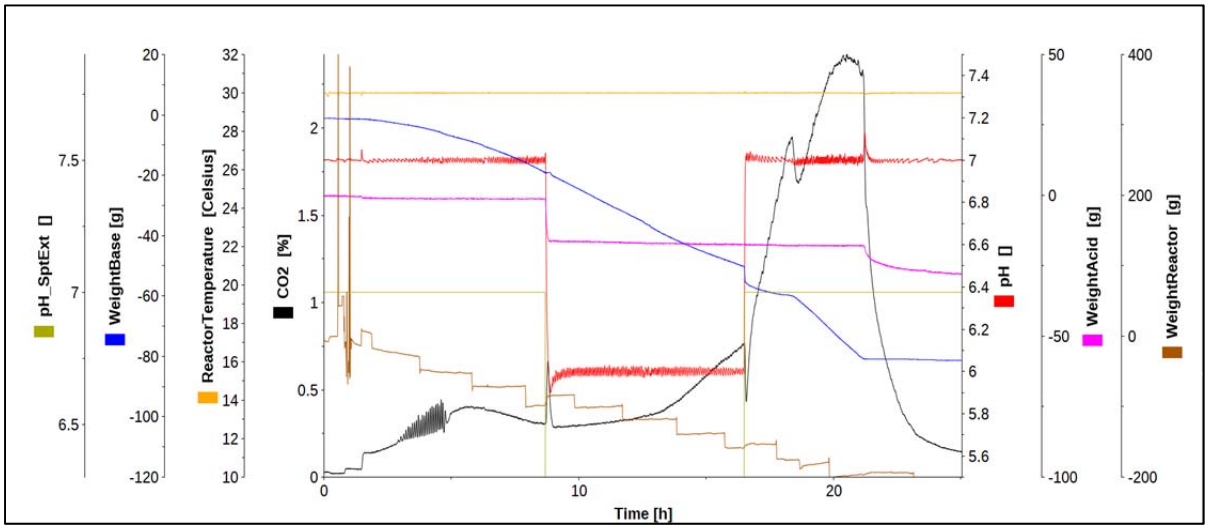

Figure 56: Overview of process parameters during batch phase cultivation with pH shift (from 7 to 6 and back to 7) as stress condition.

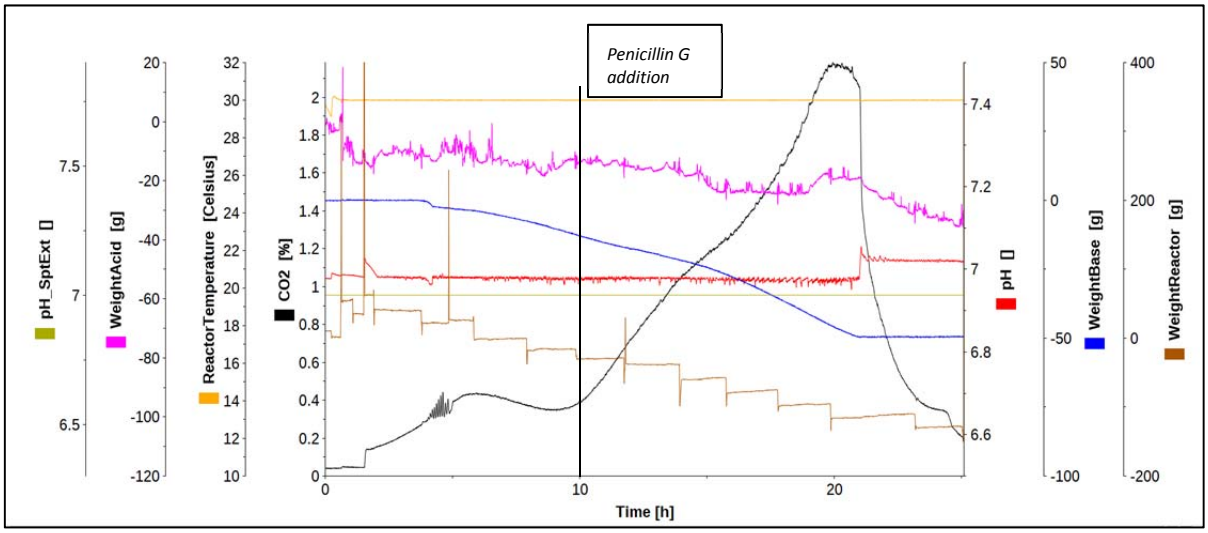

Figure 57: Overview of process parameters during batch phase cultivation with addition of Penicillin G as stress condition. Green line shows the time of Penicillin G addition.

In Figure 56 pH shift from 7 to 6 at 7 hours of cultivation and back to pH 7 at 15 hours of cultivation can be recognized. As a reference, Figure 57 with a constant pH set at 7 is shown. The pH shift relates with the CO_2 signal, which can be noticed by incline and decline of signal during pH change from 7 to 6 and later return to 7. This effect, which occurs very rapidly, can be traced to the change of carbon dioxide solubility. Moreover, higher addition of acid solution, which led to pH decrease, can be noticed. In order to return to pH 7, more base solution was added to the medium. During pH deviation, CO_2 growing slope remains flatter in comparison to the cultivation with Penicillin G addition, indicating decrease of cellular respiration (that obtain energy by breaking down sugars, fats and amino acids with oxygen as part of their metabolism). After change to pH 7, CO_2 concentration in the offgas concentration increases rapidly and exponentially until batch phase comes to the end. In Figure 57 can be seen that with Penicillin G addition carbon dioxide growth trend increased slower,

Die approbierte gedruckte Originalversion dieser Diplomarbeit ist an der TU Wien Bibliothek verfügbar.
The approved original version of this thesis is available in print at TU Wien Bibliothek.
TU Bibliothek Your knowledge hub WIEN

due to cell inhibition and change of metabolic flow for glutamate production. This needs to be further analyzed, e.g. with intracellular flux measurements in future work. Temperature during both processes was maintained constant at 30°C. Stepwise decreasing reactor volume indicates sampling points.

Conclusively can be said that extracellular pH as well as dissolved oxygen were successfully controlled, all the set points were reached what was the basis for the measurements of pH gradient. Figure 56 and Figure 57 represent controlled bioprocess conditions to contrast with shake flask and microplate experiments.

Figure 58 shows glutamate amount produced during batch cultivation with pH shift and batch cultivation with addition of Penicillin G versus cultivation time.

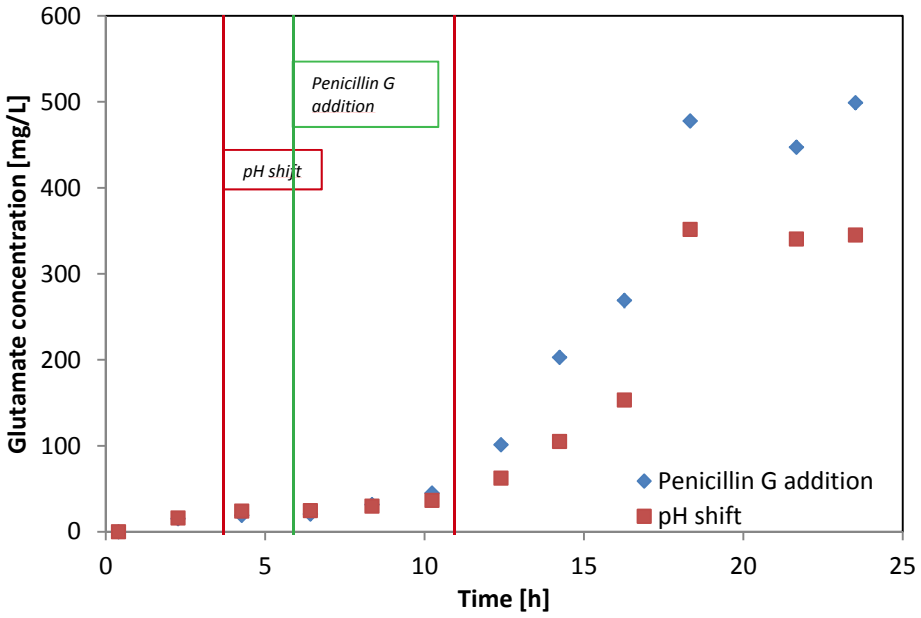

Figure 58: Glutamate production during batch cultivations with addition of Penicillin G and pH shift correspondently.

In Figure 58 can be recognized that with the addition of Penicillin G, glutamate production increased sufficiently. At the end of the processes a glutamate decrease can be observed, due to substrate limitation and metabolization of glutamate as a carbon source for cells survival. Results of these batch cultivations showed higher production of glutamate with the maximum amount of 499 mg/L in comparison to the cultivation with pH deviation with the maximum concentration of 352 mg/L. However produced amounts of glutamate are relatively small, comparing the finding of Eggeling, 2001. Gourdon et. al., 1999 reported the achievemnet of final concentration of 80 g/L glutamate with the means of temperature increase as an inducer factor. The possible reason of a low glutamate production during this study could be the addtion of pEKEx2_*pHluorin* plasmid in the strain and therefore incompatibility of recombinant sensor protein production and glutamate secretion (glutamate efflux process decribed in section 3.5).

5.5.2.1 Intracellular sensor signal

Intracellular sensor signals, like fluorescence intensity, intracellular pH, biomass specific fluorescence amount and fluorescence production rate for batch cultivations with pH shift and Penicillin G addition were calculated correspondently in order to receive better understanding of theirs dependence on external stress factors.

Fluorescence intensity trends are presented in Figure 59.

Die approbierte gedruckte Originalversion dieser Diplomarbeit ist an der TU Wien Bibliothek verfügbar.
The approved original version of this thesis is available in print at TU Wien Bibliothek.
TU Bibliothek Your knowledge hub WIEN

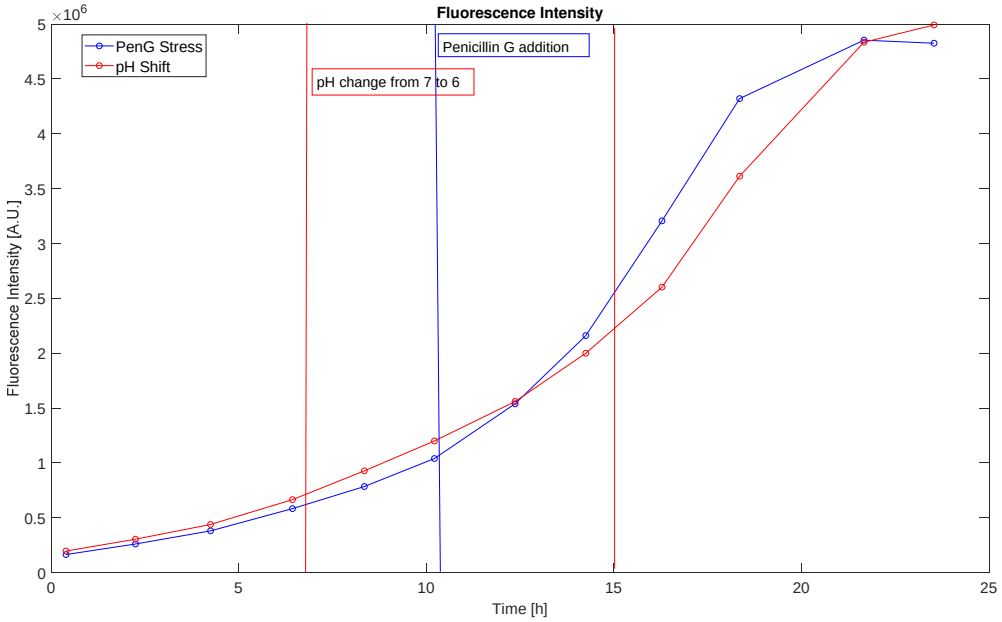

Figure 59: Biomass specific fluorescence intensity. Red marked trend: batch cultivation with pH deviation - pH shift from 7 to 6 and back to 7, illustrated by vertical red lines. **Blue marked trend:** batch cultivation with addition of Penicillin G at 10 hours of the process, illustrated by vertical blue line.

In Figure 59 can be observed that after the shift of pH from 7 to 6, fluorescence intensity became slightly higher than without any pH shift (being kept constant at pH 7). Interestingly, after addition of Penicillin G, sensor intensity became above the intensity trend of pH change. At the end of both batch cultivations, intensities of pHluorin reached the same level. It can be noticed that pH shift from pH 7 to pH 6 can increase the fluorescence intensity of produced sensor (can be further observed in Figure 60). For better understanding, biomass specific fluorescence amount and fluorescence sensor production rate are presented in Figure 60 and Figure 61.

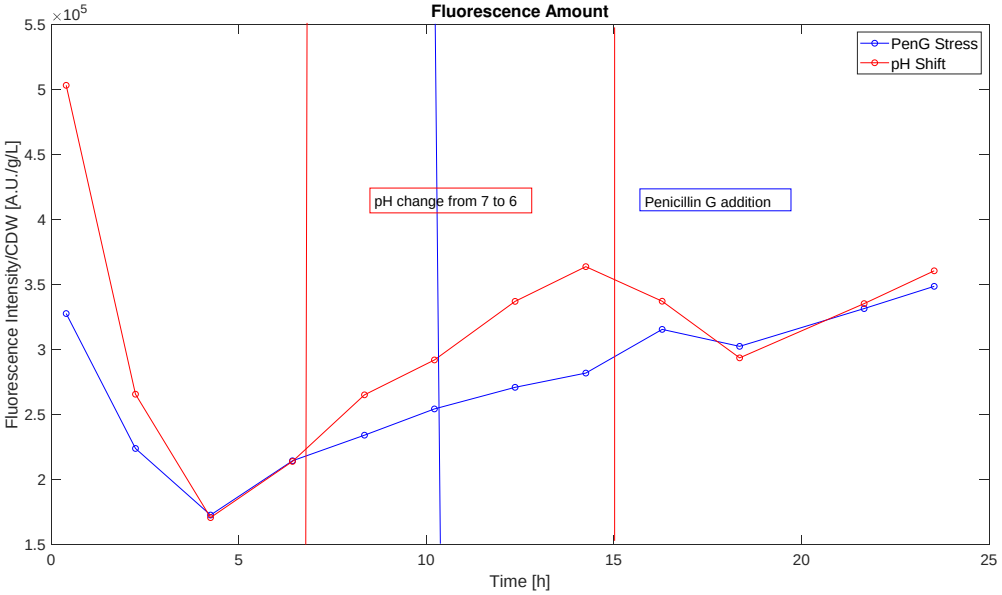

Figure 60: Biomass specific fluorescence amount. Red marked trend: batch cultivation with pH deviation - pH shift from 7 to 6 and back to 7, illustrated by vertical red lines. **Blue marked trend:** batch cultivation with addition of Penicillin G at 10 hours of the process, illustrated by vertical blue line.

Die approbierte gedruckte Originalversion dieser Diplomarbeit ist an der TU Wien Bibliothek verfügbar.
The approved original version of this thesis is available in print at TU Wien Bibliothek.

Results of first sampling points can be neglected, according to a possible explanation of uncontrolled conditions during pre-culture cultivation and measurement error of cell dry weight at the beginning of cultivation. In Figure 60 the trend of batch cultivation with pH deviation shows that biomass specific fluorescence amount after pH change to 6 increased rapidly, but decreased later, due to shift back to pH 7. The possible reason for decrease and further increase could be adaptation to new surrounding environment, adjustment for pH homeostasis, and/or higher expression, translation and correct chromophorically maturation of the sensor protein. However, Penicillin G addition did not give remarkable deviations in biomass specific fluorescence amount, except of flatter slope.

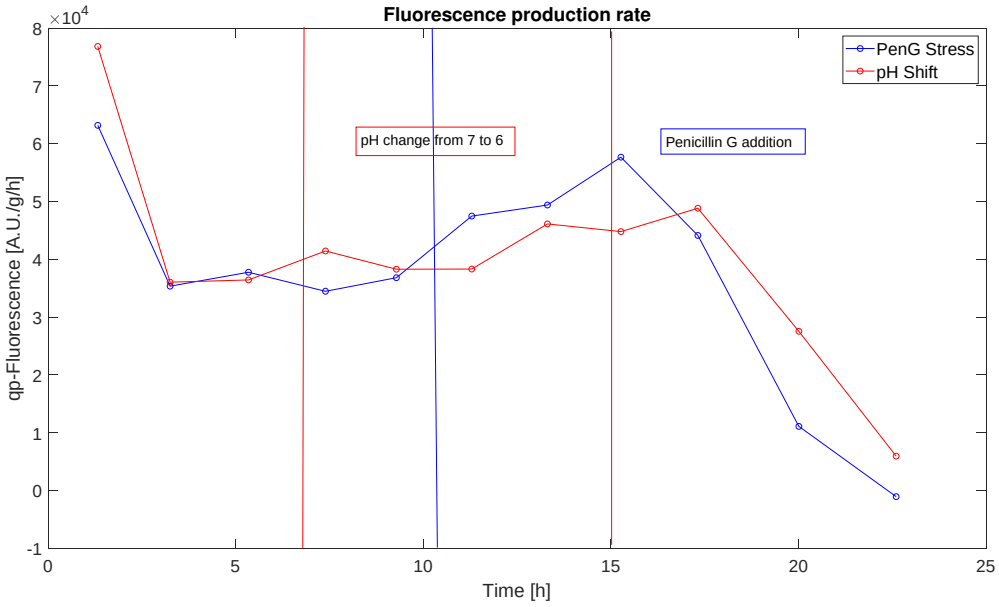

Figure 61: Fluorescence production rate. Red marked trend: batch cultivation with pH deviation - pH shift from 7 to 6 and back to 7, illustrated by vertical red lines**. Blue marked trend:** batch cultivation with addition of Penicillin G at 10 hours of the process, illustrated by vertical blue line**.**

Fluorescence production rate (q_p) was calculated according to Equation 7 and Equation 8 in 5.4.1. Here, addition of PenG shows higher q_p values than pH deviation. However, the trends of the batch cultivation after Penicillin G addition along with batch cultivation with pH shift increases and drops off at around 17 hours of the process, because of possible change of metabolic flux, substrate limitation and higher glutamate production.

Intracellular pH was calculated using linear regression function and is presented in Figure 62.

Die approbierte gedruckte Originalversion dieser Diplomarbeit ist an der TU Wien Bibliothek verfügbar.
The approved original version of this thesis is available in print at TU Wien Bibliothek.

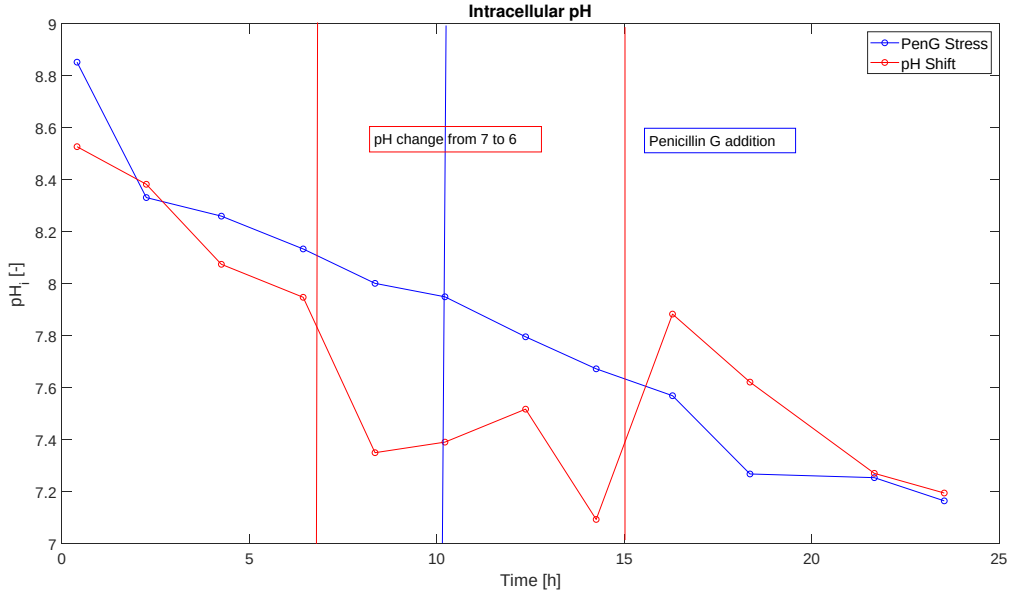

Figure 62: Intracellular pH. Red marked trend: batch cultivation with pH deviation - pH shift from 7 to 6 and back to 7, illustrated by vertical red lines. **Blue marked trend:** batch cultivation with addition of Penicillin G at 10 hours of the process, illustrated by vertical blue line.

This plot shows that Penicillin G addition does not change the trend of intracellular pH significantly. Nevertheless, changes in pH_i during pH shift can be noticed. This trend shows how intracellular pH alkalized, when external pH decreased, producing H^+ protons to achieve pH homeostasis, accordingly to Padan, 2005 (described in theoretical section 3.2). Later rush decrease and increase of pH_i indicates adjustment to newly occurred environment.

According to the obtained results, response of intracellular sensor signal to pH deviation can be detected. Addition of Penicillin G does not give visual deviations on intracellular pH, but can presumably increase fluorescence intensity.

5.5.2.2 Relation of carbon dioxide evolution rate and pH gradient

Relation of carbon dioxide evolution rate (CER) and pH gradient of batch cultivation with pH shift and Penicillin G addition were calculated and presented in Figure 63.

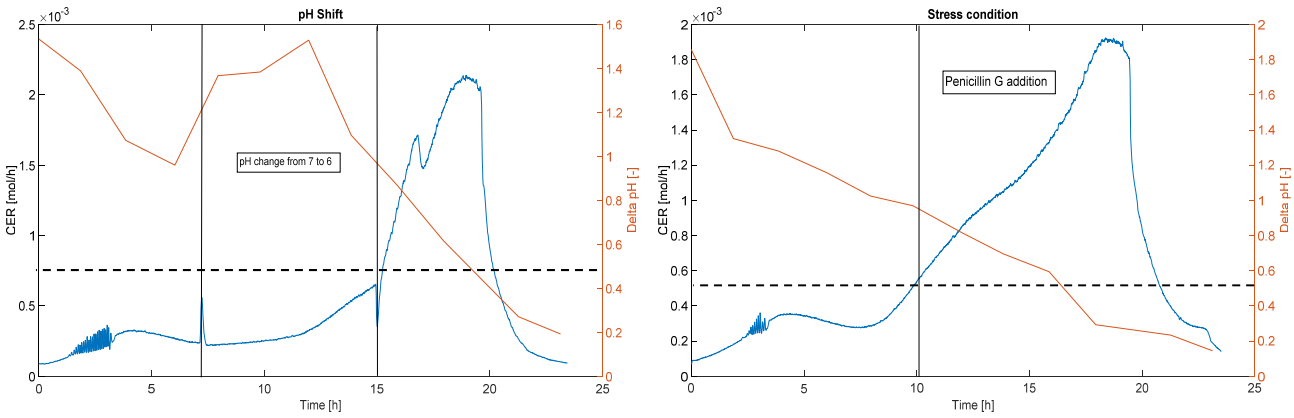

Figure 63: Relation ΔpH to Carbon Dioxide Evolution Rate (CER) against time. Left: batch cultivation with pH shift from 6 to 7 and back to pH 7. Right: batch cultivation with addition of Penicillin G. Dashed line represents pH optimum.

Relation of carbon dioxide evolution rate and pH gradient of batch cultivation with pH shift can be identified (Figure 63: Right). During pH deviation, CER incline/decline, as well as flatter slope during pH change to 6 can be recognized. Deviation of pH from 7 to 6 caused delta pH to increase and later

Die approbierte gedruckte Originalversion dieser Diplomarbeit ist an der TU Wien Bibliothek verfügbar.
The approved original version of this thesis is available in print at TU Wien Bibliothek.
TU Bibliothek Your knowledge hub WIEN

to decreases in order to achieve balance between extracellular and intercellular pH. Hypothetical optimum of 0.5 for external pH set point 7, possibly changes for external pH 6 correspondently. Therefore, after returning to pH 7, ΔpH decrease in order to achieve pH homeostasis. The fall under 0.5 indicates substrate limitation and end of the batch cultivation. In case of batch cultivation with Penicillin G addition, no significant changes can be observed (Figure 63: Left). Delta pH decreases in order to achieve the hypothetical pH optimum, but addition of external chemicals leads to its inhibition. As result of substrate limitation, pH gradient lowered down what led to the inability of the cells to maintain the pH homeostasis and eventually termination of the cultivation.

5.5.2.3 Correlation of substrate uptake rate/ respiration rates and pH gradient

Investigation of correlation existence between pH gradient and process variables was analyzed during batch cultivations with external stress conditions. Therefore, correlations of substrate uptake rate and delta pH are presented in Figure 64.

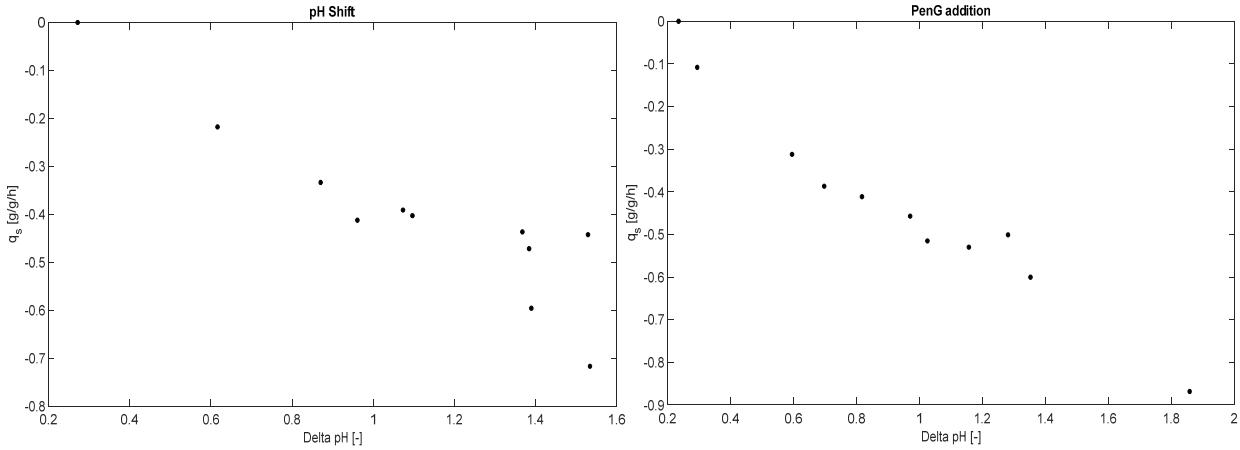

Figure 64: Correlation of substrate uptake rate (q_s) with delta pH (ΔpH). Left: batch cultivation with pH shift from 6 to 7 and back to pH 7. Right: batch cultivation with addition of Penicillin G.

Figure 64 shows the presence of linear correlation with linear trend between q_s and ΔpH in both cultivations with some outliers (especially in the case of batch cultivation with pH shift, due to pH deviations). As it can be seen, substrate uptake rate decreases with the higher pH gradient. Possible reason of it could be the energy needed for maintenance of membrane potential, what leads to the lack of energy for maintaining substrate uptake (metabolic flux). These results suggest that delta pH and therefore intracellular pH could be controlled with the means of q_s. Moreover, with the exact knowledge of membrane potential (ΔΨ) and potassium inner concentration, electrochemical potential ($\Delta\mu_{ion}$) and therefore proton motive force (PMF) can be calculated and therefore ΔpH could be possibly optimized and regulated (described in theoretical part in section 3.2).

Another investigations made was finding correlation between specific carbon dioxide evolution rate (q_{CO2}) and pH gradient (ΔpH) along with specific oxygen uptake rate (q_{O2}) and pH gradient (ΔpH). Results are presented in Figure 65.

Die approbierte gedruckte Originalversion dieser Diplomarbeit ist an der TU Wien Bibliothek verfügbar.
The approved original version of this thesis is available in print at TU Wien Bibliothek.

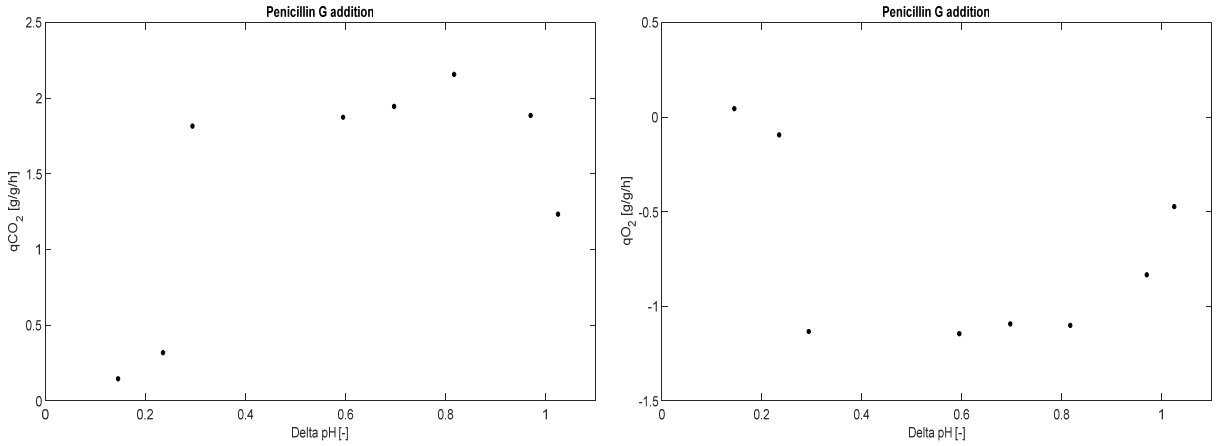

Figure 65: Left: Correlation of specific carbon dioxide evolution rate (q_{CO2}) with delta pH (ΔpH). Right: correlation of specific oxygen uptake rate (q_{O2}) with delta pH (ΔpH). Both plots were made using batch cultivation with addition of Penicillin G.

In Figure 65 correlations of specific carbon dioxide evolution rate and specific oxygen uptake rate with delta pH based on batch cultivation with addition of Penicillin G can be observed. The cultivation with pH change is not presented, due to noise contained in the data, which was caused by the pH shift. In these graphs, linear trend in ΔpH range of 0.3 to 0.8 of q_{CO2} and q_{O2} respectively can be recognized. This range seems to be the most optimal conditions for cell existence, when intracellular and extracellular pHs are reaching homeostasis. The results could signify that in this delta pH range membrane potential (according to hypothetical optimum of 0.5 (Ochrombel, 2011)) remains small and therefore respiration rates stay constant. These plots identify the correlation between respiration rates and pH gradient at optimal conditions.

The finding was also confirmed by Leyval et. al., 1997 for *Corynebacrterium glutamicum*, that ΔpH can be related to the metabolic activity of the cell such as the specific glucose uptake rate or the oxygen consumption rate, however, with the means of flow cytometry measurement, what is less beneficial as non-invasive intracellular pH sensor (described in theoretical section in 3.4) and without providing specific data in the article. Orij R B. S. et al., 2011 concluded that pH_i in yeast responds to nutritional cues and relay this information to alter cellular make-up and physiology. They also stated that the physicochemical properties of pH allow the signal to be fast, and affect multiple regulatory levels simultaneously. Hakkaart, 2019 found the correlation in *Saccharomyces cerevisiae* of pH and CO_2, particularly increase in maintenance-energy requirements and death rates in aerobic, glucose-limited cultures in case of low pH and high CO_2.

During this study, correlation of ΔpH, with the help of pHluorin sensor, with substrate uptake rate, specific carbon dioxide evolution rate and specific oxygen uptake rate in defined pH range was determined and presented. The attained results show the relevance of intracellular pH measurement and the possibilities of its further application.

Die approbierte gedruckte Originalversion dieser Diplomarbeit ist an der TU Wien Bibliothek verfügbar.
The approved original version of this thesis is available in print at TU Wien Bibliothek.
TU Bibliothek Your knowledge hub WIEN

6 Summary

The obtained results mark the importance of pH equilibrium and show its interrelation with cell growth, metabolism, and protein production. Aims set during this thesis were successfully achieved. Intracellular pH of a recombinant *Corynebacterium glutamicum* strain expressing pHluorin can be monitored during bioreactor cultivation.

Summing up, the most advantageous calibration fit and calibration equation were achieved from a linear fitting method in defined pH ranges of 6.0 - 8.3, which was used for intracellular pH evaluations. As a membrane disturbing chemical for calibration validation Nigericin in comparison to CTAB showed the best results according to statistical analysis. However, one disadvantage of Nigericin is its toxicity and cost. One of the most important outcomes and novelties of this thesis was the determination that biomass concentration is independent of fluorescence ratio, which enables applicability for bioprocesses with higher cell density. It means that the samples can be measured without extra sample manipulation, like dilution, and they can be taken directly from the bioreactor.

High throughput method is suitable for initial screening of inducer tuning. However, the investigations conducted in shake flask and microtiter plate are not transferable to bioreactor scale, due to the nature of uncontrolled conditions (DO, pH). The microtiter plate results showed that 200 µM of IPTG is sufficient enough to see fluorescence response of pHluorin sensor as intensive as in case of 1 mM or 10 mM IPTG induction. Therefore, after scaling up to bioreactor cultivation, the results showed that IPTG induction of 20 µM gives lower metabolic stress conditions while producing enough sensor in comparison with higher IPTG induction, what was not described before. Moreover, induced pre-culture for induced bioreactor cultivation is more beneficially to use in order to receive the most stable growth rate and lower fluctuations of the sensor signal.

The response of pH gradient on applying external stress conditions could be identified. It has been shown that decrease in bioreactor external medium pH can reduce the intracellular pH (pH_i), resulting in cytoplasmic acidification which in turn is primarily responsible for the metabolism shifts in response to bioreactor pH changes (Goudar, 2011). Further outcome of my study is that relation of CER and pH gradient identifies response on substrate limitation. The other result is that addition of Penicillin G did not show significant changes in intracellular pH but caused higher production of glutamate. However, produced glutamate amounts were smaller compared to literature (Eggeling, 2001; Gourdon, 1999). The possible explanation could be recombinant *Corynebacterium glutamicum* strain and its main focus on production of pHluorin sensor protein. Another novelty of this study is the discovery of correlation between pH gradient (ΔpH) and specific substrate uptake rate (q_s), giving the possibility of energy calculation, needed for H^+ maintenance and later pH gradient control during the bioprocess. One more novelty of my thesis is the existence of correlation between ΔpH and specific carbon dioxide evolution rate (q_{CO2}) along with the specific oxygen uptake rate (q_{O2}) in the optimal pH range, where the respiration rates remains constant. All these novelties show that pHluorin sensor production could be used to monitor process performance.

Die approbierte gedruckte Originalversion dieser Diplomarbeit ist an der TU Wien Bibliothek verfügbar.
The approved original version of this thesis is available in print at TU Wien Bibliothek.
TU Bibliothek Your knowledge hub WIEN

7 Outlook

In this thesis statistical methods were applied in order to find the most suitable regression fit and therefore the best calibration equation for intracellular pH evaluation. Furthermore, an MLR model was developed and used for determination of biomass dependency on the fluorescence signal. However, further chemometric analysis of calibration data for finding the most relevant regions in the fluorescence spectrum can be implemented. Therefore, principal component analysis (PCA) and partial least squares regression (PLS) methods can be applied and is part of ongoing work in the research group.

As another outlook of my thesis, further investigations on minimal induction concentration and fluorescence signal for intracellular pH determination during batch and fed-batch bioreactor cultivations can be conducted. Other investigations on verification of physiological optimum of pH gradient should be obtained.

The biggest goal and outlook of my study is to apply genetically encoded sensor for bioprocess control, which will be based on intracellular pH. This may rely on converting the analysis conducted during this thesis into an online sensor where specific wavelengths can be detected directly in the cell broth. This would be possible as the measurement is based on fluorescence ratios and no prior sample processing is required as shown in this thesis. Before this step can be taken an option may be presented by coupling the fluorescence measurement with automated sampling systems.

The intracellular pH may be further tied to other metabolic processes like ATP generation and may be interesting for fields like metabolic modelling where flow of metabolites are of particular interest. With this further knowledge of the intracellular cell status correlation with other specific functions like product formation can be obtained.

Die approbierte gedruckte Originalversion dieser Diplomarbeit ist an der TU Wien Bibliothek verfügbar.
The approved original version of this thesis is available in print at TU Wien Bibliothek.
TU Bibliothek Your knowledge hub WIEN

8 References

Anderson, R. G. (1988). A view of acidic intracellular compartments. *J. Cell Biol.*, 106, 539–543.

Araniti, F. d.-M. (2018). Flow Cytometric Measurement of Different Physiological Parameters. In Advances in Plant Ecophysiology Techniques. *Springer, Cham.*, 195-213.

Arce-Rodríguez A, V. D. (2019). Non-invasive, ratiometric determination of intracellular pH in Pseudomonas species using a novel genetically encoded indicator. *Microbial Biotechnology*, 12:1751–7915.13439.

Azmat, M., Khan, I., Cheema, H., Rajwana, I., Khan, A., & Khan, A. (2012). Extraction of DNA suitable for PCR applications from mature leaves of Mangifera indica L. *J Zhejiang Univ Sci B*, 13 (4): 239–43.

Balleza, E. K. (2018). Systematic characterization of maturation time of fluorescent proteins in living cells. *Nature methods*, 15(1), 47.

Benčina. (2013). Illumination of the spatial order of intracellular pH by genetically encoded pH-sensitive sensors. *Sensors*, 13:16736–16758.

Berger, E. A. (1973). *Proc. Nat. Acad. Sci. USA 70*, 1514-1518.

Booth. (1985). Regulation of cytoplasmic pH in bacteria. *Microbiol Review*, 49:359–78.

Booth IR, K. R. (1983). Regulation of cytoplasmic pH (pH1) in bacteria and its relationship to metabolism. *Biochem Soc Trans*, 11:70–2 .

Boyer P. D., C. R. (1973). A new concept for energy coupling in oxidative phosphorylation based on a molecular explanation of the oxygen exchange reactions. *Proc. Natl. Acad. Sci.USA*, 70: 2837-9 .

Boyer, P. D. (1997). *Annu. Rev. Biochem.* , 66, 717–749.

Bracey D, H. C.-v. (1998). Determination of the intracellular pH (pHi) of growing cells of Saccharomyces cerevisiae: the effect of reduced-expression of the membrane H+-ATPase. *J Microbiol Methods*, 31:113–125.

Chakraborty S, M. H. (2015). A FRET-Based DNA Biosensor Tracks OmpR-Dependent Acidification of Salmonella during Macrophage Infection. *PLOS Biol*, 13:e1002116.

Clarke, J. D. (2009). Cetyltrimethyl Ammonium Bromide (CTAB) DNA Miniprep for Plant DNA Isolation. *Cold Spring Harbor Protocols*.

Cotter, P. D. (2003). Surviving the acid test: responses of gram-positive bacteria to low pH. *Microbiol. Mol. Biol. Rev*, 67(3), 429-453.

Crauwels, P. S. (2018). Intracellular pHluorin as sensor for easy assessment of bacteriocin-induced membrane-damage in Listeria monocytogenes. *Frontiers in microbiology*, 9, 3038.

De Boer, H. A. (1983). The tac promoter: a functional hybrid derived from the trp and lac promoters. *Proceedings of the National Academy of Sciences*, 80(1), 21-25.

Deamer DW, N. J. (1989). Proton flux mechanisms in model and biological membranes. *J Membr Biol* , 107:91–103.

Die approbierte gedruckte Originalversion dieser Diplomarbeit ist an der TU Wien Bibliothek verfügbar.
The approved original version of this thesis is available in print at TU Wien Bibliothek.

Delvigne, F. B. (2011). Green fluorescent protein (GFP) leakage from microbial biosensors provides useful information for the evaluation of the scale-down effect. *Biotechnology journal* , 6(8), 968-978.

Eggeling, L. K. (2001). L-glutamate efflux with Corynebacterium glutamicum: why is penicillin treatment or Tween addition doing the same? *Journal of molecular microbiology and biotechnology*, 3(1), 67-68.

Evans, D. J. (1970). *J. Bacteriol.*, 104, 1203-1212.

Fisher MA, P. B. (2002). Microarray analysis of the Mycobacterium tuberculosis transcriptional response to the acidic conditions found in phagosomes. *J Bacteriol*, 184 (14): 4025-4032.

Follmann M, O. I. (2009). Functional genomics of pH homeostasis in Corynebacterium glutamicum revealed novel links between pH response, oxidative stress, iron homeostasis and methionine synthesis. *BMC Genomics*, 10:621.

Follmann, M. O. (2009). Functional genomics of pH homeostasis in Corynebacterium glutamicum revealed novel links between pH response, oxidative stress, iron homeostasis and methionine synthesis. . *BMC genomics*, 10(1), 621.

Freedman, D. A. (2009). A simple regression equation has on the right hand side an intercept and an explanatory variable with a slope coefficient. A multiple regression equation has two or more explanatory variables on the right hand side, each with its own slope coefficient. In D. A. Freedman, *Statistical Models: Theory and Practice.* (p. 26). Cambridge University Press.

Galluzzi, L. K.-S. (2017). *Molecular characterization of autophagic responses.* Academic Press (Vol. 588).

Germond, A. F. (2016). Design and development of genetically encoded fluorescent sensors to monitor intracellular chemical and physical parameters. *Biophysical reviews*, 8(2), 121-138.

Gillies RJ, U. K. (1981). 31P NMR studies of intracellular pH and phosphate metabolism during cell division cycle of Saccharomyces cerevisiae. *Proc Natl Acad Sc*, 78:2125–2129.

Gjetting SK, Y. C. (2012). Live imaging of intra- and extracellular pH in plants using pHusion, a novel genetically encoded biosensor. *J Exp Bot*, 63:3207–3218.

Goffeau, A. &. (1981). The proton-translocating ATPase of the fungal plasma membrane. . *Biochim Biophys Acta*, 639, 197-223.

Goudar, C. T. (2011). Estimating cell specific oxygen uptake and carbon dioxide production rates for mammalian cells in perfusion culture. *Biotechnology progress*, 27(5), 1347-1357.

Gourdon, P. &. (1999). Metabolic analysis of glutamate production by Corynebacterium glutamicum. *Metabolic engineering*, 1(3), 224-231.

Grillo-Hill BK, C. C.-V.-H.-V. (2015). Increased H+ efflux is sufficient to induce dysplasia and necessary for viability with oncogene expression. *Elife*, 4, e03270.

Gutmann, M. H. (1992). Carrier-mediated glutamate secretion by Corynebacterium glutamicum under biotin limitation. *Biochimica et Biophysica Acta (BBA)-Biomembranes*, 1112(1), 115-123.

Die approbierte gedruckte Originalversion dieser Diplomarbeit ist an der TU Wien Bibliothek verfügbar.
The approved original version of this thesis is available in print at TU Wien Bibliothek.
TU Bibliothek Your knowledge hub WIEN

H. Robert Horton, L. A. (2008). *Biochemie.* Deutschland. München. : Pearson Studium.

Hakkaart, X. L.-L. (2019). Physiological responses of Saccharomyces cerevisiae to industrially relevant conditions: slow growth, low pH and high CO2 levels. *Biotechnology and*.

Han, J. &. (1995, June). The influence of the sigmoid function parameters on the speed of backpropagation learning. *International Workshop on Artificial Neural Networks. Springer, Berlin, Heidelberg*, 195-201.

Hansen, L. H. (1998). The effect of the lacY gene on the induction of IPTG inducible promoters, studied in Escherichia coli and Pseudomonas fluorescens. *Current microbiology*, 36(6), 341-347.

Harold, F. M. (1969). *J. Biol.* , 244, 2261-2268.

Haugland RP, S. M. (1996). *Handbook of fluorescent probes and research chemicals*.

Haynes JA, B. M. (1990). The effect of growth conditions of Corynebacterium glutamicum on the transformation frequency obtained by electroporation. *J Gen Microbiol* , 136:255–263.

Hoischen, C. &. (1990). Membrane alteration is necessary but not sufficient for effective glutamate secretion in Corynebacterium glutamicum. . *J Bacteriol*, 172, 3409-3416.

Huber RE, K. G. (1976). A Quantitation of the factors which affect the hydrolase and transgalactosylase activities of ß-galactosidase (E. coli) on lactose. *Biochemistry* , 15:1994–2001.

Ikeda M, K. R. (1998). A novel system with positive selection for the chromosomal integration of replicative plasmid DNA in Corynebacterium glutamicum. *Microbiology*, 144:1863–1868.

Ikeda, M. &. (2003). The Corynebacterium glutamicum genome: features and impacts on biotechnological processes. *Applied microbiology and biotechnology*, 62(2-3), 99-109.

Jakob K, S. P. (2007). Gene expression analysis of Corynebacterium glutamicum subjected to long-term lactic acid adaptation. *J Bacteriol*, 189 (15): 5582-5590.

Jetten MSM, S. A. (1995). Recent advances in the physiology and genetics of amino acid-producing bacteria. *Crit Rev Biotechnol* , 15:73–103.

Kalinowski, J. B. (2003). The complete Corynebacterium glutamicum ATCC 13032 genome sequence and its impact on the production of L-aspartate-derived amino acids and vitamins. *Journal of biotechnology*, 104(1-3), 5-25.

Karasawa M, T. O. (1986). Application of protoplast fusion to the development of l-threonine and l-lysine producers. *Agric Biol Chem*, 50:339–346.

Katsumata R, I. M. (1993). Hyperproduction of tryptophan in Corynebacterium glutamicum by pathway engineering. *Biotechnology*, 11:921–925.

Katsumata R, O. A. (1984). Protoplast transformation of glutamate-producing bacteria with plasmid DNA. *J Bacteriol*, 159:306–311.

Die approbierte gedruckte Originalversion dieser Diplomarbeit ist an der TU Wien Bibliothek verfügbar.
The approved original version of this thesis is available in print at TU Wien Bibliothek.
TU Bibliothek Your knowledge hub WIEN

Kawahara Y, T.-F. K. (1997). Relationship between the glutamate production and the activity of 2-oxoglutarate dehydrogenase in Brevibacterium lactofermentum. *Biosci Biotechnol Biochem*, 61:1109–1112.

Kenton, W. (2019, 04 14). Multiple Linear Regression – MLR Definition.

Kim, J. F. (2010). Requirement of de novo synthesis of the OdhI protein in penicillin-induced glutamate production by Corynebacterium glutamicum. *Applied microbiology and biotechnology*, 86(3), 911-920.

Kimura. (2003). Metabolic engineering of glutamate production. In: Faurie R, Thommel J (eds) Adv Biochem Eng Biotechnol, vol 79. Microbial production of l-amino acids. *Springer, Berlin Heidelberg New York*, pp 37–57.

Kimura, E. Y. (1999). Glutamate overproduction in Corynebacterium glutamicum triggered by a decrease in the level of a complex comprising DtsR and a Biotin-containing subunit. . *Biosc. Biotechnol. Biochem.*, 63:1274-1278.

Kinoshita S, N. K. (1978). Amino acids. In: Rose AH (ed) Primary products of metabolism. . *Academic press, London*, pp 209–261.

Kinoshita, S. U. (1957). Studies on the amino acid fermentation. *The Journal of general and applied microbiology*, 3(3), 193-205.

Klein, W. I. (1972). *J. Biol. Chem.* , 247,7257-7265.

Koch-Koerfges. (2012). Novel Insights Into the Energy Metabolism of Corynebacterium Glutamicum by Comprehensive Analysis of Mutants Defective in Respiration Or Oxidative Phosphorylation. . *Forschungszentrum Jülich, Zentralbibliothek.*

Kresnowati MTAP, S.-M. C. (2007). Measurement of fast dynamic intracellular pH inSaccharomyces cerevisiae using benzoic acid pulse. *Biotechnol Bioeng*, 97:86–98.

Leuchtenberger. (1996). Amino acids–technical production and use. *Biotechnology: products of primary metabolism*, 465-502.

Leyval, D. D. (1997). Flow cytometry for the intracellular pH measurement of glutamate producing Corynebacterium glutamicum. *Journal of microbiological methods*, 29(2), 121-127.

Löffler G., P. P. (2007). Biochemie und Pathobiochemie. 8. Aufl. *Verlag Springer Berlin*.

Lohninger, H. (2019). *Advanced Biostatistics: Multivariate Modelling.* TU Wien.

Lund P, T. A. (2014). Coping with low pH: molecular strategies in neutralophilic bacteria. *FEMS Microbiol Rev*, 38:1091–1125.

Marešová, L. H. (2010). New applications of pHluorin-measuring intracellular pH of prototrophic yeasts and determining changes in the buffering capacity of strains with affected potassium homeostasis. *Yeast*, 27(6), 317-325.

Martinez, K. A. (2012). Cytoplasmic pH response to acid stress in individual cells of Escherichia coli and Bacillus subtilis observed by fluorescence ratio imaging microscopy. *Appl. Environ. Microbiol.*, 78(10), 3706-3714.

Die approbierte gedruckte Originalversion dieser Diplomarbeit ist an der TU Wien Bibliothek verfügbar.
The approved original version of this thesis is available in print at TU Wien Bibliothek.
TU Bibliothek Your knowledge hub WIEN

Martin-Galiano AJ, O. K. (2005). Transcriptional analysis of the acid tolerance response in Streptococcus pneumoniae. *Microbiology*, 151: 3935-3946.

Miesenböck G, D. A. (1998). Visualizing secretion and synaptic transmission with pH-sensitive green fluorescent proteins. *Nature*, 394:192–195.

Miesenbock G, D. A. (1998). Visualizing secretion and synaptic transmissionwith pH-sensitive green fluorescent protein . *Nature* , 394:192–195.

Miyawaki A, G. O. (1999). Dynamic and quantitative Ca2+ measurements using improved cameleons . *Proc Nat Acad Sci USA*, 96:2135–2140.

MJ, M. (2011). pHluorin2: an enhanced, ratiometric, pH-sensitive green florescent protein. *Adv Biosci Biotechnol*, 2:132 .

Morimoto Y V., C. Y.-S. (2010). Proton-conductivity assay of plugged and unplugged MotA/B proton channel by cytoplasmic pHluorin expressed in Salmonella. *FEBS Lett*, 584:1268–1272.

Morimoto Y V., K.-i. N. (2016). High-resolution pH imaging of living bacterial cells to detect local pH differences. *MBio*, 7:e01911-16.

Nara T, S. H. (1964). Effect of penicillin on amino acid fermentation. *Agric Biol Chem*, 28:120–124.

Nicholls, D. G. (2013). *Bioenergetics.* Academic Press.

Nifosí R, A. P. (2007). Variation of spectral, structural, and vibrational properties within the intrinsically fluorescent proteins family: a density functional study. *J Comput Chem*, 28:2366–2377.

Ochrombel. (2011). Untersuchungen zu Mechanismen der Stressantwort und des Kaliumtransportes in Corynebacterium glutamicum. *Doctoral dissertation, Universität zu Köln*, 3.

Orij R, B. S. (2011, 11 03). Intracellular pH is a tightly controlled signal in yeast. *Biochim Biophys Acta - Gen Subj* , pp. 1810:933–944.

Orij R, P. J. (2009). In vivo measurement of cytosolic and mitochondrial pH using a pH-sensitive GFP derivative in Saccharomyces cerevisiae reveals a relation between intracellular pH and growth. *Microbiology*, 155:268–278.

Padan, E. B. (2005). Alkaline pH homeostasis in bacteria: new insights. *Biochimica et biophysica acta (BBA)-biomembranes*, 1717(2), 67-88.

Pant, A. (2019, 01 13). *https://towardsdatascience.com/introduction-to-linear-regression-and-polynomial-regression-f8adc96f31cb*.

Pfefferle W, M. B. (2003). Biotechnological manufacture of lysine. In: Faurie R, Thommel J (eds) Adv Biochem Eng Biotechnol, vol. 79. Microbial production of l-amino acids. . *Springer, Berlin Heidelberg New York*, pp 59–112.

Rencher, A. C., & Christensen, W. F. (2012). Chapter 10, Multivariate regression – Section 10.1, Introduction. In A. C. Rencher, & W. F. Christensen, *Methods of Multivariate Analysis, Wiley Series in Probability and Statistics, (3rd ed.)* (p. 19). John Wiley & Sons ISBN 978111839167.

Die approbierte gedruckte Originalversion dieser Diplomarbeit ist an der TU Wien Bibliothek verfügbar.
The approved original version of this thesis is available in print at TU Wien Bibliothek.
TU Bibliothek Your knowledge hub WIEN

Rest ME van der, L. C. (1999). A heat shock following electroporation of Corynebacterium glutamicum with xenogenein plasmid DNA. *Appl Microbiol Biotechnol* , 52:541–545.

Roe AJ, O. C. (2002). Inhibition of Escherichia coli growth by acetic acid: a problem with methionine biosynthesis and homocysteine toxicity. *Microbiology*, 148 (Pt 7): 2215-2222.

Schäfer A, K. J.-F.-H. (1990). High-frequency conjugal plasmid transfer from gram-negative Escherichia coli to various gram-positive Coryneform bacteria. *J Bacteriol* , 172:1663–1666.

Schultz, C. N. (2007). Glutamate production by Corynebacterium glutamicum: dependence on the oxoglutarate dehydrogenase inhibitor protein OdhI and protein kinase PknG. *Applied microbiology and biotechnology*, 76(3), 691.

Schultz, C. N. (2007). Glutamate production by Corynebacterium glutamicum: dependence on the oxoglutarate dehydrogenase inhibitor protein OdhI and protein kinase PknG. *Applied microbiology and biotechnology*, 76(3), 691.

Schuster, S. E. (2005). pHluorin-based in vivo assay for hydrolase screening. *Analytical chemistry*, 77(9), 2727-2732.

Schwarzer A, P. A. (1991). Manipulation of Corynebacterium glutamicum by gene disruption and replacement. *Biotechnology*, 9:84–87.

Seal, H. L. (1967). The historical development of the Gauss linear model. *Biometrika*, 54 (1/2): 1–24.

Sekine H, S. T. (2001). H+-ATPase defect in Corynebacterium glutamicum abolished glutamic acid production with enhancement of glucose consumption rate. *Appl Microbiol Biotechnol*, 57:534–540.

Shen Y, R. M. (2014). pHuji, a pH-sensitive red fluorescent protein for imaging of exo- and endocytosis. *J Cell Biol*, 207:419–32.

Shen, X. H. (2012). Degradation and assimilation of aromatic compounds by Corynebacterium glutamicum: another potential for applications for this bacterium? *Applied microbiology and biotechnology*, 95(1), 77-89.

Shigu H, T. G. (1971). Studies on process of glutamic acid fermentation at the enzyme level. I. On the change of α-ketoglutaric acid dehydrogenase in the course of culture. *J Ferm Technol* , 49:400–405.

Shiio I, S. O. (1962). Effect of biotin on the bacterial formation of glutamic acid. I. Glutamate formation and cellular premeability of amino acids. *J Biochem* , 51:56–62.

Shimizu H, T. H. (2003). Effects of the changes in enzyme activities on metabolic flux redistribution around the 2-oxoglutarate branch in glutamate production by Corynebacterium glutamicum. *Bioprocess Biosyst Eng*, 25:291–298.

Shimomura O, J. F. (1962). Extraction, purification and properties of aequorin, a bioluminescent protein from the luminous hydromedusan, Aequorea. . *J Cell Comp Physiol*, 59:223–239.

Smith, K. M. (2010). Engineering Corynebacterium glutamicum for isobutanol production. *Applied microbiology and biotechnology*, 87(3), 1045-1055.

Die approbierte gedruckte Originalversion dieser Diplomarbeit ist an der TU Wien Bibliothek verfügbar.
The approved original version of this thesis is available in print at TU Wien Bibliothek.
TU Bibliothek Your knowledge hub WIEN

StatsDirect.com. (n.d.). Retrieved from https://www.statsdirect.com/help/regression_and_correlation/polynomial.htm

Südhof, T. C. (1995). The synaptic vesicle cycle: a cascade of protein–protein interactions. *Nature*, 375, 645–653 .

Suzuki, T. M. (2003). F0F1-ATPase/synthase is geared to the synthesis mode by conformational rearrangement of ϵ subunit in response to proton motive force and ADP/ATP balance. *Journal of Biological Chemistry*, 278(47), 46840-46846.

Sweeney, T. (2014). Auto-induction for over expression in E. coli. Imperial College London, London, Great Britain. Retrieved from Auto-induction for over expression in E. coli.

Takeno, S. O. (2007). Anaerobic growth and potential for amino acid production by nitrate respiration in Corynebacterium glutamicum. *Applied microbiology and biotechnology*, 75(5), 1173-1182.

Takinami K, Y. H. (1965). Biochemical effects of fatty acid and its derivatives on L-glutamic acid fermentation. Part III. Biotin-Tween 60 relationship in the accumulation of Lglutamic acid and the growth of Brevibacterium lactofermentum. *Agric Biol Chem*, 29:351-359.

Tsien, R. (1998). The green fluorescent protein. *Annu Rev Biochem*, 67:.

Udaka, S. (1960). Screening method for microorganisms accumulating metabolites and its use in the isolation of Micrococcus glutamicus. *Journal of bacteriology*, 79(5), 754.

Valkonen M, M. D. (2013). Noninvasive high-throughput single-cell analysis of the intracellular pH of Saccharomyces cerevisiae by ratiometric flow cytometry. *Appl Environ Microbiol*, 79:7179–87.

Veine, D. M. (1998). Redox potentials for yeast, Escherichia coli and human glutathione reductase relative to the NAD+/NADH redox couple: enzyme forms active in catalysis. . *Biochemistry* , 37, 15575–15582.

Wittmann, C. K. (2004). Metabolic network analysis of lysine producing Corynebacterium glutamicum at a miniaturized scale. *Biotechnology and bioengineering*, 87(1), 1-6.

Wohlrab, H. &. (1982). pH gradient-dependent phosphate transport catalyzed by the purified mitochondrial phosphate transport protein. . *J Biol Chem*, 257, 28–31.

Zhou, T. P. (2014). An insight into the sequential order in 2D correlation spectroscopy using polymer transitions: Boltzmann Sigmoid, Gaussian Cumulative, Lorentz Cumulative, and Asymmetric Sigmoid. Findings in experiments and simulations. . *Vibrational Spectroscopy*, 70, 137-161.

Die approbierte gedruckte Originalversion dieser Diplomarbeit ist an der TU Wien Bibliothek verfügbar.
The approved original version of this thesis is available in print at TU Wien Bibliothek.

9 List of figures

Figure 1: Scanning electron microscopy of *Corynebacteium glutamicum*. Scanning electron microscopy was performed in CeNSE, IISc, Bangalore. 9

Figure 2: History of amino acid fermentation and strain development technology in *Corynebacterium glutamicum* (Ikeda, 2003). 9

Figure 3: Overview of membrane-bound electron transport and ATP synthesis in *Corynebacterium glutamicum* (Koch-Koerfges, 2012). The energy released in the electron transport chain reactions is used to build up a proton concentration gradient across the membrane. For this purpose, protons are transported from the cytoplasm into the membrane, when electrons from reduced substrates flow through the complexes of the electron transport chain. At the time protons flow back into the cytoplasm through ATP synthase, the free enthalpy stored in the proton gradient is used for building ATP from ADP and P_i (H. Robert Horton, 2008). 11

Figure 4: Model for the function of potassium in the pH homeostasis of *C.glutamicum.* Under neutral pH conditions at pH_{in} = pH_{ex} = 7.5, the proton motive force (PMK) is determined solely by the value of the membrane potential (Ψ), while the respiratory chain (R) is fully active ↑ (A). If the external pH drops to 6.0, a proton gradient (ΔpH) occurs across the membrane, which causes a higher PMK value. Due to the increased PMK, the respiratory chain (R) is only partially active ↓ and protons can enter the cell (B). The influx of potassium ions by CglK into the cytoplasm leads to the lowering of membrane potential (C) due to the shift of positive charges. Thus, the PMK is also lowered, so that the respiratory chain is again fully active, and proton-exporting systems (X) can regulate the pH in the cell (D) (Ochrombel, 2011). 12

Figure 5: pHluorin gene expression under control of *lac* operon and induction with IPTG. The *tac* promotor has the same working principal as *lac* promotor. Figure above: without addition of IPTG the regulator gene is expressed and the repressor protein is synthesized with binding sites for inducer and the operator region. The repressor protein binds to the operator region, covering part of the promoter region where RNA polymerase attaches. RNA polymerase cannot bind to the promoter region so the target gene is not transcribed to mRNA and cannot be later translated into the protein. Figure below: after addition of IPTG, the inducer binds to the other site on the repressor protein, causing the repressor protein to change shape and dissociate from the operator region. The promoter region is now unblocked so RNA polymerase can bind to it and initiate transcription, and the target protein can be expressed (Sweeney, 2014). 13

Figure 6: Fluorescence intensity signal [A] versus wavelength [nm] of expressed pHluorin sensor in *Corynebacterium glutamicum* with OD_{600} 1 at pH 6.0 and 8.3..... 15

Figure 7: “S” shape curve of Boltzmann sigmoid function (Zhou, 2014). 18

Figure 8: Fluorescence intensity signal [A] versus wavelength [nm] of expressed pHluorin sensor in *Corynebacterium glutamicum* with OD_{600} of 1 at different pH values. 28

Figure 9: Polynomic fit with the use of CTAB for the cells with optical densities 1, 10, 25 and 50. As black lines relevant confidence intervals (95 % level of significance) are presented. 29

Die approbierte gedruckte Originalversion dieser Diplomarbeit ist an der TU Wien Bibliothek verfügbar.
The approved original version of this thesis is available in print at TU Wien Bibliothek.

Figure 10: 3D model of polynomic fit with the use of CTAB for the cells with optical densities 1, 10, 25 and 50. 30
Figure 11: Statistical results, calculated in MATLAB of polynomic fits with an order 3. 30

Figure 12: Statistical results, calculated in MATLAB of polynomic fits with an order 2. 31

Figure 13: Boltzmann sigmoidal fit with the use of CTAB for the cells with optical densities 1, 10, 25 and 50. As black lines relevant confidence intervals (95 % level of significance) are presented. 31

Figure 14: 3D model of Boltzmann sigmoidal fit with the use of CTAB for the cells with optical densities 1, 10, 25 and 50. 32

Figure 15: Linear fit with the use of CTAB for the cells with optical densities 1, 10, 25 and 50. As black lines relevant confidence intervals (95 % level of significance) are presented. 33

Figure 16: MLR model of the cells with optical densities 1, 10, 25 and 50 (with the use of CTAB). Blue squares correspond to experimental data, whereas black squares represent simulated data. 34

Figure 17: Polynomic fit with the use of Nigericin for the cells with optical densities 1, 10, 25 and 50. As black lines relevant confidence intervals (95 % level of significance) are presented. 35

Figure 18: 3D model of polynomic fit with the use of Nigericin for the cells with optical densities 1, 10, 25 and 50. 35

Figure 19: Statistical results, calculated in MATLAB of polynomic fits with an order 2. 36

Figure 20: Statistical results, calculated in MATLAB of polynomic fits with an order 3. 36

Figure 21: Boltzmann sigmoidal fit with the use of Nigericin for the cells with optical densities 1, 10, 25 and 50. As black lines relevant confidence intervals (95 % level of significance) are presented. ... 37

Figure 22: 3D model of Boltzmann sigmoidal fit with the use of Nigericin for the cells with optical densities 1, 10, 25 and 50. 37

Figure 23: Linear fit with the use of Nigericin for the cells with optical densities 1, 10, 25 and 50. As black lines relevant confidence intervals (95 % level of significance) are presented. 38

Figure 24: MLR model of the cells with optical densities 1, 10, 25 and 50 (with the use of Nigericin). Blue squares correspond to experimental data, whereas black squares represent simulated data. 39

Figure 25: Cross-validation of OD variable. pH estimation for OD 10, using calibration equation of linear, polynomic and Boltzmann sigmoidal fitting of OD 1 calibration data set. Measured pH of OD 10. 40

Figure 26: Cross-validation of OD variable. pH estimation for OD 25, using calibration equation of linear, polynomic and Boltzmann sigmoidal fitting of OD 1 calibration data set. Measured pH of OD 25. 40

Die approbierte gedruckte Originalversion dieser Diplomarbeit ist an der TU Wien Bibliothek verfügbar.
The approved original version of this thesis is available in print at TU Wien Bibliothek.
TU Bibliothek Your knowledge hub WIEN

Figure 27: Cross-validation of OD variable. pH estimation for OD 50, using calibration equation of linear, polynomic and Boltzmann sigmoidal fitting of OD 1 calibration data set. Measured pH of OD 50. 41
Figure 28: Root Mean Square Errors of calibration equations of linear regression, polynomial regression and sigmoidal fit based on: calibration of OD 10, 25, 50 for OD 1 (A), calibration of OD 1, 25, 50 for OD 10 (B), calibration of OD 1, 10, 50 for OD 25 (C), calibration of OD 1, 10, 25 for OD 50 (D). 42

Figure 29: Sigmoidal fitting of CTAB (left) and Nigericin (right) dataset with OD 1, 10, 25 and 50. Red line represents OD=1, blue line – OD=10, turquoise line represents OD=25 and pink line represents OD=50. Black lines from both sides represent confidence intervals for each OD. 42

Figure 30: Plot fluorescence ratios against pH for CTAB (right) and Nigericin (left) datasets with error bars (triplicate measurement). 43

Figure 31: Biomass concentration of shake flask cultivation: blue lines– addition of Tween 40, red lines – control run without any stress addition, green lines – addition of Penicillin G. 44

Figure 32: Left: intracellular pH versus cultivation time of three experiments in biological duplicates. Right: pH gradient versus cultivation time of three experiments in biological duplicates.. 45

Figure 33: Optical density at 600 nm versus time in hours of IPTG concentration tuning with non-induced pre-culture at different inducer concentrations. 47

Figure 34: Optical density at 600 nm versus time in hours of IPTG concentration tuning with induced pre-culture at different inducer concentrations. 47

Figure 35: Intracellular pH (pHi) versus time in hours of IPTG concentration tuning with non-induced pre-culture at different inducer concentrations. 48

Figure 36: Intracellular pH (pHi) versus time in hours of IPTG concentration tuning with induced pre-culture at different inducer concentrations. 48

Figure 37: Fluorescence sensor amount versus time in h. Left: IPTG concentration tuning with non-induced pre-culture at different inducer concentrations. Right: IPTG concentration tuning with induced pre-culture at different inducer concentrations. 49

Figure 38: Optical density at 600 nm versus time in hours of experimental set with induced pre- and main culture (0.5 mM IPTG) and addition of different concentrations of Penicillin G in the range of 150 U/L – 1150 U/L. 49

Figure 39: Intracellular pH versus time in hours of experimental set with induced pre- and main culture (0.5 mM IPTG) and addition of different concentrations of Penicillin G in the range of 150 U/L – 1150 U/L. 50

Figure 40: Biomass specific fluorescence amount versus time in hours of experimental set with induced pre- and main culture (0.5 mM IPTG) and addition of different concentrations of Penicillin G

Die approbierte gedruckte Originalversion dieser Diplomarbeit ist an der TU Wien Bibliothek verfügbar.
The approved original version of this thesis is available in print at TU Wien Bibliothek.
TU Bibliothek Your knowledge hub WIEN

in the range of 150 U/L – 1150 U/L. 50

Figure 41: Fluorescence intensity of non-induced cultivation, non-induced pre-culture and induced (20 µM IPTG) main culture cultivation, induced pre- and main culture (200 µM) cultivation, induced pre- and main culture (20 µM) cultivation, induced pre- and main culture (1 mM) cultivation. 51

Figure 42: Intracellular pH of not-induced cultivation, non-induced pre-culture and induced (20 µM IPTG) main culture cultivation, induced pre- and main culture (200 µM) cultivation, induced pre- and main culture (20 µM) cultivation, induced pre- and main culture (1 mM) cultivation. A represents graph of fluorescence signals of the first batch samples, B shows fluorescence signals of the last batch samples and C represents fluorescence signals of the last fed-batch samples. 52

Figure 43: pH gradient calculated out of intracellular and extracellular pH. The results are presented for non-induced cultivation, non-induced pre-culture and induced (20 µM IPTG) main culture cultivation, induced pre- and main culture (200 µM) cultivation, induced pre- and main culture (20 µM) cultivation, induced pre- and main culture (1 mM) cultivation. 53

Figure 44: Biomass specific fluorescence amount of non-induced cultivation, non-induced pre-culture and induced (20 µM IPTG) main culture cultivation, induced pre- and main culture (200 µM) cultivation, induced pre- and main culture (20 µM) cultivation, induced pre- and main culture (1 mM) cultivation. 54

Figure 45: Fluorescence production rate of non-induced cultivation, non-induced pre-culture and induced (20 µM IPTG) main culture cultivation, induced pre- and main culture (200 µM) cultivation, induced pre- and main culture (20 µM) cultivation. 55

Figure 46: Interrelationship between pHluorin fluorescence per biomass and IPTG concentration added during batch cultivations. Errors bars represent variability in fluorescence level during the entire process time course. 56

Figure 47: Maximum growth rate (μ_{max}) in dependence of different IPTG induction conditions. Errors bars represent variability in fluorescence level during the entire process time course. 57

Figure 48: Fluorescence intensity of extracellular sensor of non-induced cultivation, non-induced pre-culture and induced (20 µM IPTG) main culture cultivation, induced pre- and main culture (200 µM) cultivation, induced pre- and main culture (20 µM) cultivation. 58

Figure 49: Biomass specific fluorescence amount of non-induced cultivation, non-induced pre-culture and induced (20 µM IPTG) main culture cultivation, induced pre- and main culture (200 µM) cultivation, induced pre- and main culture (20 µM) cultivation. 58

Figure 50: Fluorescence production rate of non-induced cultivation, non-induced pre-culture and induced (20 µM IPTG) main culture cultivation, induced pre- and main culture (200 µM) cultivation, induced pre- and main culture (20 µM) cultivation. 59

Figure 51: Relation ΔpH to Carbon Dioxide Evolution Rate (CER) against time of non-induced cultivation (A), non-induced pre-culture and induced (20 µM IPTG) main culture cultivation (B), induced pre- and main culture (20 µM) cultivation (C), induced pre- and main culture (200 µM)

Die approbierte gedruckte Originalversion dieser Diplomarbeit ist an der TU Wien Bibliothek verfügbar.
The approved original version of this thesis is available in print at TU Wien Bibliothek.
TU Bibliothek Your knowledge hub WIEN

cultivation (D), induced pre- and main culture (1 mM) cultivation (E). Green lines separate batch and fed-batch phases. 60

Figure 52: Plot A: substrate uptake rate and glucose concentration against time; Plot B: substrate uptake rate against pH gradient; Plot C: growth rate and pH gradient against time of non-induced pre-culture and with 20 µM IPTG induced main culture cultivation. Green lines separate batch and fed-batch phases. 62

Figure 53: Plot A: Substrate uptake rate and glucose concentration against time; Plot B: substrate uptake rate against pH gradient; Plot C: growth rate and pH gradient against time of induced pre-culture and with 200 µM IPTG induced main culture cultivation. Green lines separate batch and fed-batch phases. 63

Figure 54: Relation ΔpH to Carbon Dioxide Evolution Rate (CER) against time of induced cultivation (1 mM IPTG) with substrate limitation and pH shift (from 6 to 7 and return). The green line divides batch
from fed-batch phase. Dashed line represents hypothetical pH optimum. 64

Figure 55: Relation ΔpH to Carbon Dioxide Evolution Rate (CER) against time of induced cultivation (1 mM IPTG) with pH shift (from 6 to 7 and return). The green line divides batch from fed-batch phase. Dashed line represents pH optimum. 65

Figure 56: Overview of process parameters during batch phase cultivation with pH shift (from 7 to 6 and back to 7) as stress condition. 66

Figure 57: Overview of process parameters during batch phase cultivation with addition of Penicillin G as stress condition. Green line shows the time of Penicillin G addition. 66

Figure 58: Glutamate production during batch cultivations with addition of Penicillin G and pH shift correspondently. 67

Figure 59: Biomass specific fluorescence intensity. Red marked trend: batch cultivation with pH deviation - pH shift from 7 to 6 and back to 7, illustrated by vertical red lines. Blue marked trend: batch cultivation with addition of Penicillin G at 10 hours of the process, illustrated by vertical blue line. 68

Figure 60: Biomass specific fluorescence amount. Red marked trend: batch cultivation with pH deviation - pH shift from 7 to 6 and back to 7, illustrated by vertical red lines. Blue marked trend: batch cultivation with addition of Penicillin G at 10 hours of the process, illustrated by vertical blue line. 68

Figure 61: Fluorescence production rate. Red marked trend: batch cultivation with pH deviation - pH shift from 7 to 6 and back to 7, illustrated by vertical red lines. Blue marked trend: batch cultivation with addition of Penicillin G at 10 hours of the process, illustrated by vertical blue line. 69

Figure 62: Intracellular pH. Red marked trend: batch cultivation with pH deviation - pH shift from 7 to 6 and back to 7, illustrated by vertical red lines. Blue marked trend: batch cultivation with addition of Penicillin G at 10 hours of the process, illustrated by vertical blue line. 70

Die approbierte gedruckte Originalversion dieser Diplomarbeit ist an der TU Wien Bibliothek verfügbar.
The approved original version of this thesis is available in print at TU Wien Bibliothek.
TU Bibliothek Your knowledge hub WIEN

Figure 63: Relation ΔpH to Carbon Dioxide Evolution Rate (CER) against time. Left: batch cultivation with pH shift from 6 to 7 and back to pH 7. Right: batch cultivation with addition of Penicillin G. Dashed line represents pH optimum. 70

Figure 64: Correlation of substrate uptake rate (q_s) with delta pH (ΔpH). Left: batch cultivation with pH shift from 6 to 7 and back to pH 7. Right: batch cultivation with addition of Penicillin G. 71

Figure 65: Left: Correlation of specific carbon dioxide evolution rate (q_{CO2}) with delta pH (ΔpH). Right: correlation of specific oxygen uptake rate (q_{O2}) with delta pH (ΔpH). Both plots were made using batch cultivation with addition of Penicillin G. 72

Die approbierte gedruckte Originalversion dieser Diplomarbeit ist an der TU Wien Bibliothek verfügbar.
The approved original version of this thesis is available in print at TU Wien Bibliothek.

10 List of tables

Table 1: Elements and their purpose in gene expression system under control of *lac* operon 13
Table 2: Advantages and disadvantages/problems of MLR (Lohninger, 2019)..... 17
Table 3: Advantages and disadvantages of polynomial regression (Pant, 2019)..... 18
Table 4: Advantages and disadvantages of Boltzmann sigmoidal fit 19
Table 5: 2TY medium components..... 20
Table 6: Acid and base components..... 20
Table 7: CGXII medium components 21
Table 8: Carbon source and antifoam 21
Table 9: CTAB solution..... 21
Table 10: IPTG solution..... 21
Table 11: Antibiotic component..... 22
Table 12: Nigericin solution..... 22
Table 13: Penicillin solution..... 22
Table 14: stock solution of pH buffers 22
Table 15: PBS buffer components 22
Table 16: Trace element solution components..... 23
Table 17: pH adjustment chemical..... 23
Table 18: Tween 40 specifications 23
Table 19: Shake flask experiment description..... 24
Table 20: Tuning of inducer. Concentrations of IPTG used during bioreactor cultivation..... 25
Table 21: Batch and fed-batch cultivations conducted in DasGip bioreactor system. 25
Table 22: Batch cultivations conducted in 3.5-L-Labfors reactor..... 26
Table 23: R^2 value for the polynomic regression model of third order for different OD_{600} and biomass concentrations..... 30
Table 24: R^2 values of the regression models for different OD_{600} values and therefore different cell concentrations [g/L] 33
Table 25: R^2 value for the curves regressed using a polynomic model of order 3 for Nigericin 35
Table 26: R^2 value for the curves regressed using a linear model for Nigericin..... 38
Table 27: R^2 and RMSE for fitting methods applied for OD 10..... 41
Table 28: R^2 and RMSE for fitting methods applied for OD 25..... 41
Table 29: R^2 and RMSE for fitting method applied for OD 50 41
Table 30: Cultivation parameters used for 3 different experiments during high-throughput screening 46
Table 31: Cultivation parameters used during five batch and fed-batch cultivations 51
Table 32: Cultivation parameters used for investigating pH dynamics during carbon starvation, external pH changes and stress addition 64
Table 33: Chemical list..... 89
Table 34: Equipment list..... 90
Table 35: pH buffers used for sensor calibration 91
Table 36: pH values prepared vs pH values measured after cell addition at different biomass concentrations..... 91

Die approbierte gedruckte Originalversion dieser Diplomarbeit ist an der TU Wien Bibliothek verfügbar.
The approved original version of this thesis is available in print at TU Wien Bibliothek.

11 Attachments

Chemicals:

Table 33: Chemical list

Chemical	Company	Article number
3-morpholino propane sulfonacid (MOPS)	Carl Roth, Germany	6979.4
Agar, Bacteriological European Type (Ingredient) for microbiology	AppliChem, Germany	402302.121
Ammonia solution 25 %	Carl Roth, Germany	5460.2
Ammonium sulfate	Carl Roth, Germany	9218.2
Biotin	Carl Roth, Germany	3822.3
Calcium chloride dihydrate	Carl Roth, Germany	5239.3
Copper(II) sulfate pentahydrate	Carl Roth, Germany	8175.1
Cetyltrimethylammoniumbromide	Carl Roth, Germany	9161.1
D(+) glucose monohydrate	Carl Roth, Germany	6887.5
Dipotassium hydrogen phosphate	Carl Roth, Germany	P749.3
Disodium hydrogenphosphate dihydrate	Carl Roth, Germany	T877.1
Ethanol	Carl Roth, Germany	P076.1
Hydrochloric acid 32%	Carl Roth, Germany	X896.1
IPTG	Carl Roth, Germany	2316.4
Iron(II) sulfate heptahydrate	Carl Roth, Germany	P015.2
Kanamycin sulfate	Carl Roth, Germany	T832.2
Magnesium sulfate heptahydrate	Carl Roth, Germany	8283.3
Manganese sulfate monohydrate	Carl Roth, Germany	7347.1
Nickel(II) chloride hexahydrate	De Haën, Germany	31462
Nigericin	Sigma Aldrich, Israel	N7143
Penicillin G	AppliChem, Germany	A1837.0025
Phosphoric acid 85 %	Carl Roth, Germany	9079.3
Polypropylene glycol 2000	Sigma Aldrich, Spain	81380
Potassium chloride	Carl Roth, Germany	HN02.3
Potassium dihydrogen phosphate	Carl Roth, Germany	3904.3
Sodium chloride	Carl Roth, Germany	3957.2
Tryptone (Ingredient) for microbiology	AppliChem, Germany	103682.121
Tween 40	Carl Roth, Germany	8240
Urea	Carl Roth, Germany	X999.3
Yeast extract	Carl Roth, Germany	2363.5
Zinc sulfate heptahydrate	Carl Roth, Germany	T884.1

Die approbierte gedruckte Originalversion dieser Diplomarbeit ist an der TU Wien Bibliothek verfügbar.
The approved original version of this thesis is available in print at TU Wien Bibliothek.
TU Bibliothek Your knowledge hub WIEN

Equipment:

Table 34: Equipment list

Device	Company	Type	Specifications
Analytical balance (1)	Mettler Toledo, USA	ME204	max= 220 g, d= 0.0001 g
Analytical balance (2)	Sartorius, Germany	TE214S	max= 210 g, d= 0.0001 g
Balance	Sartorius, Germany	Extend	max= 8200 g, d= 0.1 g
Balance for reactor	KERN & Sohn, Germany	KMS-TM	max= 35 kg, d= 1 g
Balance for reactor	Mettler Toledo, Switzerland	MS8001TS/00	max= 8200 g, d= 0.1 g
Black microplate, 96-Well	Greiner Bio-One GmbH, Germany	655900	Flat bottom (chimney well), PS, non-binding
Cedex Bio HT Analyzer	Roche, Switzerland	06608116001	Glucose Bio HT, Glutamate Bio HT, Lactate Bio HT, NH_3 Bio HT
Centrifuge	Sigma, USA	3-18KS	-
DasGip bioreactors	Eppendorf, Germany	DASGIP Parallel Bioreactor System DR03F	V_{min}= 700 mL, V_{max}= 2700 mL, $V_{typical}$= 2000 mL, 2 x Rushton
DO sensor Labfors 5	Infors HT, Switzerland	Visiferm Arc 325	-
DO sensor DasGip	Hamilton, USA	Ref.243666-231	DO ECS 225
Fogale biomass sensor	FOGALE nanotech, France	RS 232 C	Standard for rack mounting: 450 x 270 x 150 mm (19", 3U) Stainless IP 65 enclosure: 350 x 170 x 460 mm
Labfors 5 bioreactor	Infors AG, Switzerland	Infors Labfors 5 K166041	volume: 3.5 L glass vessel stirrer: double 6-blade disc, 2 x Rushton
Lucullus PIMS	Applikon Biotechnology, USA	-	-
µClear® 96 Well Cell Culture Microplates, Black, CELLSTAR®	Greiner Bio-One GmbH, Germany	655090	Flat bottom (chimney well), PS, TC, lid with condensation rings, sterile
Mili Q water: SYNERGY UV HIGH FLOW (1/PK)	Merck Millipore, USA	SYNSVHF00	-
Offgas analyzer	BlueSens, Germany	BlueInOne Ferm	-
pH electrode for Labfors 5	Mettler Toledo, Switzerland	32899	diameter: 12 mm, length: 325 mm
pH electrode for DASGIP	Hamilton, USA	EasyFerm Plus PHI K8 225	
pH probes	Xylem Analytics, Germany	pH 320, SenTix 50	pH-combined electrode
Photometer	Thermo Scientific, USA	Genesys 20	Absorption measurement in linear range: 0.2-0.8 A.
Rotary shaker	Infors HT, Switzerland	Multitron	-
Tecan Infinite 200	Tecan Gmbh, Austria	Infinite 200	Multifunctional 6 to 384-well microplates reader with injection option, fluorescence and absorbance measurement

Die approbierte gedruckte Originalversion dieser Diplomarbeit ist an der TU Wien Bibliothek verfügbar.
The approved original version of this thesis is available in print at TU Wien Bibliothek.

Table 35: pH buffers used for sensor calibration

pH	V (K_2HPO_4) [µL]	V (KH_2PO_4) [µL]
6.0	264	1736
6.2	384	1616
6.4	556	1444
6.6	762	1238
6.8	994	1006
7.0	1230	770
7.2	1434	566
7.4	1604	396
7.6	1732	268
7.8	1816	184
8.0	1880	120
8.1	1912	88
8.2	1944	56
8.3	1964	36

2 mL of the concentrated buffer was dissolved in Mili Q water to 20 mL.

Table 36: pH values prepared vs pH values measured after cell addition at different biomass concentrations

pH prepared	pH measured for OD - 1	pH measured for OD - 10	pH measured for OD - 25	pH measured for OD - 50
6.0	6.2	6.2	6.2	6.2
6.4	6.4	6.4	6.4	6.4
6.8	6.8	6.8	6.8	6.8
7.0	7.0	7.0	7.0	7.0
7.2	7.2	7.2	7.2	7.2
7.4	7.4	7.4	7.4	7.4
7.6	7.6	7.6	7.6	7.6
7.8	7.8	7.8	7.7	7.7
8.0	8.0	8.0	7.8	7.8
8.3	8.3	8.13	8.0	7.8
8.7 *(adjusted with 0.5 M KOH)*	8.6	8.23	8.1	8
9.0 *(adjusted with 0.5 M KOH)*	8.8	8.35	8.1	8
9.6 *(adjusted with 0.5 M KOH)*	9	8.5	8.2	8.1
10 *(adjusted with 0.5 M KOH)*	9.3	8.5	8.2	8.2

Die approbierte gedruckte Originalversion dieser Diplomarbeit ist an der TU Wien Bibliothek verfügbar.
The approved original version of this thesis is available in print at TU Wien Bibliothek.